MAREES TERRESTRES

BULLETIN D'INFORMATIONS

N° 88

30 OCTOBRE 1982

Association Internationale de Geodesie

Commission Permanente des Marees Terrestres

Editeur Prof. Paul MELCHIOR

Observatoire royal de Belgique

Avenue Circulaire 3

1180 Bruxelles

TABLE DES MATIERES N°88

A MULTI INPUT-SINGLE OUTPUT MODEL FOR EARTH TIDE DATA

F. De Meyer
Royal Meteorological Institute
Avenue Circulaire 3
1180 Brussels, Belgium

ABSTRACT

A multi input-single output (MISO) model is applied to Earth tide data to obtain frequency-dependent transferfunctions that describe the tidal characteristics in a similar sense to what can be deduced from traditional harmonic analysis.

The model expresses the tide as a weighted sum of present and past values of the tidal input channels and it allows the input of subsystems describing other influencing phenomena. The choice of a limited number of response weights severely truncates the impulse responses, with a result that the transferfunctions are continuous and smooth in the tidal wave bands. The transferfunctions can be interpreted directly in terms of the amplitude and phase factors of the tidal constituents as a function of frequency. Problems and criteria concerning the smoothness of the transferfunctions and the number of response coefficients are discussed. A method is developed for computing confidence intervals for the frequency responses from an estimate of the variance of the extraneous noise. The MISO-model neglects the existence of sharp resonance peaks and therefore smoothes out the effect of the Earth's liquid core.

1 INTRODUCTION

Munk and Cartwright (1966) have developed a response method for the analysis and prediction of ocean tides in which the input functions are the time-variable spherical harmonics of the gravitational potential on the Earth's surface. The radiative input is taken to represent nongravitational effects. A wider application of the response method is used by Cartwright (1968) in an analysis of sea level variations, where the tidal contributions are supplemented with additional inputs to include the effects of tide-surge interaction, external surges and local weather. These are the major departures from the traditional approach in which the tidal oscillations are described by the amplitudes and phase lags for a finite, predetermined set of cosine functions of precisely known frequencies. Unlike the conventional harmonic methods of tidal analysis, the response procedure expresses the tide as a weighted sum of past, present and future values of a relatively small number of time-varying input channels. The realistic features of the admittance functions being continuous and smooth are successfully approximated in this nonharmonic algorithm.

It has been suggested by Zetler et al. (1970) that the response method is ideally suited for the analysis of Earth tide data. Its extension to Earth tides is given by Lambert (1974) and a review is presented by Yaramanci (1978). In this paper a multichannel model is discussed for taking into account the theoretical tidal variations, meteorological and associated phenomena. The model can include inputs representing atmospheric loading and on-site temperature fluctuations, which are known to influence underground observations. The method is based on the same principles as the response procedure in the sense that the results of the analysis are given in terms of functions of frequency, called transferfunctions, which reveal directly the frequency responses of the physical system under study as distinct from the astronomical context of the problem.

Fundamentally the aim of an Earth tidal analysis is to estimate the reponse function of the Earth in order to compare it with a theoretical geophysical model. The harmonic method suffers from the apparent incapacity of incorporating noise contributions which are inevitably present in the tidal records. The input-output model is interesting for Earth tide analysis because the response of the physical system to the tidal gravitational potential can be automatically separated from other disturbances at the tidal frequencies. Since the analysis of Earth tide data should include input functions representing effects of

local or global nature, the essential object of this approach is to isolate the linear part of the response of the Earth to the purely gravitational forces from the effects of other perturbations at the tidal periods that are ultimately the result of meteorological processes or nonlinear sea level interaction.

The input-output model differs from the harmonic viewpoint mainly in the princile that all possible input candidates are treated a priori on equal level with the tides. The input channels are used to express the response of the Earth to external forces which are more or less known, whatever their origin. Seperate transferfunctions can be calculated for distinct, sufficiently uncorrelated inputs, whose spectral lines are not normally seperable from one another by a least squares harmonic analysis. It is expected that the great variety to use the MISO model will increase the geophysical information.

The method is applied to observed hourly tilt readings of two Verbaandert-Melchior pendulums from the station Dourbes (λ = 04°36'E, φ = 50°06'N) in an area of moderate oceantide influence. Astronomical prejudice as to what tidal frequencies are present is weakened, thus allowing freely for the presence of background noise. A description of the Dourbes station has been given by Dopp (1964) and Melchior (1978, p. 363).

2. THE MULTI INPUT-SINGLE OUTPUT MODEL.

Suppose that the noise-free output $y^\circ(t)$ of a linear dynamic system at time t is generated by m deterministic input signals $u_1^\circ(t)$, ..., $u_m^\circ(t)$. It is then assumed that the linear system can be adequately represented by the discrete convolution equation

$$y^\circ(t) = \sum_{k=1}^{m} \sum_{j=0}^{\infty} h_{kj} \; u_k^\circ (t - j \, \Delta t_k) \quad , \qquad (2.1)$$

where the Δt_k denote appropriate time lags. The use of positive lags is avoided since it obviously violates causality. An equivalent statement is that the system, described by Eq.(2.1), is physically realizable. The weights (h_{k0}, h_{k1},...) are the ordinates of the impulse response function for the input channel number k, which represents the response of the system to a unit impulse.

Let z be the backward shift operator (Robinson, 1980), that is,

$$z^j u_k^\circ(t) = u_k^\circ (t - j \, \Delta t_k) \quad , \; j = 0, 1, 2, \ldots, \qquad (2.2.)$$

and define the z-transform of the impulse reponse by the power series

$$H_k(z) = \sum_{j=o}^{\infty} h_{kj} z^j \quad . \qquad (2.3)$$

Then the basic deterministic equation (2.1) can be expressed in the convenient shorthand

$$y^\circ(t) = \sum_{k=1}^{m} H_k(z)\, u_k^\circ(t) \quad , \qquad (2.4)$$

where the transferfunction $H_k(z)$ expresses the modulation effects in translating the given input $u_k^\circ(t)$ into the output $y^\circ(t)$.

Knowledge of the transferfunction $H_k(z)$ completely determines the dynamic response of the linear system to the input in the kth channel. The z-transform evaluated on the unit circle $z = e^{-2\pi i f \Delta t_k}$ of the complex z-plane corresponds to the discrete Fourier transform of the impulse response

$$H_k(f) = \sum_{j=o}^{\infty} h_{kj}\, e^{-2\pi i j f \Delta t_k} \quad , \qquad (2.5)$$

where f denotes frequency. The complex transferfunction $H_k(f)$ is commonly expressed in polar form

$$H_k(f) = G_k(f) e^{i \Phi_k(f)} \quad . \qquad (2.6)$$

Munk and Cartwright (1966) refer to $H_k(f)$ as the admittance function. Writing $Y^\circ(f)$ and $U_k^\circ(f)$ for the Fourier transforms of $y^\circ(t)$ and $u_k^\circ(t)$, the convolution relation (2.1) is equivalent to

$$Y^\circ(f) = \sum_{k=1}^{m} H_k(f) U_k^\circ(f) \qquad (2.7)$$

in view of the convolution theorem of Fourier transforms. The gain or amplitude response $G_k(f)$ therefore represents the amplification by the system on passing an input harmonic wave with frequency f through the channel number k and the phase response $\Phi_k(f)$ determines the phase shift that will be observed in the output at the frequency f.

It will evidently be impossible to parameterize the multi input-single output (MISO) model in Eq. (2.1) in terms of discrete impulse responses of infinite extent. If an infinite lag structure is the correct description of the true process, then by using approximants of finite order there is the risk to commit a misspecification error of generally unknown proportions, especially without prior information.

Discrete dynamic systems can frequently be represented by the linear difference equation model

$$\sum_{j=o}^{p} b_j y^\circ(t-j\,\Delta\,t) = \sum_{k=1}^{m} \sum_{j=o}^{q_k} a_{kj} u_k^\circ\,(t-j\,\Delta\,t_k) \quad , \; b_o = 1, \qquad (2.8)$$

of which the dynamical character is as far as desired identical with the true system response ; Δ t is the sampling period of the output $y^\circ(t)$. Here the orders p, q_1, ..., q_m are assumed to be known a priori. Equation (2.8) describes a transferfunction model where the dynamical behaviour of the output is explained in terms of its own past values and the present and past values of the input signals. Note that for m=1 a single input - single output (SISO) model is obtained.

It is clear that in practice one very seldom has definitive information concerning the orders of the numerical scheme or even that the finite parameter representation is efficient. Box and Jenkins (1970) and Bennet (1979) discuss this problem of identification. In this connection the overall criterion of parsimony, which is an efficiency or statistical estimation constraint, is often used as "Occam's razor" (Tukey, 1961). Apart from the exigence that the proposed model be consistent with the entire set of observations, this principle states that the model be simple in the sense that a more elaborate model is only accepted if a better or more parsimonious one is not available. This is important with the algorithm suggested in Eq.(2.8) since "overfitting" tends to provide impulse response weights whose absolute values are too large and whose signs may actually reverse with negligible changes in the data for increasing orders p and q_1, ..., q_m.

The use of the backward shift operator allows us to write Eq.(2.8) in the equivalent expression

$$B(z)y^\circ(t) = \sum_{k=1}^{m} A_k\,(z)u_k^\circ\,(t) \quad , \qquad (2.9)$$

where $z^j y^\circ(t) = y^\circ(t-j\,\Delta\,t)$ and

$$B(z) = \sum_{j=o}^{p} b_j z^j \quad , \quad A_k(z) = \sum_{j=o}^{q_k} a_{kj} z^j \qquad (2.10)$$

are polynomials in arguments of z, operating on the theoretical deterministic output $y^\circ(t)$ and input $u_k^\circ\,(t)$, respectively ; (b_o, b_1, ..., b_p) is the autoregressive (AR) operator and (a_{ko}, a_{k1}, ..., a_{kq_k}) the moving-average (MA) operator associated with the channel number k.

Comparing Eq. (2.9) with (2.4) it is concluded that the transferfunction $H_k(z)$ is approximated by the ratio of two polynomials in z (Padé approximant)

$$H_k(z) = B^{-1}(z)A_k(z) \quad . \qquad (2.11)$$

The impulse response for input number k can then be explicitely obtained by formal division of the polynomial $A_k(z)$ by B(z). In order that the polynomial B (z) be invertible it must be necessarily required that all the roots of B(z), which are termed the poles of the MISO model, are situated outside the unit circle $|z| = 1$ of the complex z-plane. This is called the stability criterion or minimum-delay property (Robinson, 1980) and it ensures stationarity for the input-output model, since we then may expand $B^{-1}(z)$ in a series of positive powers of z which will converge uniformly in a region including the unit circle. The strength of the Padé approximant evidently is that it approximates an infinite power series $H_k(z)$ by the ratio of two polynomials of finite order. In terms of the frequency f, Eq. (2.11) reads

$$H_k(f) = \sum_{j=o}^{q_k} a_{kj} e^{-2\pi ijf\Delta t_k} \Big/ \sum_{j=o}^{p} b_j e^{-2\pi ijf\Delta t} \quad . \qquad (2.12)$$

However, some poles may occur very near unity in the complex z-plane. This introduces a limited form of statistical non-stationarity in which the time series is showing a stochastically varying bias or trend. The backward difference operator ∇ is defined by

$$\nabla\, y^o(t) = y^o(t) - y^o(t-\Delta t) = (1-z)y^o(t) \qquad (2.13)$$

On differencing Eq. (2.4) we obtain

$$\nabla\, y^o(t) = \sum_{k=1}^{m} H_k(z) \quad \nabla\, u_k^o(t) \quad , \qquad (2.14)$$

which shows that the incremental changes $\nabla y^o(t)$ and $\nabla\, u_k^o(t)$ satisfy the same transferfunction model as do $y^o(t)$ and $u_k^o(t)$. This procedure allows for limited removal of non-stationary effects in time series observations by differencing the data. If the non-stationary part (drift) of $y^o(t)$ is mainly concentrated at the low frequencies, its effect can be greatly attenuated by fitting the model (2.14) instead of (2.4), since the operator (1-z) essentially has the properties of a high-pass filter. The Padé approximant then becomes

$$B(z)\,\nabla\, y^{\circ}(t) = \sum_{k=1}^{m} A_k(z) \quad \nabla\, u_k^{\circ}(t) \qquad . \qquad (2.15)$$

Nevertheless this method does not provide for more general non-stationary behaviour in which the parameters that characterize the polynomials $B(z)$ and $A_k(z)$ themselves vary as functions of time.

In practice the true output $y^{\circ}(t)$ and inputs $u_k^{\circ}(t)$ will be subjected to error, such that noisy measurements are available

$$y(t) = y^{\circ}(t) + \eta(t) \quad , \quad u_k(t) = u_k^{\circ}(t) + \xi_k(t). \qquad (2.16)$$

Then the multivariate model (2.8) can be represented in terms of the observed output and inputs as

$$\sum_{j=o}^{p} b_j y(t-j\,\Delta\,t) = \sum_{k=1}^{m} \sum_{j=o}^{q_k} a_{kj} u_k(t-j\,\Delta\,t_k) + \varepsilon(t), \; b_o = 1, \qquad (2.17)$$

or equivalently

$$B(z)y(t) = \sum_{k=1}^{m} A_k(z) \quad u_k(t) + \varepsilon(t) \qquad (2.18)$$

with the model error given by

$$\varepsilon(t) = \sum_{j=o}^{p} b_j \quad \eta(t-j\,\Delta\,t) - \sum_{k=1}^{m} a_{kj} \quad \xi_k(t-j\,\Delta\,t_k) \quad . \qquad (2.19)$$

An analoguous expression can be written when $y(t)$ and $u_k(t)$ are replaced by $\nabla\, y(t)$ and $\nabla\, u_k(t)$, respectively. Besides "ignored" variables the model noise $\varepsilon(t)$ consequently includes input and output disturbances. This result illustrates the fact that the noise element in the model (2.18) will in general be autocorrelated (red or coloured noise) and has a pattern which is itself controlled by a transferfunction relationship, since the errors $\eta(t)$ and $\xi_k(t)$, $k=1,2,\ldots,m$, will be internally dependent. Furthermore it follows that $\varepsilon(t)$ cannot implicitely be assumed to be uncorrelated with the observed input and output signals since $\varepsilon(t)$, $y(t)$ and $u_k(t)$ partly depend on $\eta(t)$ and $\xi_k(t)$.

3. LEAST SQUARES ESTIMATION OF THE MODEL PARAMETERS.

Let us assume that the continuous output $y(t)$ and inputs $u_k(t)$, $k = 1, 2, \ldots, m$, are digitized with the same sampling interval Δt. Defining the row vectors $\underline{x}^T(t) = [-y(t-\Delta t), \ldots, -y(t-p\Delta t), u_1(t), \ldots, u_1(t-q_1\Delta t_1), \ldots, u_m(t), \ldots, u_m(t-q_m \Delta t_m)]$ and $\underline{\theta}^T = (b_1, \ldots, b_p, a_{10}, \ldots, a_{1q_1}, a_{mo}, \ldots, a_{mq_m})$ we obtain from Eq. (2.17) the shorthand relation of the form

$$y(t) = \underline{x}^T(t)\,\underline{\theta} + \varepsilon(t) \quad . \tag{3.1}$$

The transpose of any column vector $\underline{a}$ and matrix A is denoted by $\underline{a}^T$ and A^T. The elements of the parameter vector $\underline{\theta}$ are then to be estimated from N simultaneous observations of the inputs and the output at the time instants $k\,\Delta t$, $1 \leq k \leq N$. The entire set of N linear equations (3.1) can also be written in the vector matrix formulation as

$$\underline{y} = X\,\underline{\theta} + \underline{\varepsilon} \tag{3.2}$$

with $\underline{y}^T = [y(\Delta t), \ldots, y(N\Delta t)]$, $\underline{\varepsilon}^T = [\varepsilon(\Delta t), \ldots, \varepsilon(N\,\Delta t)]$ and X the data matrix with rows the values of the vectors $\underline{x}^T(t)$ at the time points $k\,\Delta t$, $1 \leq k \leq N$.

Minimization of the sum of squares error criterion

$$S(\underline{\theta}) = \underline{\varepsilon}^T\underline{\varepsilon} = (\underline{y} - X\,\underline{\theta})^T(\underline{y} - X\,\underline{\theta}) \tag{3.3}$$

with respect to the parameter vector $\underline{\theta}$ gives the normal equations for the least squares estimate $\hat{\underline{\theta}}$ of the linear model (3.2)

$$A\,\hat{\underline{\theta}} = \underline{b} \tag{3.4}$$

where $A = X^TX$ is the normal matrix, whose elements are the cross-covariances between the regression variables and $\underline{b} = X^T\underline{y}$.
This is accomplished by setting the matrix derivatives

$\partial S/\partial\underline{\theta} = -2\,X^T(\underline{y}-X\underline{\theta})$ of $S(\underline{\theta})$ with respect to $\underline{\theta}$ equal to zero at $\underline{\theta} = \hat{\underline{\theta}}$. If the nonnegative definite normal matrix A is nonsingular, the solution is given by the matrix inversion of Eq. (3.4)

$$\hat{\underline{\theta}} = A^{-1}\underline{b} \tag{3.5}$$

To determine uniquely all $n=p+q_1+ \ldots +q_m$ coefficients in the parameter vector $\underline{\theta}$ it is necessary that the normal matrix is of full rank n or det A $\neq 0$ for estimation problems involving least squares.

Hoerl and Kennard (1970) focus attention on the inadequacy of least squares for ill-conditioned (nonorthogonal) problems. The symmetric covariance matrix of the estimate $\hat{\underline{\theta}}$ is defined by

$$V = E\{[\hat{\underline{\theta}} - E(\hat{\underline{\theta}})][\hat{\underline{\theta}} - E(\hat{\underline{\theta}})]^T\} \quad , \tag{3.6}$$

where E denotes the mathematical expectation operator. The elements v_{jj} along the main diagonal of V are the estimated variances of the components of the vector $\hat{\underline{\theta}}$. The covariance matrix of the parameter errors $\hat{\underline{\theta}} - \underline{\theta}$ is denoted by

$$P = E[(\hat{\underline{\theta}} - \underline{\theta})(\hat{\underline{\theta}} - \underline{\theta})^T] = V + \underline{\beta}\underline{\beta}^T \quad , \tag{3.7}$$

where $\underline{\beta} = E(\hat{\underline{\theta}}) - \underline{\theta}$ is the bias of the estimate.

Substitution of (3.2) into (3.5), together with $\underline{b} = X^T\underline{y}$, shows that $\hat{\underline{\theta}} = \underline{\theta} + (X'X)^{-1} X^T \underline{\varepsilon}$ and the bias is therefore $\underline{\beta} = E[(X'X)^{-1}X^T\underline{\varepsilon}]$. If the independent variables are nonstochastic and if $\underline{\varepsilon}$ is a zero mean vector, uncorrelated with the regressors (i.e., the columns of the matrix X), then it follows that $\hat{\underline{\theta}}$ is an unbiased estimate of $\underline{\theta}$. The covariance matrix of the least squares parameter estimate is in this case

$$V = E[(X^TX)^{-1}X^T\varepsilon\varepsilon^TX(X^TX)^{-1}] = (X^TX)^{-1}X^T \psi X(X^TX)^{-1}$$

with $\psi = E(\underline{\varepsilon}\underline{\varepsilon}^T)$ the residual covariance matrix. Should $\underline{\varepsilon}$ be purely white noise with constant variance σ_ε^2, then the covariance matrix ψ of the extraneous noise becomes diagonal, i.e., $\psi = \sigma_\varepsilon^2 I$, and

$$V = \sigma_\varepsilon^2 (X^TX)^{-1} \quad . \tag{3.8}$$

A reasonable measure for the deviation of $\hat{\underline{\theta}}$ from $\underline{\theta}$ is given by the Euclidian distance L_n, where

$$L_n^2 = (\hat{\underline{\theta}} - \underline{\theta})^T(\hat{\underline{\theta}} - \underline{\theta}) \tag{3.9}$$

nd the total mean square error is defined by

$$E(L_n^2) = \text{Tr } P = \text{Tr } V + \underline{\beta}^T\underline{\beta} \qquad (3.10)$$

where Tr V denotes the sum of the diagonal elements (trace) of the matrix V. The first term in Eq. (3.10) is the sum of variances or the total variance of the parameter estimates and the second term can be interpreted as the square of the bias introduced by $\underline{\hat{\theta}}$.

In this connection it is convenient to work with normalized observations. Denoting by y_k en x_{kj} the elements of the vector $\underline{y}$ and the matrix X, respectively, we suppose that all variates considered have zero mean or that the arithmetical means have been subtracted from the individual values. The standardized data are defined by

$$y_k^* = y_k / \sigma_y, \; x_{kj}^* = x_{kj}/\sigma_j \quad , \quad \varepsilon_k^* = \varepsilon_k/\sigma_y \quad , \qquad (3.11)$$

with $1 \leq k \leq N$ and $1 \leq j \leq n$; σ_y and σ_j are the standard deviations of the output y and the independent variable x_j, such that y_k^* and x_{kj}^* are expressed in standard measure (zero mean, unit variance). Then the expression (3.2) is replaced by the normalized regression model

$$\underline{y}^* = X^* \; \underline{\theta}^* + \underline{\varepsilon}^* \qquad (3.12)$$

in terms of the scaled parameters

$$\theta_j^* = \sigma_j \; \theta_j \; / \; \sigma_y \qquad , \; 1 \leq j \leq n \qquad . \qquad (3.13)$$

To simplify the notations we will drop the asterisks and the discussion will concern the standardized model (3.12). The least squares estimate of the normalized parameter vector is then obtained from the normal equations (3.4), with $A = X^TX/N$ the correlation matrix of dimension n ; X now stands for the scaled matrix X^*. The diagonal elements of A are equal to one and the off-diagonal elements are the estimated correlation coefficients between the normalized variables x_i and x_j. The elements b_j of the vector $\underline{b} = X^T\underline{y}/N$ are the correlations between the dependent variable y and the regressors x_j.

Substitution of Eq. (3.8) into (3.10) shows that the properties of the least squares estimator can be examined by considering the expected value of the squared Euclidian distance of $\underline{\hat{\theta}}$ from $\underline{\theta}$

$$E(L_n^2) = \sigma_\varepsilon^2 \text{Tr } (X^TX)^{-1} + \underline{\beta}^T \underline{\beta} \qquad (3.14)$$

in terms of the correlation matrix X^TX. Equivalently

$$E(\hat{\underline{\theta}}^T\hat{\underline{\theta}}) = \underline{\theta}^T\underline{\theta} + \sigma_\varepsilon^2 \, \mathrm{Tr}\,(X^TX)^{-1} + \underline{\beta}^T\underline{\beta} \quad . \qquad (3.15)$$

If $\lambda_1 \geq \lambda_2 \geq \ldots \geq \lambda_n$ are the eigenvalues of the normal matrix X^TX it follows that

$$\mathrm{Tr}\,(X^TX) = \sum_{j=1}^{n} \lambda_j = n \qquad (3.16)$$

since all the diagonal elements of X^TX are equal to 1. Note that the eigenvalues λ_j are real and nonnegative because X^TX is a symmetrical and nonnegative matrix. The values λ_j/n can therefore be considered as percentages of the total variance explained by the regression variables. It also follows that

$$E(L_n^2) = \sigma_\varepsilon^2 \sum_{j=1}^{n} 1/\lambda_j + \sum_{j=1}^{n} \beta_j^2 > \sigma_\varepsilon^2/\lambda_n \quad . \qquad (3.17)$$

In consequence a lower bound for the average squared distance between $\hat{\underline{\theta}}$ and $\underline{\theta}$ is $\sigma_\varepsilon^2 / \lambda_n$.

If X^TX has one or more small eigenvalues, $E(L_n^2)$ can become very large and $\hat{\underline{\theta}}$ is then expected to be far distant from the true parameter vector $\underline{\theta}$. In particular, the worse the conditioning of X^TX, which can be measured by the condition number λ_1/λ_n, the more $\hat{\underline{\theta}}$ can be expected to be too long. Equation (3.15) shows that the least squares method can lead to an overinflation of the parameter estimates when X^TX does not have a uniform eigenvalue spectrum. This serious deficiency is the condition of overfitting mentioned by Munk and Cartwright (1966). In this case the least squares approach may give coefficients whose absolute values are too large and whose signs may actually reserve with small changes in the data.

Linear dependance or high correlation between the explanatory variables in a linear model is called collinearity. In practical cases we can encounter partial, not perfect, collinearity between the variables such that det X^TX is small. This problem inevitably results from the unavoidable correlation existing between the interdependent regressors in the input-output model (2.17). The consequence of strong correlations among the regression variables (one or more small eigenvalues) is that there will be a high degree of uncertainty in the parameter estimates, since the variance of the parameters is proportional to $1/\lambda_j$. The implicit indeterminacy of the model orders also makes the system poorly identifiable. When an ill-conditioned normal matrix X^TX is to be inverted a conventional computer algorithm will indeed provide an inverse, but the limited precision can be the source of untrustworthy answers. Use of multiprecision arithmetic is recommended in these circumstances but will not necessarily guarantee a more reliable result.

The determinant of X^TX is numerically equal to the product of its eigenvalues and if at least one eigenvalue is small the normal matrix is nearly singular, which implies almost linear dependance between various explanatory variables. This happens when the rank of X^TX is less than its order. In the absence of any a priori knowledge, the importance of possible collinearity can be weighed by computing the eigenvalues and the condition number of X^TX and by a careful inspection of the parameter covariance matrix.

Consider the canonical form

$$A = \Phi \Lambda \Phi^{-1} \tag{3.12}$$

of the normal matrix with $\Lambda = \text{diag}(\lambda_1, \ldots, \lambda_n)$ the diagonal matrix of the eigenvalues λ_j and $\Phi = (\underline{\varphi}_1, \ldots, \underline{\varphi}_n)$ the nxn modal matrix with colums the eigenvectors $\underline{\varphi}_j$ of A.

Since Φ is a unitary matrix, i.e., $\Phi^T = \Phi^{-1}$, it follows that

$$A \Phi = \Phi \Lambda \tag{3.19}$$

The equation

$$A = \Phi \Lambda \Phi^T = \sum_{j=1}^{n} \lambda_j \underline{\varphi}_j \underline{\varphi}_j^T \tag{3.20}$$

represents the eigenvalue decomposition of A. Inverting Eq. (3.20) we find

$$A^{-1} = (\Phi^T)^{-1}\Lambda^{-1}\Phi^{-1} = \Phi \Lambda^{-1}\Phi^T = \sum_{j=1}^{n} \lambda_j^{-1} \underline{\varphi}_j \underline{\varphi}_j^T \tag{3.21}$$

provided all $\lambda_j \neq 0$. If we omit from the summation in Eq. (3.21) all the terms for which $\lambda_j = 0$ we obtain the pseudoinverse matrix A^+ of A (Penrose, 1955).

When there are collinearities in the independent variables, i.e., when one or more eigenvalues are nearly zero, it follows from Eqs. (3.5) and (3.21) that there is no reliance on the individual coefficients θ_j in a regession analysis embodying all the variables. Therefore it appears reasonable to concentrate on that part of A^{-1} which is most affected by the smallness of the eigenvalues of A. A rejection test can be constructed by choosing a cut-off number depending on the magnitude of the real eigenvalues. From the small size of $\lambda_{r+1}, \ldots, \lambda_n$ it seems safe in neglecting the contributions of these sources and the cut-off eigenvalue λ_r is selected. We then define the pseudo inverse by

$$A^+ = \sum_{j=1}^{r} \lambda_j^{-1} \underline{\varphi}_j \underline{\varphi}_j^T \tag{3.22}$$

Since $Tr\,(A^{+})^{-1} = \sum_{j=1}^{r} \lambda_j$ we can use the measure $1/n \sum_{j=1}^{r} \lambda_j$ to decide that the first r of the eigenvalues account for nearly the whole of the variation and that the contribution of the other (n-r) is small. Using A^{+} instead of A^{-1} in Eq. (3.5) a parameter estimate is obtained with an expected value of the squared Euclidian distance

$$E(L_r^2) = \sigma_\varepsilon^2 \sum_{j=1}^{r} 1/\lambda_j + \sum_{j=1}^{n} \beta_j^2 > \sigma_\varepsilon^2/\lambda_r \quad . \tag{3.23}$$

The lower bound for the average squared distance between $\hat{\underline{\theta}}$ and $\underline{\theta}$ is therefore decreased to $\sigma_\varepsilon^2/\lambda_r$.

4. CONFIDENCE LIMITS FOR THE TRANSFERFUNCTIONS.

Once the coefficients $\hat{\theta}_j$ of the transferfunction model are obtained we need to estimate confidence limits for the amplitude and phase responses as a function of frequency so that the frequency variations of the individual input transferfunctions can ultimately be interpreted in terms of the physics of the Earth tidal system. The fundamental theorem for the variance σ_F^2 and the covariance σ_{FG}^2 of functions F(θ) and G (θ) states that

$$\sigma_F^2 = \sum_{i=1}^{n} \sum_{j=1}^{n} \frac{\partial F}{\partial \theta_i} \frac{\partial F}{\partial \theta_j} v_{ij} \quad , \tag{4.1}$$

$$\sigma_{FG}^2 = \sum_{i=1}^{n} \sum_{j=1}^{n} \frac{\partial F}{\partial \theta_i} \frac{\partial G}{\partial \theta_j} v_{ij} \quad , \tag{4.2}$$

where v_{ij} are the elements of the covariance matrix V of the n parameters $\hat{\theta}_j$ (Cameron, 1960), wich are estimated by the corresponding elements of the matrix $\hat{\sigma}_\varepsilon^2 (X^T X)^{-1}$ under the standard assumptions of uncorrelated and constant variance errors. An unbiased estimate of the variance of the extraneous noise is obtained by $\hat{\sigma}_\varepsilon^2 = \hat{\underline{\varepsilon}}^T \hat{\underline{\varepsilon}} / (N-n-1)$, with $\hat{\underline{\varepsilon}}$ the N-vector of observed residuals. We then have the approximate 100(1-α) % confidence interval $\hat{\theta}_j \pm t_{1-\alpha/2} \sigma_{jj}$ for any of the parameters θ_j ; σ_{jj} is the estimated standard error of $\hat{\theta}_j$ and $t_{1-\alpha/2}$ is the α % point of a t-distribution with N-n degrees of freedom.

Omitting the subscript k, the following expressions for the variance and covariance of the real and imaginary parts R(f) and I(f) of the transferfunction $H(f) = R(f) + iI(f) = G(f)\, e^{i\Phi(f)}$ for the input number k are obtained in terms of the elements of the covariance matrix of the model parameters

$$\sigma_R^2(f) = \sum_{i=1}^{n} \sum_{j=1}^{n} \frac{\partial R}{\partial \theta_i}(f) \frac{\partial R}{\partial \theta_j}(f) v_{ij} , \qquad (4.3)$$

$$\sigma_I^2(f) = \sum_{i=1}^{n} \sum_{j=1}^{n} \frac{\partial I}{\partial \theta_i}(f) \frac{\partial I}{\partial \theta_j}(f) v_{ij} , \qquad (4.4)$$

$$\sigma_{RI}^2(f) = \sum_{i=1}^{n} \sum_{j=1}^{n} \frac{\partial R}{\partial \theta_i}(f) \frac{\partial I}{\partial \theta_j}(f) v_{ij} . \qquad (4.5)$$

Applying Eqs. (4.1) and (4.2) to the functions $G(f) = [R^2(f) + I^2(f)]^{1/2}$ and $\phi(f) = \tan^{-1}[I(f)/R(f)]$, the variances of the amplitude and phase responses as a function of frequency are given by

$$\sigma_G^2(f) = \cos^2\phi(f)\,\sigma_R^2(f) + \sin^2\phi(f)\,\sigma_I^2(f) + \sin 2\phi(f)\,\sigma_{RI}^2(f), \qquad (4.5)$$

$$\sigma_\phi^2(f) = [\cos^2\phi(f)\,\sigma_R^2(f) + \sin^2\phi(f)\,\sigma_I^2(f) - \sin 2\phi(f)\,\sigma_{RI}^2(f)] / G^2(f) . \qquad (4.6)$$

The 100 (1- α)% confidence intervals for G(f) and $\phi(f)$ follow by substituting (4.5) and (4.6) in the relations $G(f) \pm t_{1-\alpha/2}\sigma_G(f)$ and $\phi(f) \pm t_{1-\alpha/2}\,\sigma_\phi(f)$, respectively.

Since

$$\frac{\partial R}{\partial \theta_j} = \mathrm{Re}\left\{\frac{\partial H}{\partial \theta_j}\right\} \quad \text{and} \quad \frac{\partial I}{\partial \theta_j} = \mathrm{Im}\left\{\frac{\partial H}{\partial \theta_j}\right\}$$

we only have to use the partial derivatives

$$\frac{\partial H_k}{\partial a_j} = e^{-2\pi ijf\,\Delta t_k/B_k}(f) \quad \text{and} \quad \frac{\partial H_k}{\partial b_j} = -A_k(f)\, e^{-2\pi ijf\,\Delta t_k/B_k^2}(f)$$

in the expressions for $\partial R_k/\partial a_j$, $\partial R_k/\partial b_j$, $\partial I_k/\partial a_j$ and $\partial I_k/\partial b_j$ for the channel number k.

5. APPLICATION OF THE MISO MODEL TO EARTH TIDES OBSERVATIONS.

The system describing the Earth is assumed to be linear, stable and time-invariant, where many forces act as input to generate the particular observed signal as the output of this system (e.g. tilt, gravity, strain). Due to the complexity of the real Earth, the term "system" is to be interpreted as a mathematical black box description of the behaviour of the Earth to the composition of these forces. In that sense the MISO model describes the relation between the input channels and the output and involves no real parameters of physical importance. However, the transferfunctions reveal directly the frequency responses of the true system under study as distinct from the astronomical context of the problem. The principle advantage of this method apparently lies in the fact that separate transferfunctions can be constructed for sufficiently uncorrelated inputs.

Effective use of the model (2.17) requires that we adopt consistent procedures for deciding on the relevant nongravitational input functions to be included in the analysis and for choosing the appropriate number of lags to fit the transferfunction for each input signal. By including all workable inputs in the model we attempt to account for the entire information content of the data, but it is important to avoid the condition of overfitting. One approach to the problem of deciding upon the inclusion of a particular input is to introduce all suspected channels from the start in a lumped response analysis. An input is then rejected on the basis of unacceptably large confidence limits produced in the transferfunctions.

Slow variations, of any origin (rheologic, thermic, molecular), in the instrumental conditions produce a socalled "drift" of the instrumental zero in Earth tide observations. External effects acting upon or inside the Earth's crust superpose themselves on the drift, such as changes in the underground water level, atmospheric pressure or other unknown local disturbances. From the viewpoint of harmonic analysis it is very difficult to separate such irregular phenomena from the tidal constituents. In order to suppress the long period contributions, the MISO model in the form of Eq. (2.15) is selected in this connection and no autoregressive operator is introduced (p=1), so that the coefficients a_{kj} have the meaning of impulse response weights h_{kj} in Eq. (2.1).

Among many inputs from meteorological, loading and tectonic origin the tidal potential is all-important and theoretically best known. The first four input channels are generated by the harmonic model and correspond to the main frequency bands of the gravitational potential. These functions are computed hour by hour from the time-harmonic expansions of the Cartwright-Tayler-Edden (1971, 1973) model.
The input functions $u_1(t)$, $u_2(t)$, $u_3(t)$ and $u_4(t)$ are confined to the long-period (LP), diurnal (D), semi-diurnal (SD) and ter-diurnal (TD) frequency bands, respectively. The transferfunctions may then be interpreted directly in terms of the amplitude and phase factors of the tidal constitutents as a function of frequency.

Since the tidal line spectrum is superimposed on a continuum the use of the convolution method permits to include a complete set of realistic input functions. The existence of the noisy spectrum carries some obligation to incorporate the features in the tide records that cannot be accounted for by the gravitational tide-producing forces. Solar radiation affects Earth tides observations mainly through gravitational and surface loading effects of moving air masses, through heating and cooling of the ground and through meteorological effects on sea level. It may be important to include input functions expressing specifically air pressure and temperature disturbances in the vicinity of the observation site. Indeed, noise is generated in the tidal wave bands as a result of temperature variations acting on the instruments, which combine their effect into a S_1 meteorlogical wave and as a result also of atmospheric pressure fluctuations, which produce a S_2 meteorological component. In consequence the inputs $u_5(t)$ and $u_6(t)$ respectively correspond to the interpolated hourly means of the barometric pressure (in mbar) and air temperature (in degrees centigrade), measured at the synoptic station Florennes (λ = 4°39'E, φ = 50° 14'N), situated about 18 km north of the station Dourbes (λ = 4°36'E, φ = 50°06'N).
Air pressure variations are expected to be more important than thermic influences, since temperature variations cannot be transmitted very deeply in the crust and the horizontal pendulumns are installed in a cavity of dimension 6m x 6m at a depth of 46 m.

Hydrological disturbances are probably the major long-period influences experienced in tidal measurements because changes in the flood of a neighbouring river may produce important deformations of the galery where the instruments are installed. Therefore the input channel u_7 (t) includes the interpolated hourly means of the level (in cm) of the river Viroin, situated south of the station at a distance of 2 km.

Geophysical considerations and experience indicate a continuous and rather smooth response of the Earth to the body forces within the band of frequencies covered by a particular tidal species. This implies a severe truncation in the impulse responses. A fundamental decision is to be made about each response concerning its length q_k and the lag interval Δt_k. Increasing the sampling rate Δt_k leads to a smaller bandwidth over which H_k (f) is defined and increasing the length q_k of the input channel number k entails more allowed oscillations for the transferfunctions. Since our knowledge is limited to a few narrow frequency bands, there is no need to fit H_k (f) for all frequencies. Considering that the long-period band extends from 0 to 0.0061 cph (cycles per hour), the diurnal band from 0.0341 to 0.0464 cph, the semi-diurnal band from 0.0744 to 0.0867 cph and the terdiurnal band drom 0.1177 to 0.1239 cph, the effective band widths Δf_1 = 0.0061, Δf_2 = 0.0123, Δf_3 = 0.0123 and Δf_4 = 0.0062 cph are obtained.

The Fourier series (2.5) has periodicity $1 / \Delta t_k$ in frequency, which is of course unrealistic from the physical viewpoint because of the repetition of the response spectrum, but quite acceptable when dealing with the question of sampling the system function provided that $1 / \Delta t_k > 2 \Delta f_k$, with Δf_k the bandwidth within which the spectrum G_k (f) is confined. This gives an estimate $\Delta t_k = 1/2 \Delta f_k$ for the optimum lag interval ; in particular Δt_1 = 81.96, $\Delta t_2 = \Delta t_3$ = 40.64 and Δt_4 = 80.64 hours. Continuation of the Fourier series at frequencies higher than the Nyquist frequency $1/2 \Delta t_k$ is termed spectrum folding. Geometrically we can interprete this effect as if the frequency axis would be folded in the points $j/2 \Delta t_k$, j = 0, $\pm$ 1, $\pm$ 2, ... To represent the transferfunction H_k (f) optimally in the wave band k, the integer j and time resolution Δt_k should be chosen such that $j/2 \Delta t_k$ nearly coincides with the beginning of the wave band k. For example, choosing Δt_2 = 43 hours and j = 3 for the D-band gives $j/2 \Delta t_2$ = 0.0349 cph, Δf_2 = 0.0116 cph and the transferfunction H_2 (f) is restricted to the frequency interval (0.0349, 0.0465) cph.

In a similar way we obtain Δt_1 = 82 h (j=0), Δt_3 = 40 h (j=6) and Δt_4 = 81 h (j=19), confining the computed transferfunctions of the LP, SD and TD waves to the frequency intervals (0, 0.0061) cph, (0.0750, 0.0875) cph and (0.1173, 0.1235) cph, respectively. The imposed periodic representation of the H_k (f) inevitably makes the corresponding Fourier series invalid outside the known bands.

The smoothness of the actual transferfunction H_k (f) depends on the number of response weights and it is important to decide what the maximum lags q_k should be. If the number of lags is increased there is a danger that the frequency curves will become distorted in their attempt to adapt to the smaller tidal constituents, which are more perturbed by the presence of extraneous noise than the major tidal waves. Extending q_k therefore is suspected to introduce artificial fluctuations in the amplitude and phase response functions. Writing $q_k \Delta t_k = 1/f_k$, truncation of the impulse response at the lag q_k implies that any change of the frequency response with a spectral wavelength smaller than f_k cannot be detected by the Fourier series representation. We have chosen a priori q_k = 6 for the inputs k = 1, 2, 3 and q_4 = 2, which means that any oscillation of the response function with a spectral wavelength smaller than 0.1 cpd (cycles per day) will be smoothed out in the D- and SD-bands.

The foregoing choice deliberately neglects the existence of very sharp resonance peaks and therefore the presence of the Earth's liquid core which has the effect of introducing a resonance in the diurnal frequency band, associated with the nutations of the Earth's axis in space. Fitting the Earth tides observations with only a few impulse response coefficients inevitably smoothes out the core effect, which distorts the amplitude of diurnal Earth tide constituents by a few percent over a relatively narrow band centered on the frequency of resonance.

For the three perturbation inputs u_5 (t), u_6 (t) and u_7 (t) we have chosen a priori Δt_k = 5 hours and q_k = 4, k = 5, 6, 7. Since the distortion of the Earth tides by oceanic influences cannot be ignored, the MISO model could include shallow water interaction and raditional inputs from oceanic tides. The nonlinear sea level inputs can also be included in the response analysis of Earth tide observations (especially tilt) taken near the coast of shallow seas. Because the additional input has totally or partly the same frequencies as the tidal inputs, sea level response has not been included in this analysis.

6. ANALYSIS OF TILT OBSERVATIONS.

A multi response analysis was performed on a 3287 day series of hourly observations for the time interval 1/1/1969 - 31/12/1977, recorded with the Verbaandert-Melchior EW pendulum n° 28 and NS pendulum N° 7 at the station of Dourbes, situated at 140 km from the North Sea in an area of moderate ocean tide influence. This epoch was selected because the hourly data of all input and output channels were available. Table 1 shows the impulse response coefficients h_{kj} and the estimated standard errors Δh_{kj} for the pendulum n° 28, obtained with the least squares method. The matrix inversion in Eq. (3.5) was performed in double precision arithmetic.

The terminology will be as that used by Draper and Smith (1966) and Agterberg (1974). The total sum of squares TSS = $9.793\ 10^5$ mseca^2 refers to the sum of squares of the deviations of the differences $\nabla y(t) = y(t) - y(t - \Delta t)$ from their mean, yielding a variance 12.6 m seca^2 of the output channel. Since the sum of squares due to the regression is SSR= $9.634\ 10^5$ m seca^2, a residual sum of squares RSS = $1.584\ 10^4$ m seca^2 is obtained, which estimates the residual variance as $\hat{\sigma}_\varepsilon^2$ = 0.204 m seca^2. A measure of the overall fit of the MISO model is the multiple correlation coefficient R, where R^2 = SSR/TSS = 0.9838, which gives the percentage explained sum of squares ESS = 100 R^2 = 98.4 %.

The determinant of the normal matrix was $6\ 10^{-15}$, together with a condition number 5923, given minimum and maximum eigenvalues λ_{min} = $6.04\ 10^{-4}$ and λ_{max} = 3.57. By dropping the two smallest eigenvalues the pseudo inverse method was also applied and the corresponding solutions h_{kj} and Δh_{kj} are summarized in Table 1. Then the (n-2) eigenvalues account for 99.98 % of the total sum of squares. It is interesting to note that the impulse response weights and their estimated standard errors, obtained with the least squares and pseudo inverse procedure, can be quite different,especially for the semi-diurnal band, but no significant differences between the transferfunctions are obtained by the two algorithms.

Table 2 shows the solutions h_{kj} and Δh_{kj} for the NS pendulum with the least squares method. The following statistical interpretation was obtained : TSS = $1.762\ 10^6$ mseca^2, SSR = $1.669\ 10^5$ mseca^2, RSS = $9.304\ 10^3$ mseca^2, $\hat{\sigma}_\varepsilon^2$ = 0.123 mseca^2, R^2 = 0.9472, ESS = 94.7 %. Dropping the two smallest eigenvalues still explains 99.98 % of the total sum of squares ;

e determinant of the normal matrix was $2\ 10^{-18}$ with a condition number 5941.

For the EW pendulum the corresponding amplitude and phase response curves for the three tidal wave bands and the perturbation inputs are represented in Fig. 1 along with the 98 % confidence limits. It is remarked that the standard errors in both amplitude and phase are smallest at the frequencies of the major harmonic constituents in each frequency band. Because the transferfunctions derived from the impulse response weights take the form of the familiar ratios γ of the observed to the theoretical amplitudes and the differences κ between the observed and theoretical phases of the tidal waves, the comparison between the γ- and κ- factors, obtained from Venedikov's harmonic analysis and the MISO model, is summarized in Table 3 (De Meyer, 1980). A similar comparison for the NS pendulum is compiled in Table 4 and the transferfunctions are shown in Fig. 4.

Apart from a long-period perturbation barometric pressure produces a tilt effect of 0.08 mseca/mbar in the semi-diurnal band of the EW-component and 0.09 mseca/mbar in the NS-component. We also observe an influence of 0.03 mseca/degree centigrade (EW) and 0.04 mseca/degree centigrade (NS) in the diurnal band, due to atmospheric temperature variations. Expressing the level of the river in cm, the nearby Viroin introduces an effect of 0.1 mseca/cm in the SD-band of both components, while it does not seem to perturb the D-band.

Figures 2 and 5 show examples of the observed residual series for the two instruments concerned. Figures 3.a and 6.a represent the residual periodograms in the frequency interval $0 \leq f \leq 0.18$ cph, while Figures 3.b and 6.b illustrate the residual power spectrum estimates in the frequency interval $0 \leq f \leq 0.03$ cph. A coloured noise spectrum with important contributions at the low frequencies and increased noise levels in the main tidal bands are observed. An incomplete description of the data by a linear model arises when Earth tide measurements from areas affected by shallow loading are analyzed, thus introducing nonlinear waves which disturb the astronomical components. The fact that these shallow water waves actually disturb the records at the station Dourbes (140 km from the North Sea) is clearly demonstrated by the residual periodograms. For the identification of the shallow water constituents the terminology of Rossiter and Lennon (1968) is used.

The diurnal group of tidal lines appears to be adequately represented by the MISO model. The diurnal band is characterized by a small increase in the background noise, probably of meteorological origin. Important residual power is observed in Figures 3.a and 6.a in the semi-diurnal band and a number of lines surrounding M_2 is indicated. In the ter-diurnal band the background noise is fairly low, but in the quarterdiurnal band the waves MN_4, M_4 and MS_4 can be identified, especially for the EW instrument. Much of the variance of the noise process therefore goes into these nonlinear disturbances. The residual spectrum smoothly fills the space between the tidal bands and rises sharply towards zero frequency, reflecting a similar pattern in meteorological spectra. In the low-frequency range lines at the annual and semi-annual periods are noted. The residual record is consequently associated with shallow water loading and irregular oscillations due to meteorological phenomena.

7. CONCLUSIONS.

The harmonic analysis of Earth tide observations gives a pointwise response function with undefined estimates between. Since the weaker lines are hopelessly contaminated by the noise, this accounts for the inconsistencies from different instruments and time intervals. The input-output approach alternatively leads to a more systematic procedure and gives a good description with a relatively small number of impulse response coefficients. An advantage of the MISO model is that several inputs can be included a priori in the analysis and that one can increase the number of subsystems for other influencing phenomena. Although it is not claimed that the proposed method improves the geophysical information given by the harmonic method, it is clear that this algorithm gives an equivalent precision with a lesser number of tidal constants and that the relative advantage of the MISO model over the harmonic procedure increases with the complexity of the spectral inputs.

It is important to note that no filtering of the data is needed, that no elimination of the drift is necessary and that only direct computations and measurements of the input channels are used. The resolution of very close waves does not arise explicitily although this method underestimates the statistical reliability of the minor tidal constituents and smoothes ont the resonance amplification of nearly diurnal Earth tides.

ıe Fourier transform of the impulse response weights gives a filtered estimate of the transferfunctions. The results show a changing but relatively smooth transition of the frequency responses across the tidal species, but it is argued that the transferfunctions obtained contain potentially useful information on the importance of the input channels and especially of the ocean tide influence.

Table 1

Impulse response weights HP 28VM - Least squares estimation

J	k = 2		k = 3		k = 4	
	h_{2j}	Δh_{2j}	h_{3j}	Δh_{3j}	h_{4j}	Δh_{4j}
0	0.6281	0.040	0.8021	0.041	0.7847	0.398
1	0.0276	0.042	-0.0570	0.024	0.1432	0.222
2	-0.0664	0.060	-0.0225	0.077	-0.0471	0.398
3	0.0008	0.060	-0.0537	0.031		
4	0.0241	0.060	0.0327	0.077		
5	0.0330	0.042	-0.0529	0.024		
6	0.0259	0.040	0.0236	0.041		
j	k = 5		k = 6		k = 7	
	h_{5j}	Δh_{5j}	h_{6j}	Δh_{6j}	h_{7j}	Δh_{7j}
0	0.1214	0.025	-0.0068	0.019	-0.0130	0.082
1	0.0874	0.026	0.0136	0.019	-0.0678	0.107
2	0.0389	0.026	0.0160	0.019	-0.0407	0.107
3	0.0059	0.026	0.0063	0.019	-0.0192	0.107
4	-0.0146	0.025	-0.0039	0.019	-0.0865	0.081

Impulse response weights HP 28VM - Pseudoinverse estimation

j	k = 2		k = 3		k = 4	
	h_{2j}	Δh_{2j}	h_{3j}	Δh_{3j}	h_{4j}	Δh_{4j}
0	0.6078	0.035	0.7099	0.008	0.7845	0.398
1	-0.0054	0.029	-0.0105	0.013	0.1433	0.222
2	-0.1255	0.026	-0.1979	0.008	-0.0473	0.398
3	-0.0514	0.030	0.0001	0.020		
4	-0.0349	0.026	-0.1427	0.008		
5	0.0000	0.029	-0.0063	0.013		
6	0.0058	0.035	-0.0069	0.008		

Table 2

Impulse response weights HP 7 VM - Least squares estimation

j	k = 1		k = 2		k = 3		k = 4	
	h_{1j}	Δh_{1j}	h_{2j}	Δh_{2j}	h_{3j}	Δh_{3j}	h_{4j}	Δh_{4j}
0	0.7506	0.607	0.5420	0.074	0.9124	0.046	0.7737	0.225
1	0.0747	0.349	0.4984	0.078	0.3882	0.027	-0.0545	0.125
2	0.0627	0.625	-0.2523	0.114	-0.1581	0.086	-0.0457	0.225
3	-0.0599	0.465	0.3864	0.107	0.2951	0.035		
4	-0.0154	0.623	-0.1983	0.114	-0.3547	0.087		
5	0.2167	0.350	0.0409	0.079	0.0890	0.027		
6	0.1188	0.603	-0.0604	0.075	-0.1610	0.046		

j	k = 5		k = 6		k = 7	
	h_{5j}	Δh_{5j}	h_{6j}	Δh_{6j}	h_{7j}	Δh_{7j}
0	-0.1190	0.011	-0.0150	0.008	0.0099	0.035
1	-0.0390	0.011	-0.0108	0.008	-0.0401	0.046
2	0.0178	0.011	-0.0100	0.008	-0.0176	0.046
3	0.0323	0.011	0.0174	0.008	-0.0521	0.045
4	0.0207	0.011	0.0021	0.008	-0.0834	0.034

Table 3

Comparison harmonic and MISO analysis HP 28 VM

(least squares)

Tidal wave	Venedikov method				MISO model			
	γ	$\Delta\gamma$	κ	$\Delta\kappa$	γ	$\Delta\gamma$	κ	$\Delta\kappa$
SIGMQ1	0.6605	0.3657	-83.13	31.72	0.5490	0.0176	-1.13	1.86
2Q1	0.4814	0.1113	-6.27	13.25	0.5476	0.0141	2.17	1.55
SIGMA1	0.1829	0.0916	8.31	28.68	0.5475	0.0116	2.93	1.34
Q1	0.6033	0.0142	5.25	1.35	0.5840	0.0070	8.02	0.63
RHO1	0.5058	0.0742	7.91	8.41	0.5949	0.0066	8.31	0.59
O1	0.6510	0.0027	6.59	0.23	0.6492	0.0018	6.58	0.16
TAU1	0.8295	0.2034	-37.70	14.05	0.6472	0.0021	6.13	0.18
NO1	0.6630	0.0309	4.58	2.67	0.6764	0.0051	5.41	0.42
KI1	0.9605	0.1725	5.65	10.29	0.6846	0.0051	5.27	0.42
PI1	0.6305	0.0991	2.93	9.00	0.7299	0.002	1.98	0.16
P1	0.7097	0.0058	2.39	0.47	0.7334	0.0016	1.27	0.13
S1	2.1067	0.3561	25.61	9.61	0.7361	0.0013	0.51	0.10
K1	0.7450	0.0019	-0.27	0.14	0.7377	0.0012	-0.30	0.09
PSI1	0.5557	0.2410	-0.52	24.85	0.7382	0.0014	-1.45	0.11
PHI1	0.8902	0.1367	-11.35	8.80	0.7375	0.0018	-2.40	0.14
TETA1	0.5984	0.1744	17.85	16.70	0.6661	0.0084	-11.08	0.74
J1	0.6090	0.0334	1.26	3.14	0.6431	0.0101	-11.96	0.91
SO1	0.7666	0.2036	-19.07	15.22	0.5529	0.0129	-3.98	1.33
OO1	0.5360	0.0515	-10.75	5.51	0.5617	0.0133	-1.63	1.30
NU1	0.4862	0.2695	28.93	31.75	0.6712	0.0322	-6.41	2.73
3N2	0.8953	0.2099	19.89	13.44	0.6924	0.0138	4.93	1.33
EPS2	1.2911	0.0881	4.51	3.91	0.7013	0.0107	5.73	1.11
2N2	0.8431	0.0252	7.59	1.71	0.7787	0.0051	7.43	0.29
MU2	1.1990	0.0207	-5.65	0.99	0.7899	0.0052	7.14	0.31
N2	0.8256	0.0032	4.34	0.22	0.8220	0.0022	3.91	0.16
NU2	0.7782	0.0168	6.72	1.24	0.8207	0.0021	3.52	0.15
M2	0.8152	0.0006	3.40	0.04	0.8139	0.0005	3.61	0.03
LAMB2	1.0894	0.0800	46.98	4.21	0.8572	0.0019	2.75	0.11
L2	0.8930	0.0194	14.18	1.24	0.8626	0.0024	2.07	0.14
T2	0.8079	0.0215	4.13	1.52	0.8319	0.0013	-2.81	0.09
S2	0.8243	0.0013	-3.18	0.09	0.8230	0.0010	-3.08	0.07
K2	0.8158	0.0043	-2.87	0.30	0.8030	0.0019	-3.36	0.13
ETA2	0.7308	0.0731	-13.06	5.73	0.7333	0.0034	6.09	0.53
2K2	0.4024	0.2008	-49.93	28.59	0.8541	0.0301	8.11	1.47
M3	0.8760	0.0198	8.26	1.30	0.8653	0.0236	8.09	1.56

Table 4

Comparison harmonic and MISO analysis HP 7 VM
(least squares)

Tidal wave	Venedikov method				MISO model			
	γ	$\Delta\gamma$	κ	$\Delta\kappa$	γ	$\Delta\gamma$	κ	$\Delta\kappa$
SA					1.1369	0.6017	-5.12	29.37
SSA					1.1036	0.5815	-10.06	26.52
MSM					0.5868	0.1934	9.42	17.99
MM					0.7258	0.1732	15.61	13.89
MSF					0.8403	0.0689	-29.15	3.41
MF					0.6546	0.0418	-32.39	3.66
MSTM					0.7887	0.1483	11.16	11.28
MTM					0.8275	0.1410	6.27	9.72
MSQM					0.6902	0.4552	-1.94	38.71
MQM					0.6852	0.5058	-0.20	42.30
SIGMQ1	2.7733	1.4382	-54.14	29.72	0.9155	0.0651	-150.75	2.57
2Q1	0.5658	0.4300	57.62	43.53	0.9487	0.0610	131.85	1.37
SIGMA1	0.8596	0.3653	-69.50	24.34	0.9725	0.0579	121.17	1.45
Q1	1.0473	0.0562	58.59	3.07	1.0717	0.0309	66.02	1.44
RHO1	1.7356	0.2966	69.85	9.79	1.0683	0.0262	59.49	1.17
O1	0.9483	0.0106	29.43	0.64	0.9392	0.0063	28.74	0.38
TAU1	1.9518	0.8021	34.38	23.55	0.9073	0.0072	25.28	0.46
NO1	0.8770	0.1028	41.12	6.72	0.7292	0.0174	13.81	1.25
KI1	0.8776	0.6887	41.59	44.96	0.7028	0.0172	13.25	1.34
PI1	0.8266	0.3946	-2.72	27.35	0.6007	0.0065	17.38	0.71
P1	0.5095	0.0231	26.00	2.60	0.5955	0.0052	18.69	0.56
S1	16.0622	1.4193	71.42	5.02	0.5928	0.0044	20.13	0.44
K1	0.5957	0.0075	21.31	0.72	0.5929	0.0042	21.65	0.41
PSI1	0.9047	0.9603	15.44	60.82	0.5959	0.0047	23.20	0.48
PHI1	0.2085	0.5447	-4.03	149.65	0.6020	0.0057	24.73	0.62
TETA1	0.2655	0.6967	-14.01	150.33	0.7806	0.0300	30.73	2.09
J1	0.6138	0.1264	21.83	11.80	0.8246	0.0346	29.70	2.38
SO1	1.9378	0.8112	14.32	23.98	1.0086	0.0466	14.93	2.59
OO1	0.9327	0.2065	2.30	12.68	1.0142	0.0505	12.08	2.32
NU1	0.4877	1.0522	-21.43	123.64	0.9583	0.1097	0.56	6.54
3N2	1.0066	0.2282	-49.36	12.99	1.1966	0.0268	7.36	1.61
EPS2	1.2187	0.0954	7.41	4.48	1.2558	0.0212	6.56	1.27
2N2	0.6324	0.0272	-26.58	2.47	1.4383	0.0076	-9.61	0.43
MU2	1.2770	0.0244	1.53	1.01	1.4198	0.0080	-12.59	0.47
N2	0.5332	0.0035	-24.59	0.37	1.0919	0.0046	-24.37	0.24
NU2	0.3980	0.0182	-33.09	2.62	1.0362	0.0042	-24.18	0.23
M2	0.4439	0.0006	-14.65	0.08	0.8865	0.0009	-14.53	0.06
LAMB2	0.6220	0.0868	89.42	8.00	0.8959	0.0027	-10.11	0.29
L2	0.3492	0.0215	52.29	3.53	0.8967	0.0037	-9.22	0.35
T2	0.5059	0.0233	-12.33	2.64	1.0412	0.0026	-4.44	0.14
S2	0.5319	0.0014	-5.18	0.15	1.0699	0.0021	-4.76	0.11
K2	0.5368	0.0047	-6.40	0.50	1.1314	0.0038	-6.11	0.19
ETA2	0.5584	0.0789	-18.32	8.09	1.3816	0.0029	-36.09	0.58
2K2	0.1939	0.2181	-79.38	64.44	0.8614	0.0522	-99.12	2.30
M3	0.7925	0.0179	-5.97	1.29	0.9079	0.0241	-5.07	1.71

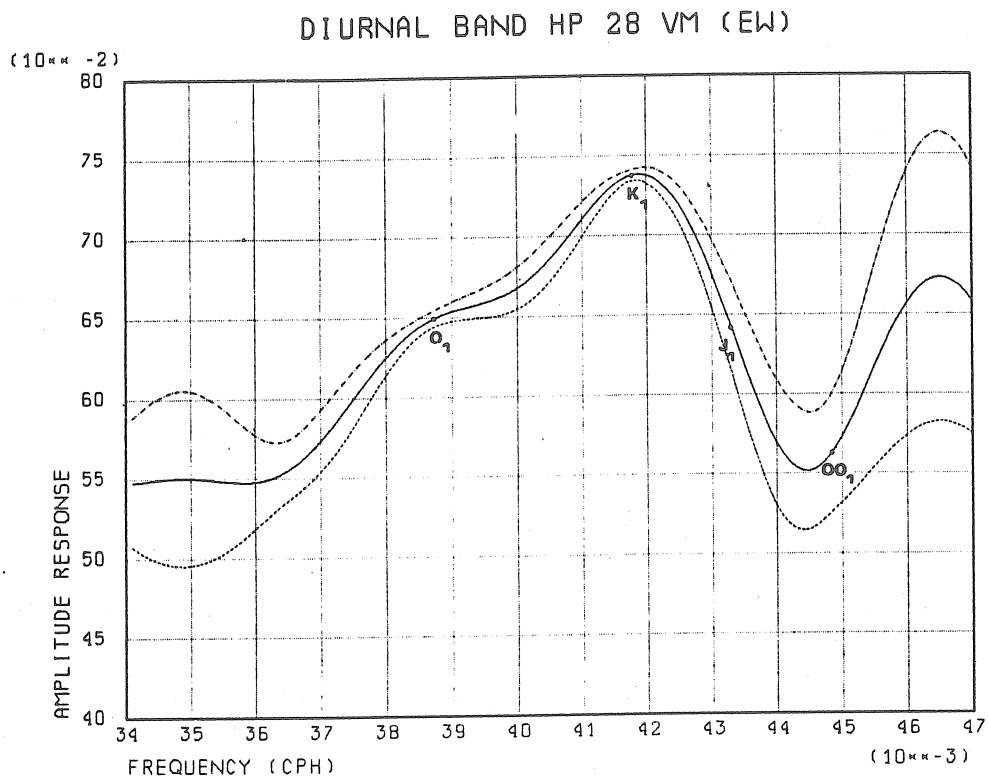

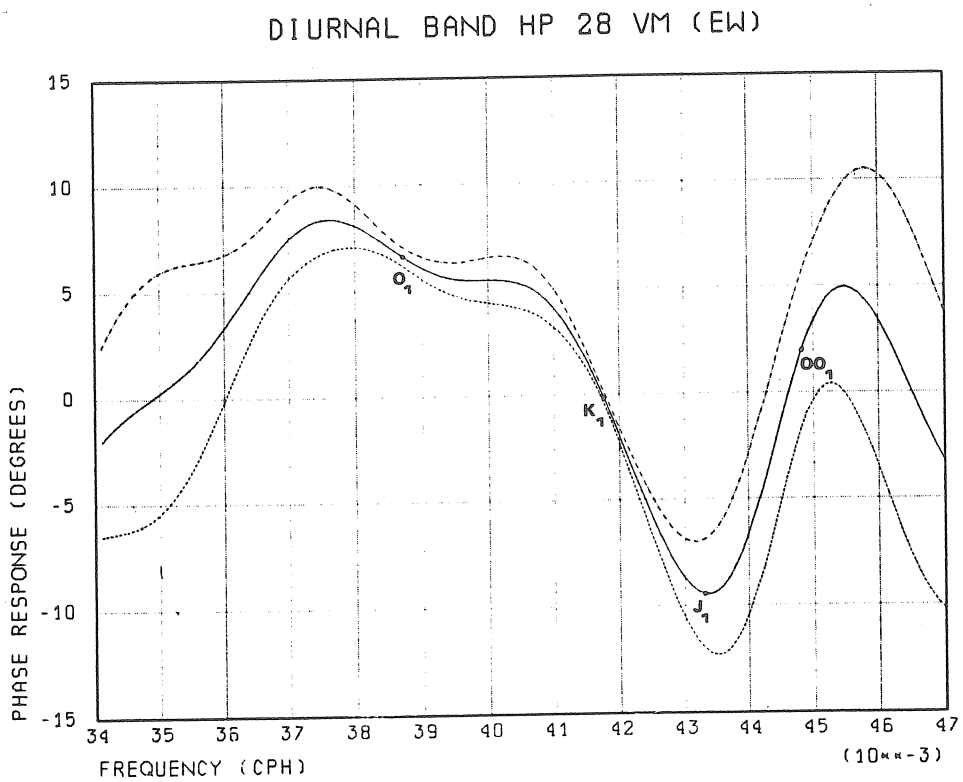

Fig. 1.a. Transferfunction in the diurnal frequency band corresponding to H_2 (f). Note the smoothing of the diurnal resonance effect.

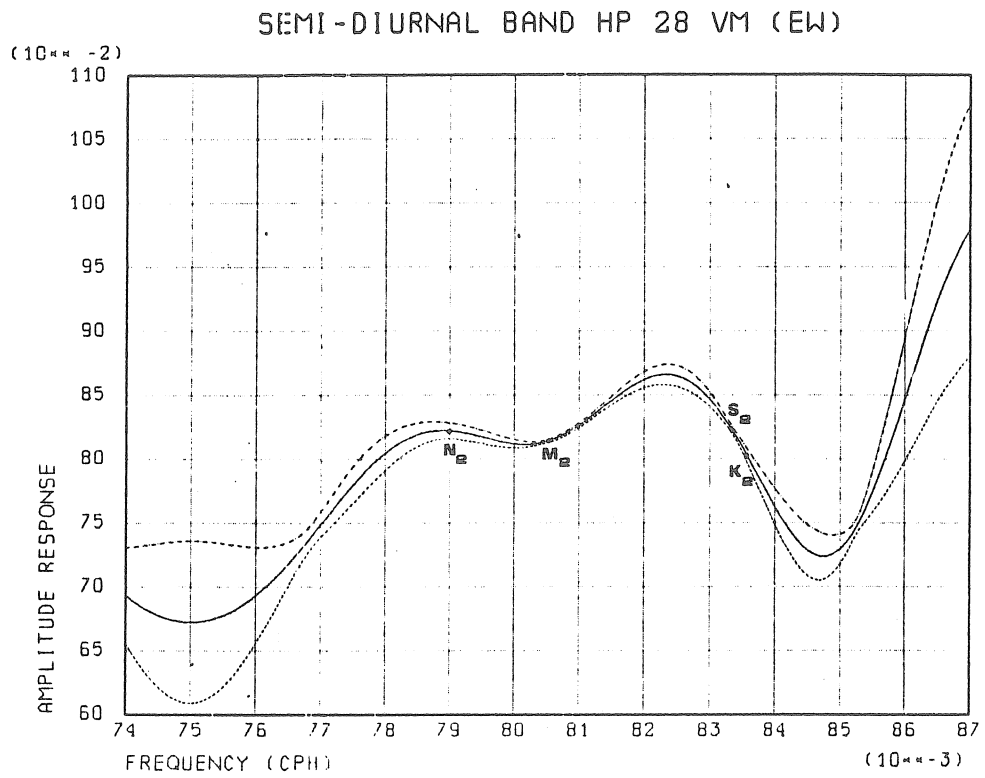

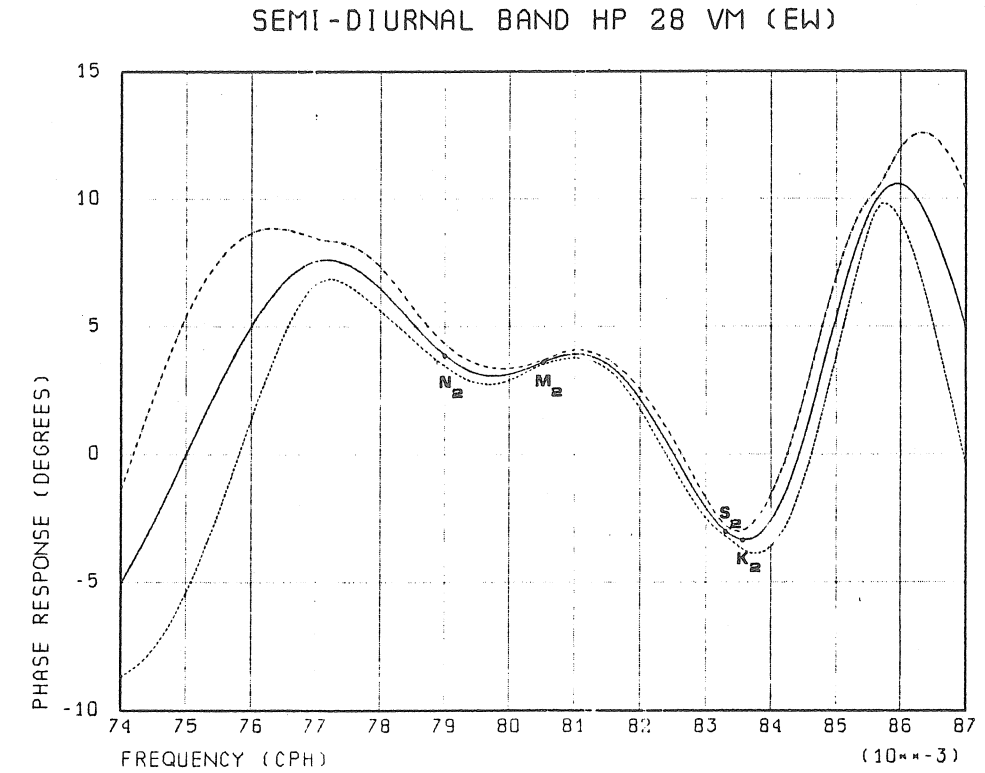

Fig. 1.b. Transferfunction in the semi-diurnal frequency band corresponding to H_3 (f).

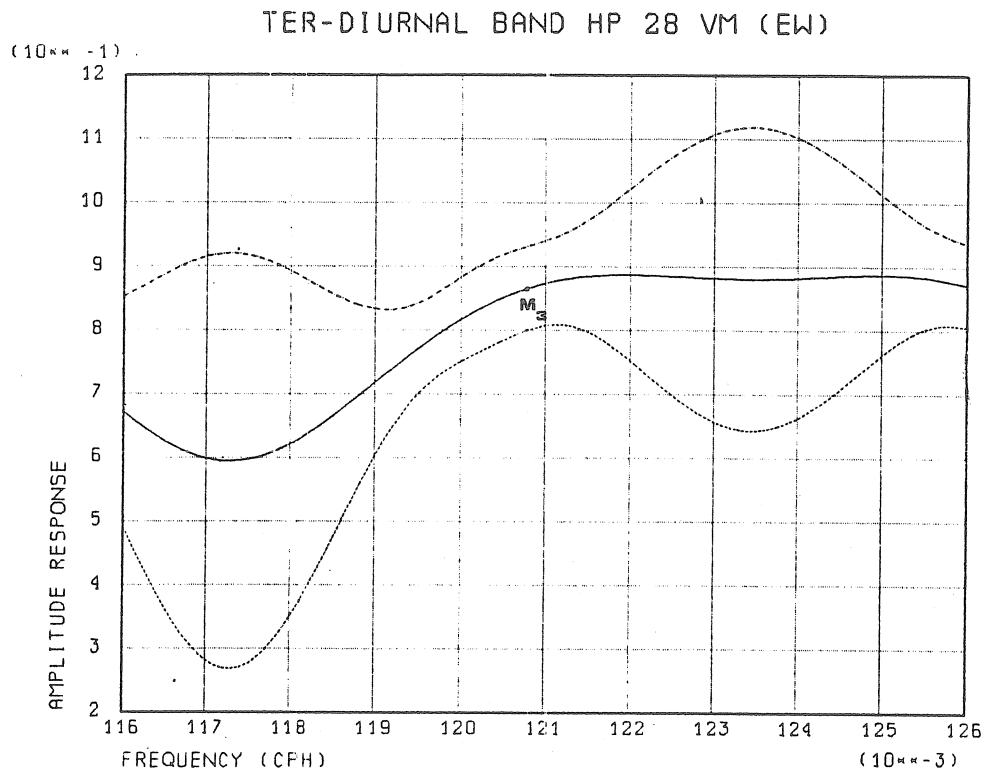

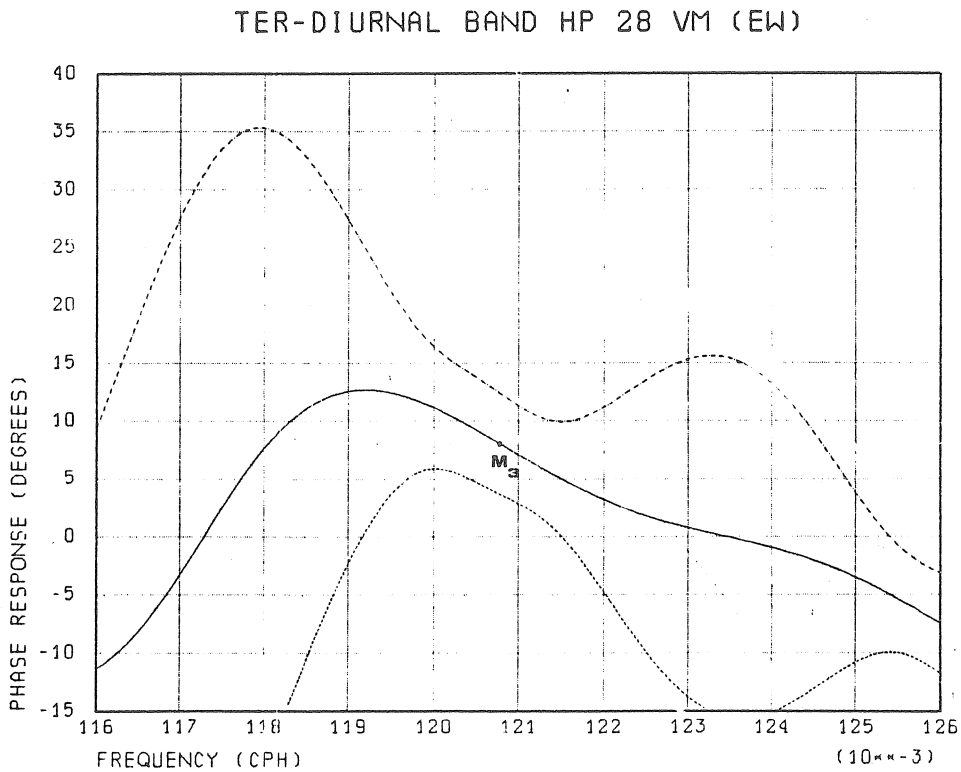

Fig. 1.c. Transferfunction in the ter-diurnal frequency band corresponding to H_4 (f).

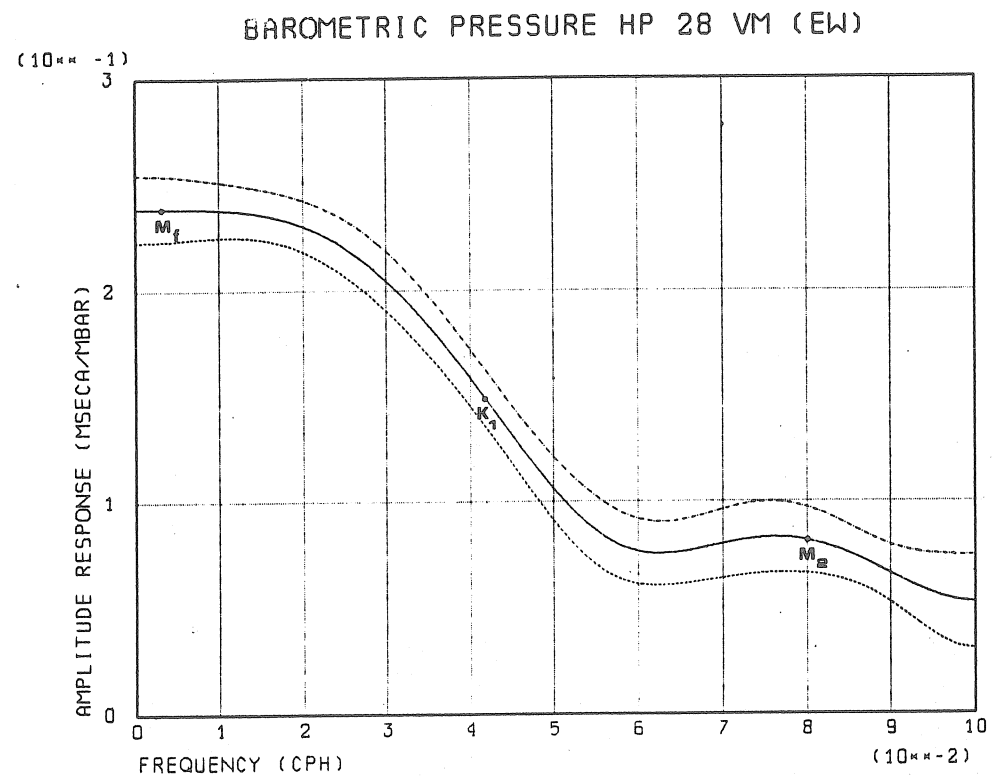

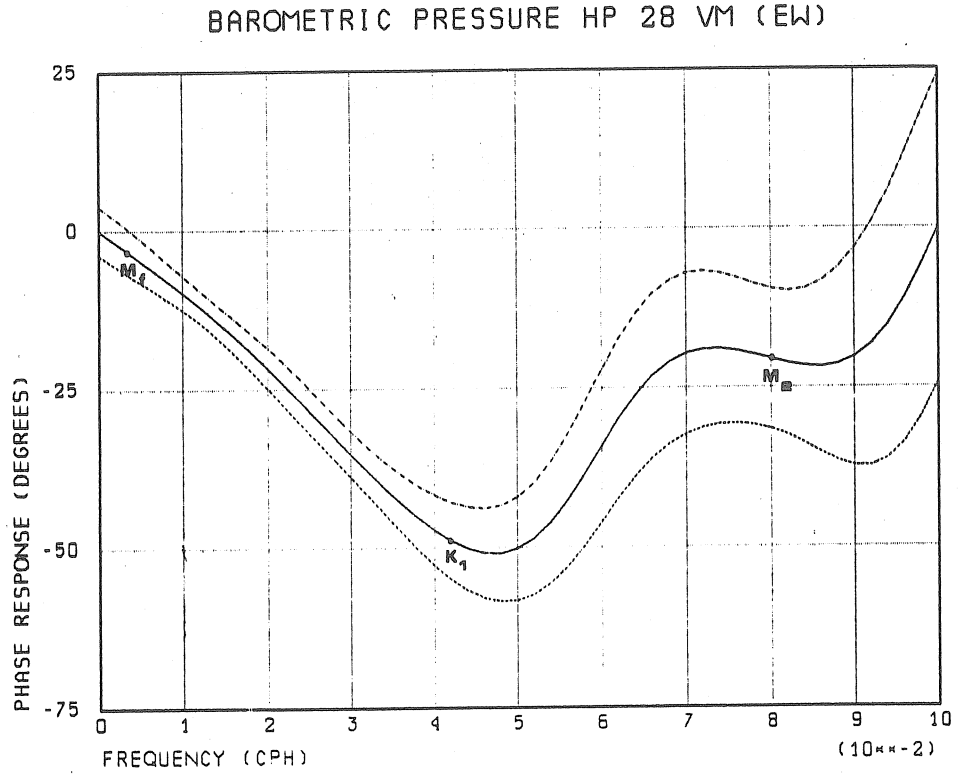

Fig. 1.d. Transferfunction of the barometric pressure corresponding to $H_5(f)$.

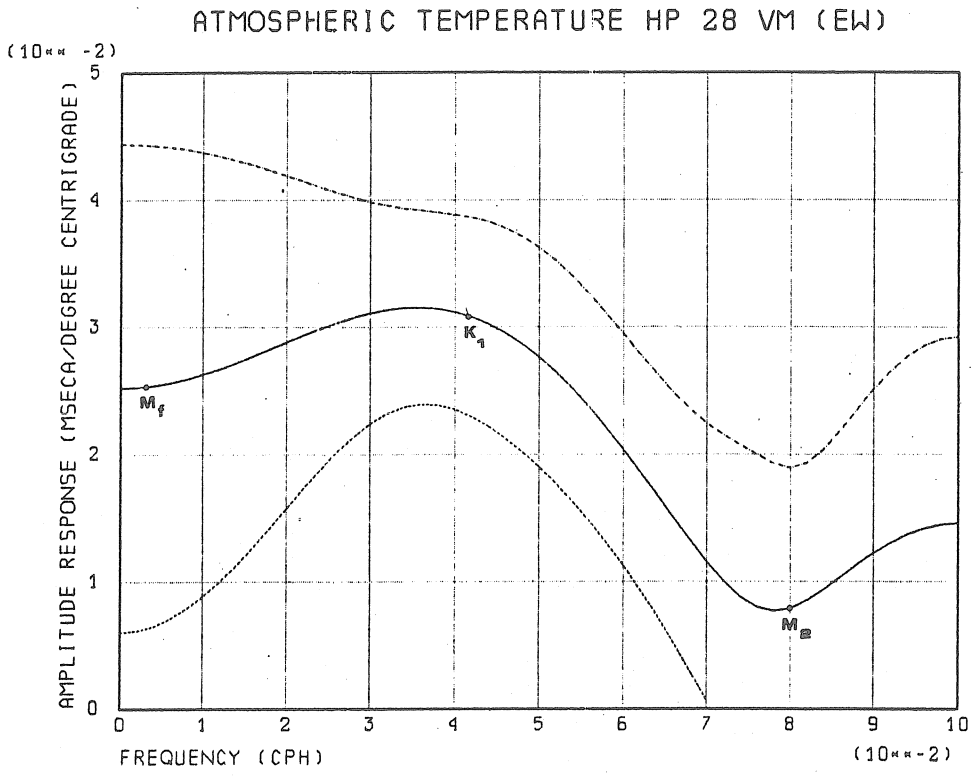

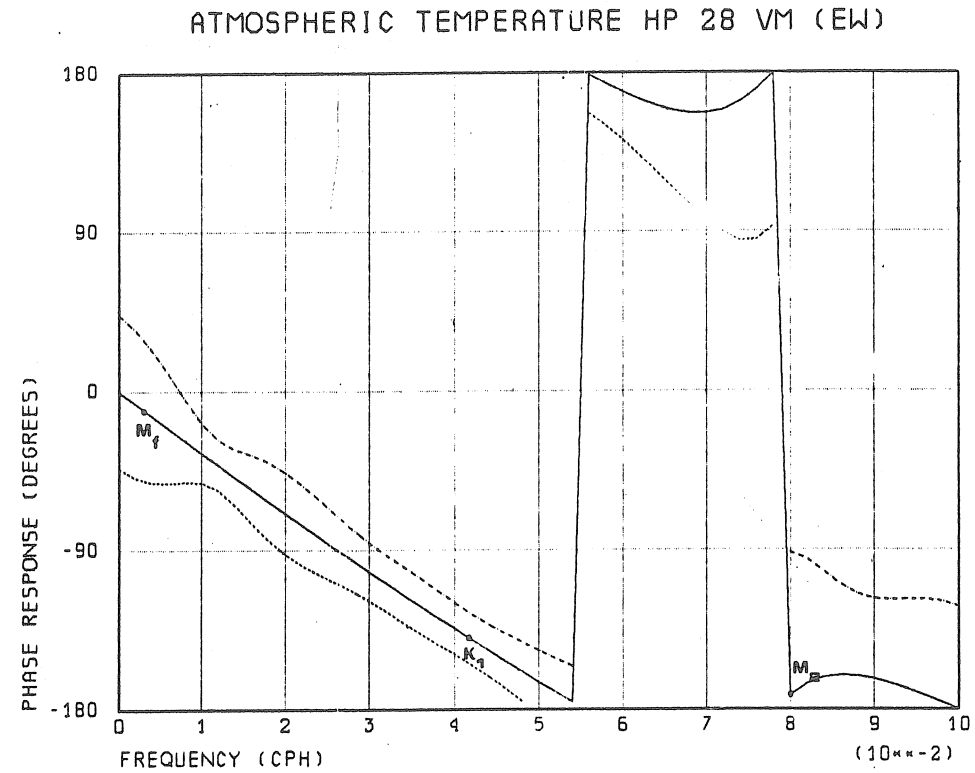

Fig. 1.e. Transferfunction of the atmospheric temperature corresponding to H_6 (f).

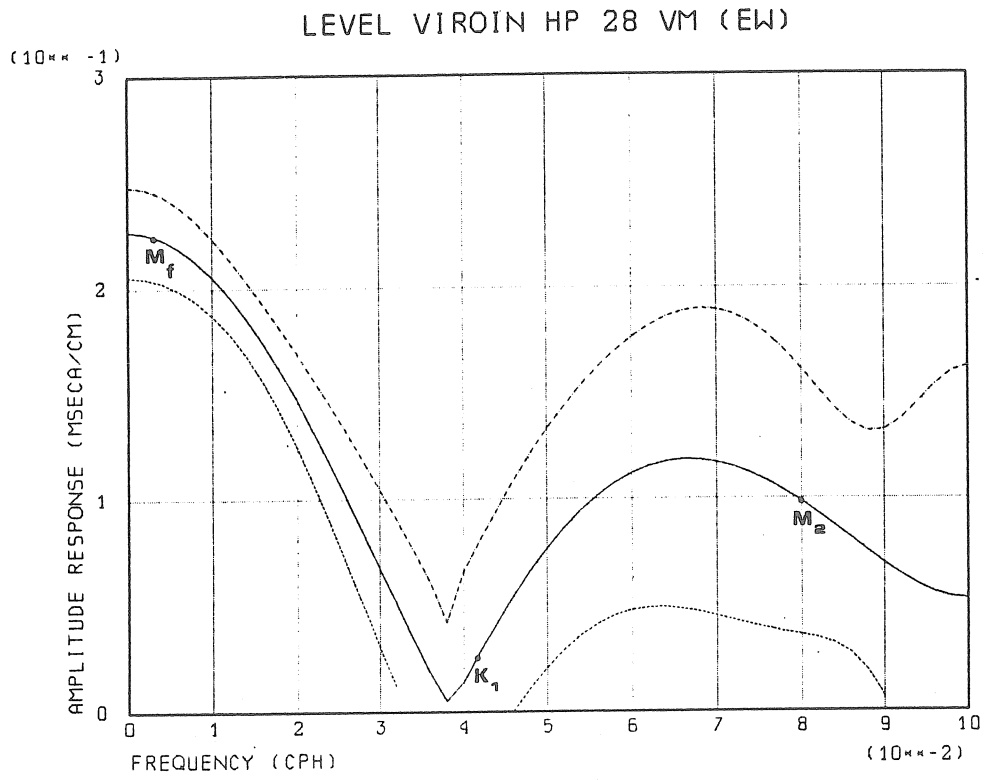

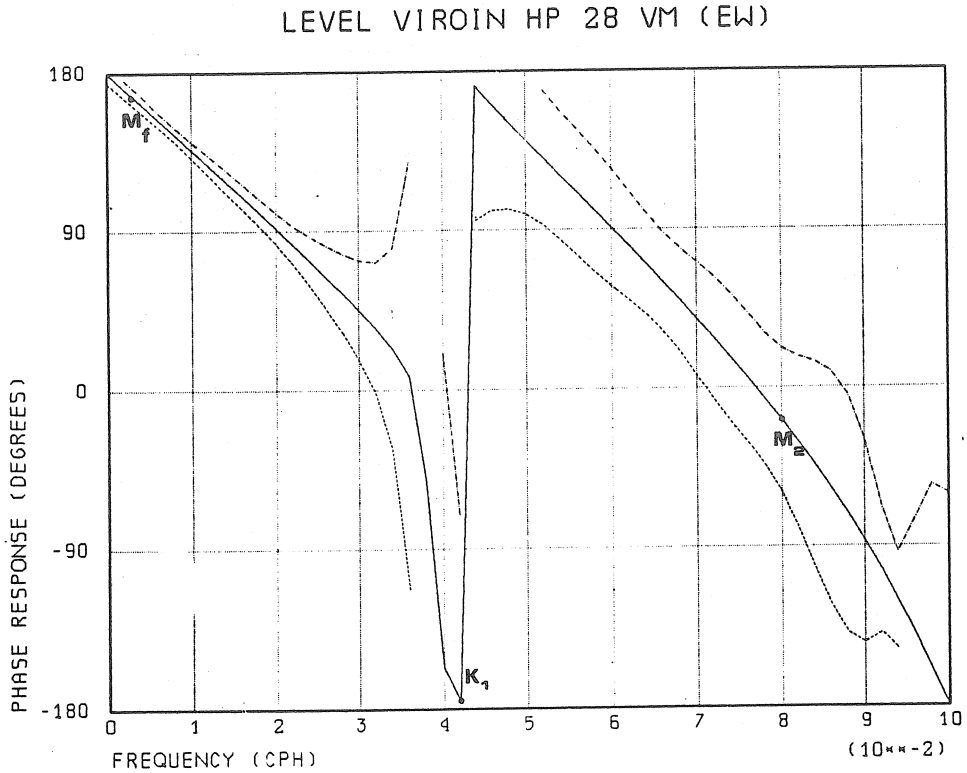

Fig. 1.f. Transferfunction of the Viroin level corresponding to H_7 (f).

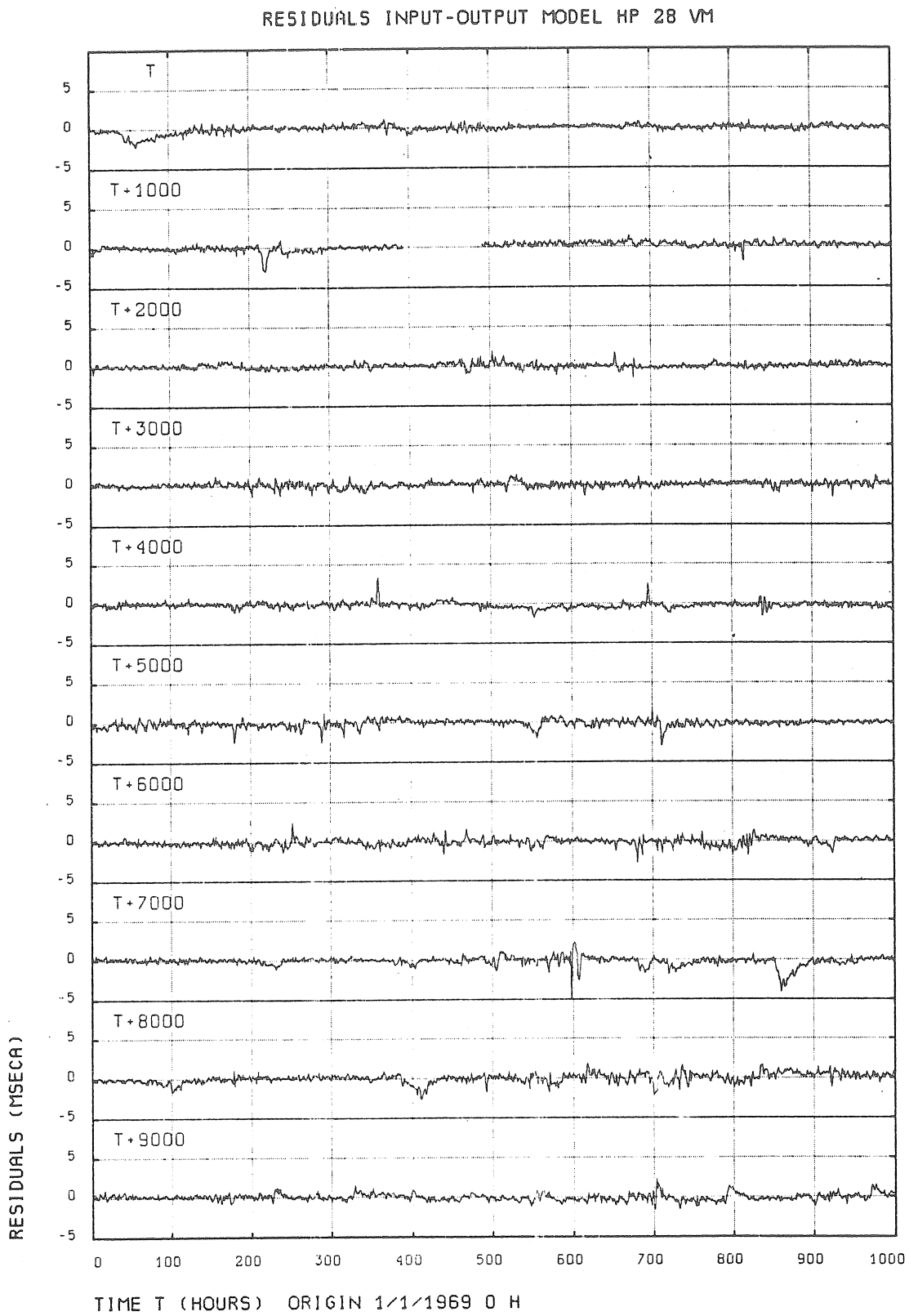

Fig. 2. Observed residuals of the MISO model.

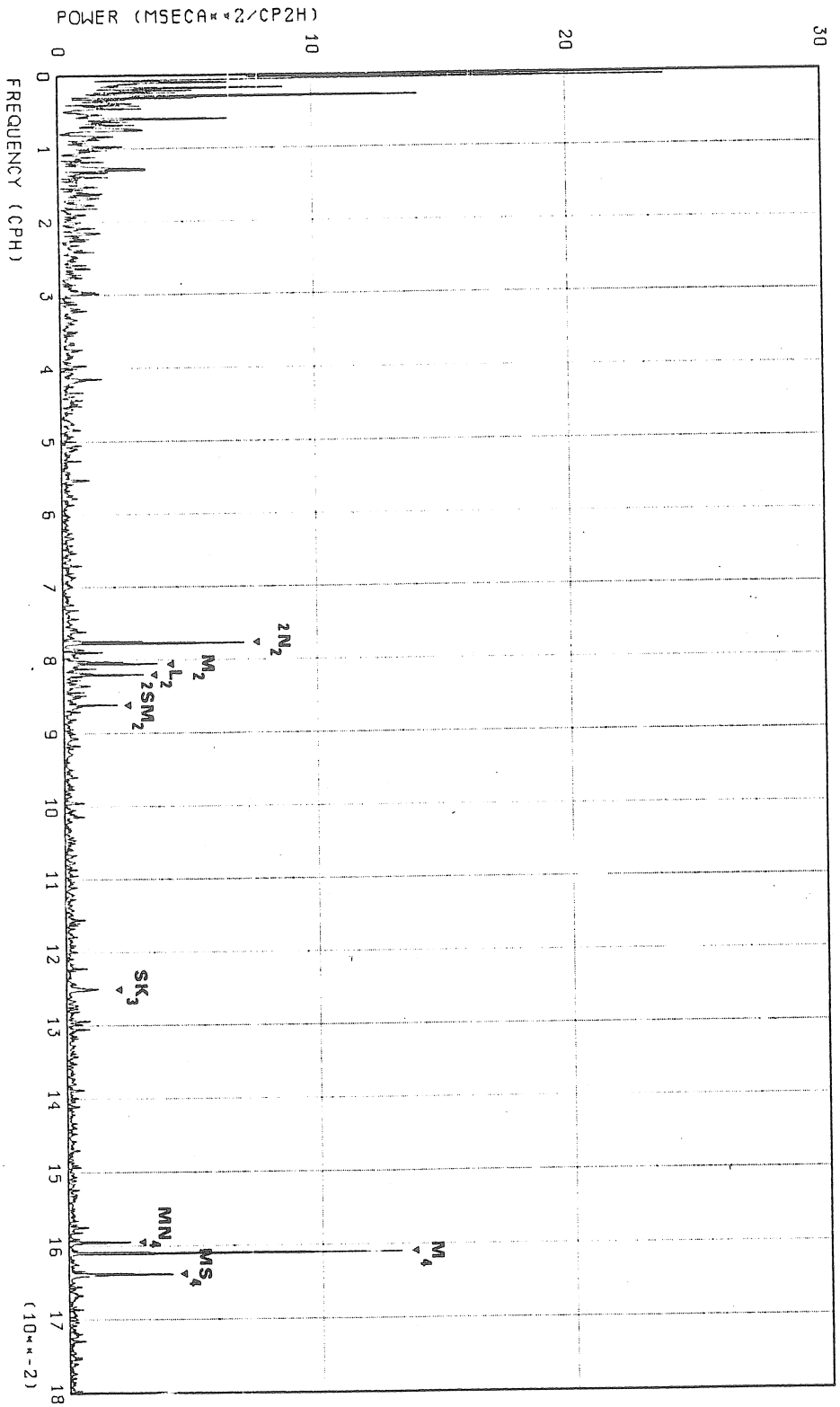

Fig.3.a. Residual power spectrum in the frequency interval $0 \leq f \leq 0.18$ cph.

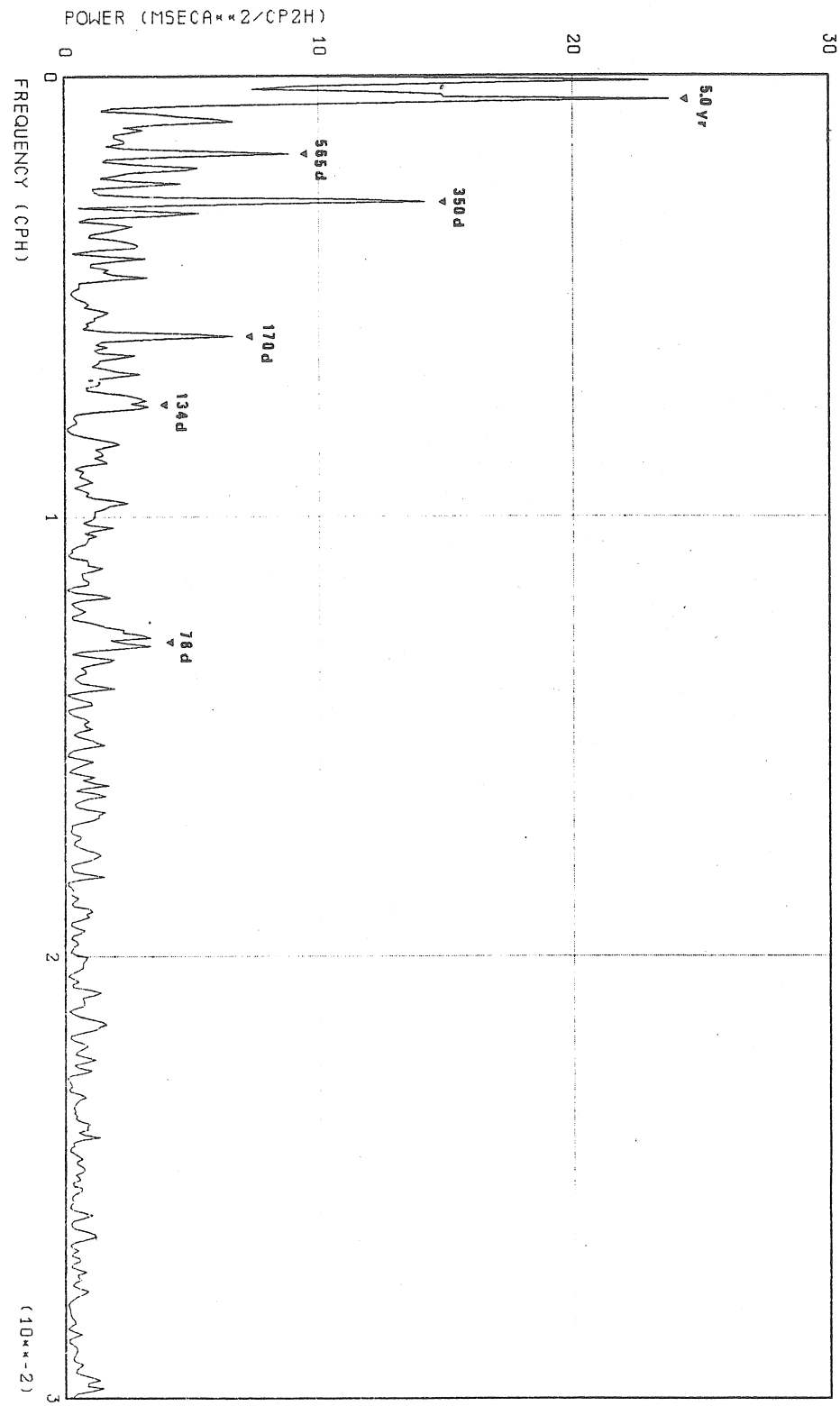

Fig. 3.b. Residual power spectrum in the frequency interval $0 \lesssim f \lesssim 0.03$ cph.

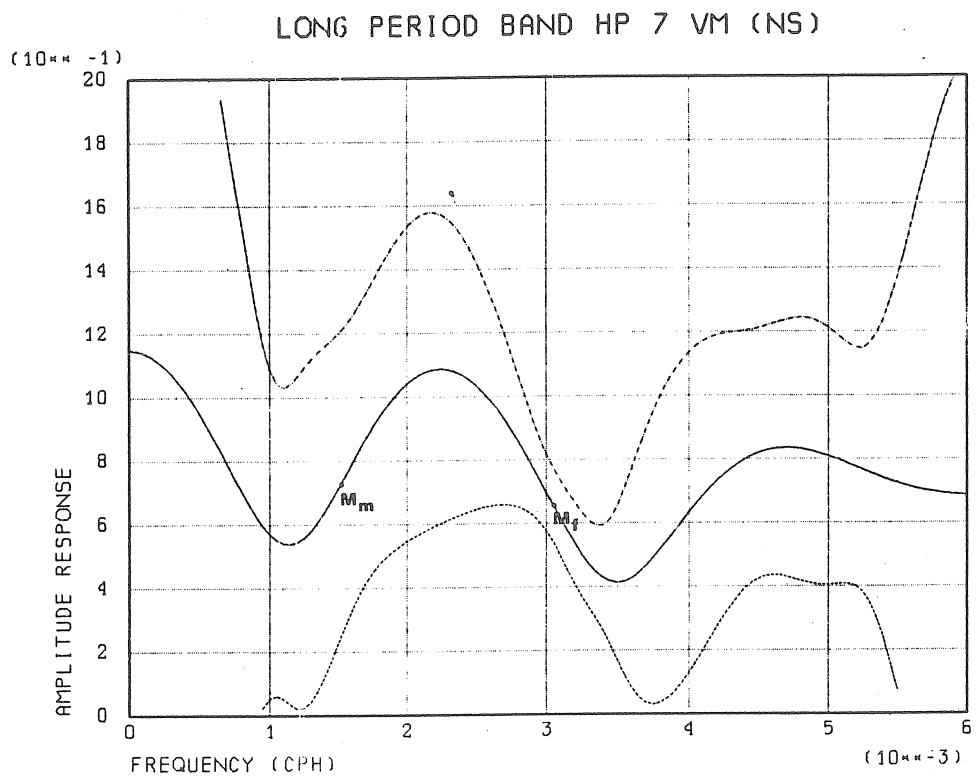

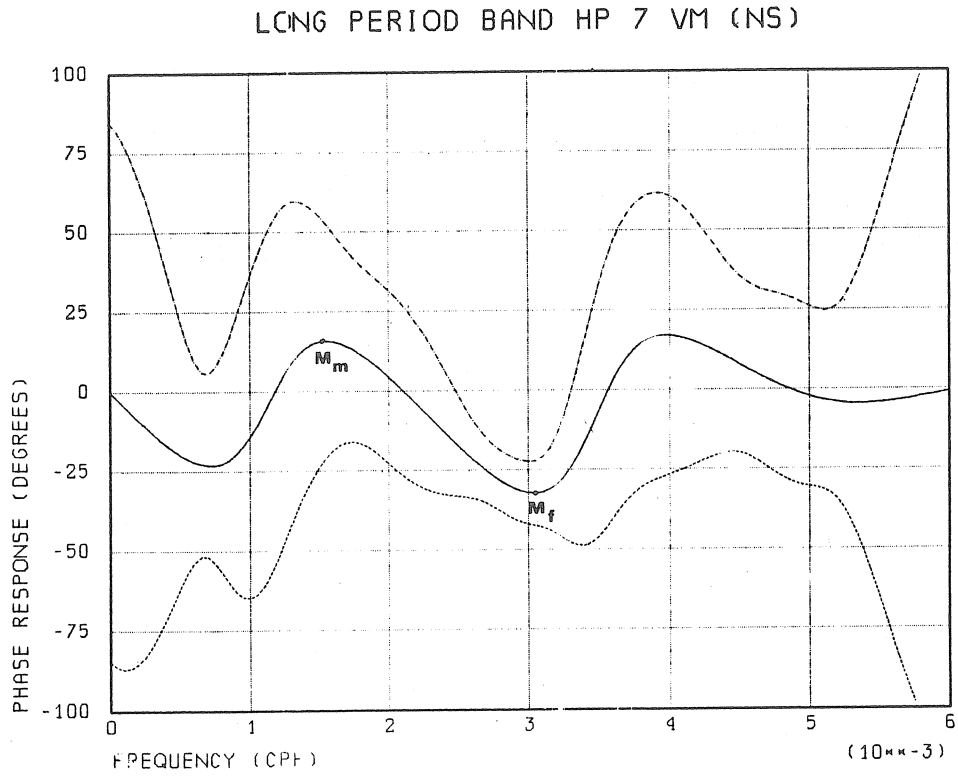

Fig. 4.a. Transferfunction in the low frequency band $0 \leq f \leq 0.006$ cph corresponding to $H_1(f)$.

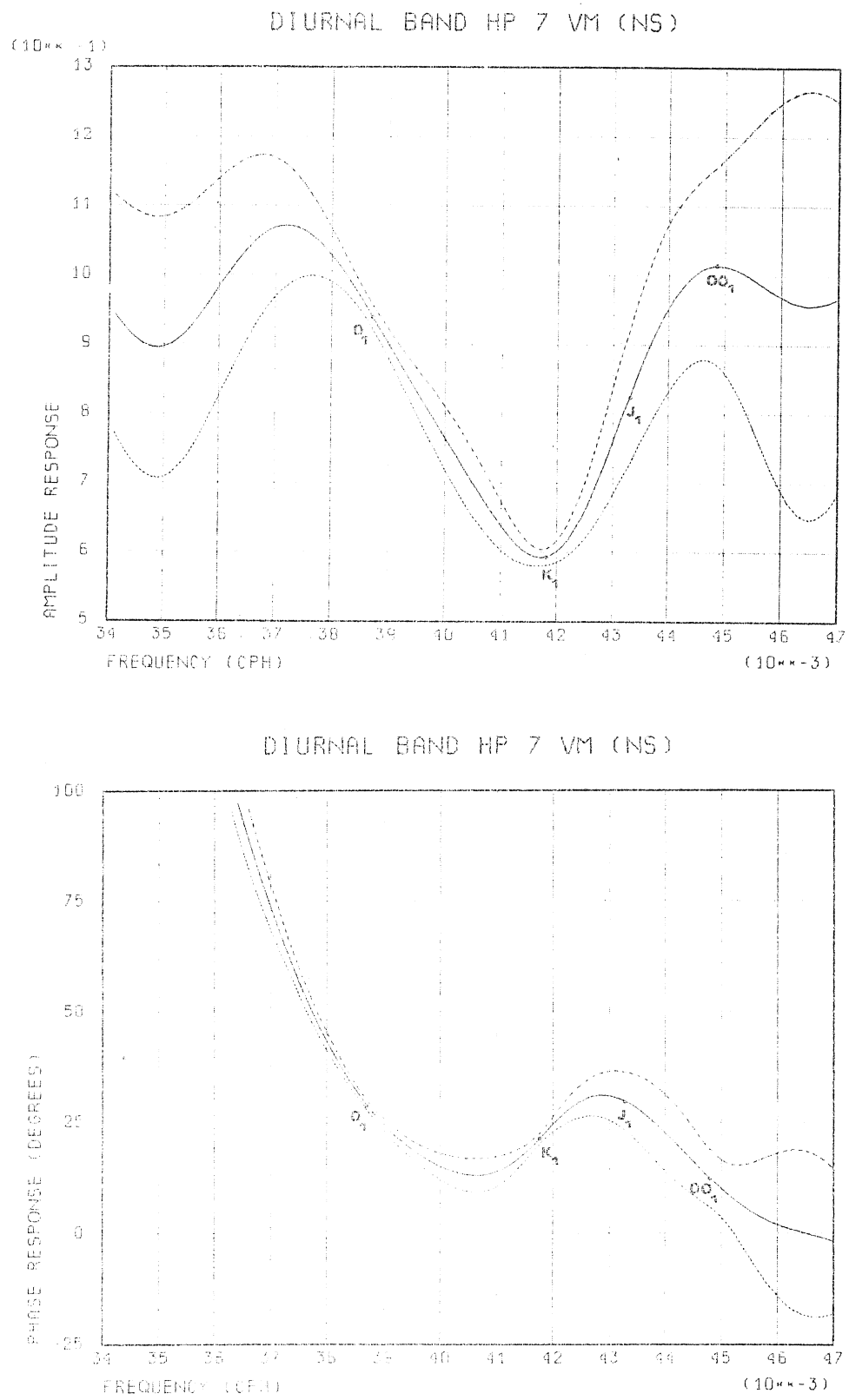

Fig. 4.b. Transfer function in the diurnal frequency band corresponding to $H_z(f)$.

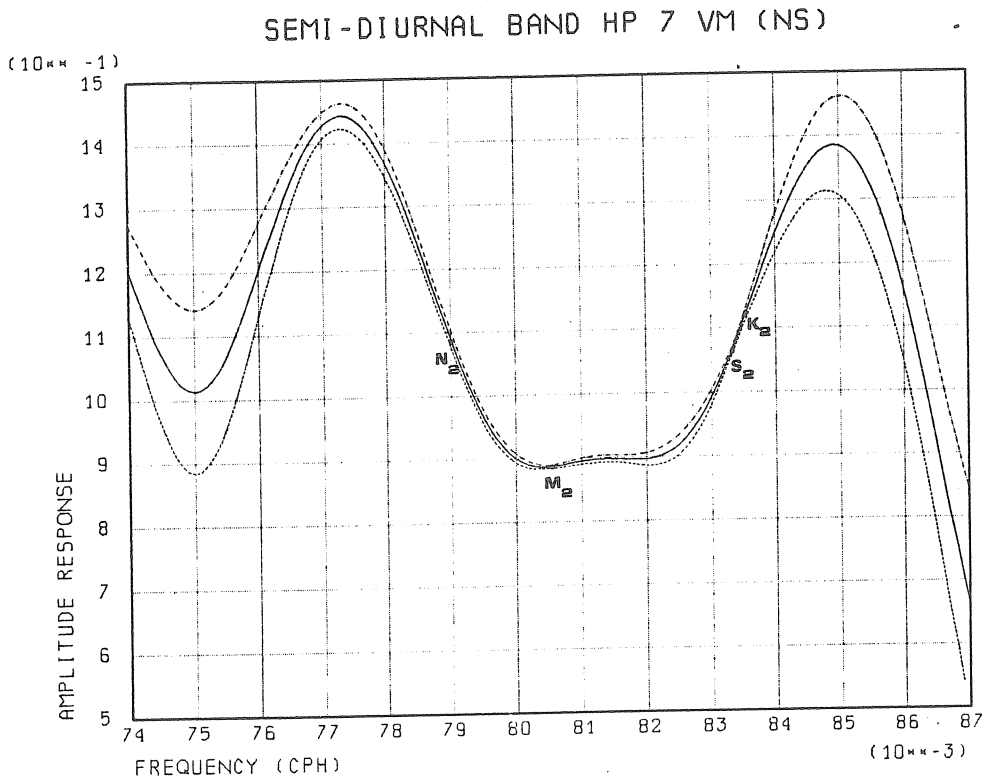

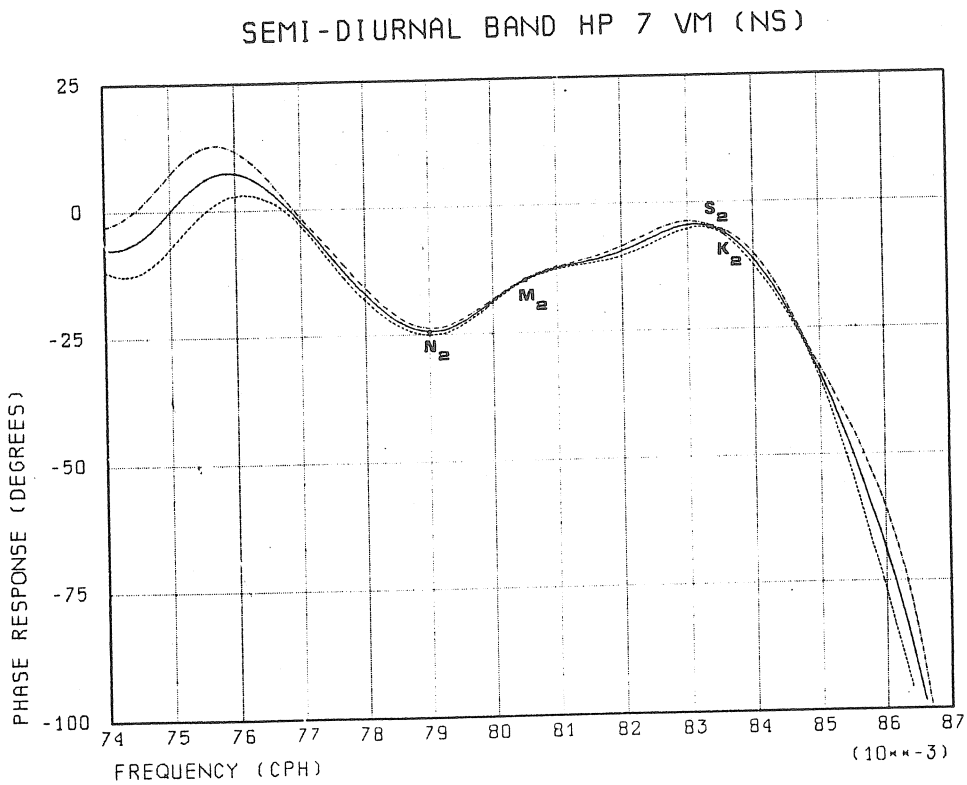

Fig. 4.c. Transferfunction in the semi-diurnal frequency band corresponding to $H_3(f)$.

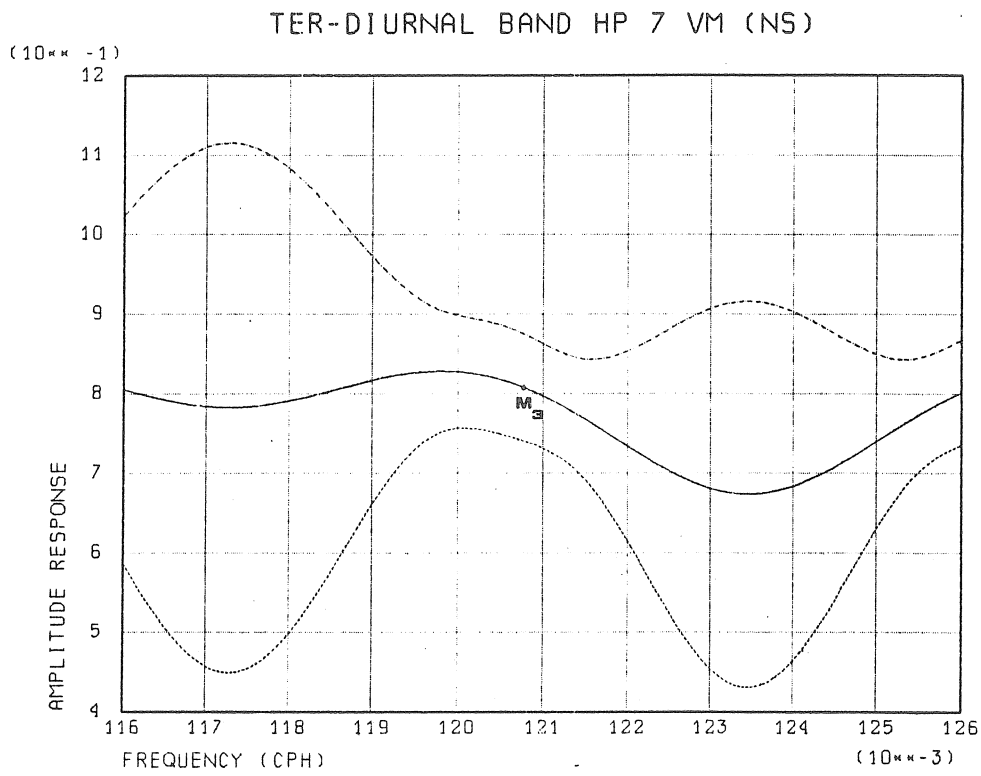

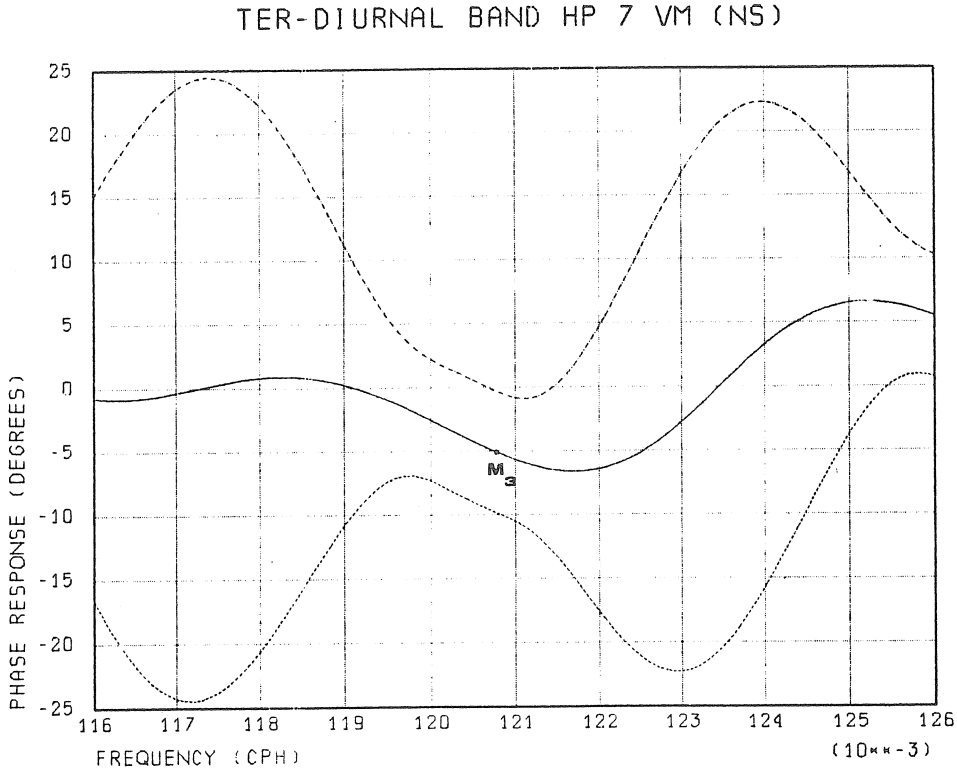

Fig. 4.d. Transferfunction in the ter-diurnal frequency band corresponding to $H_4(f)$.

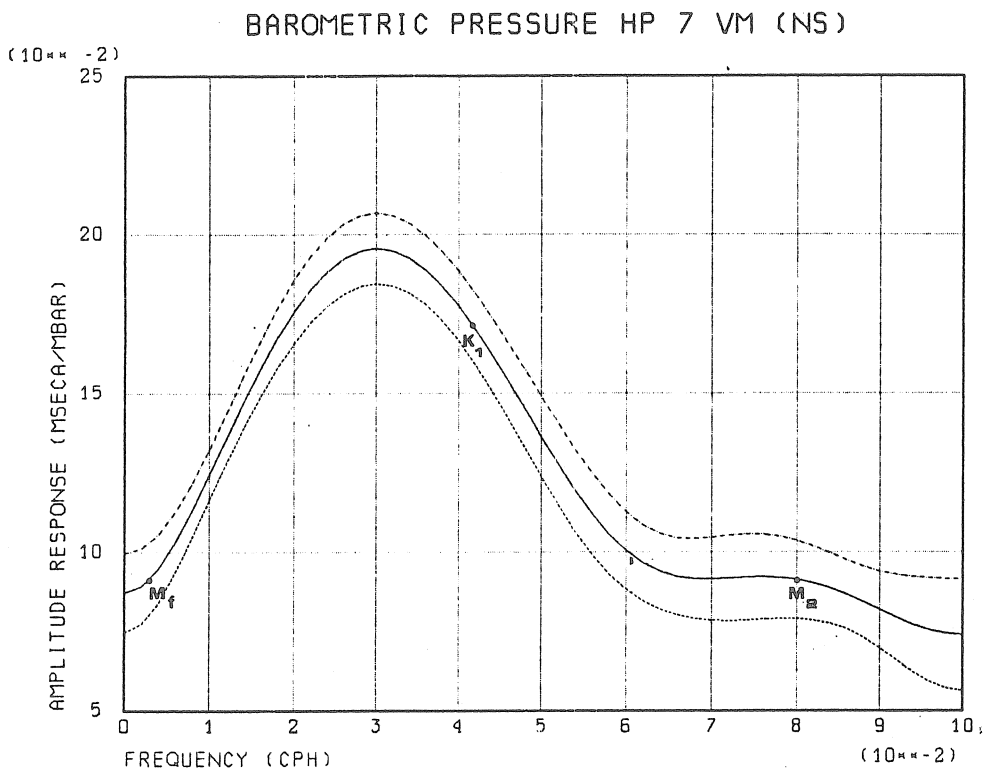

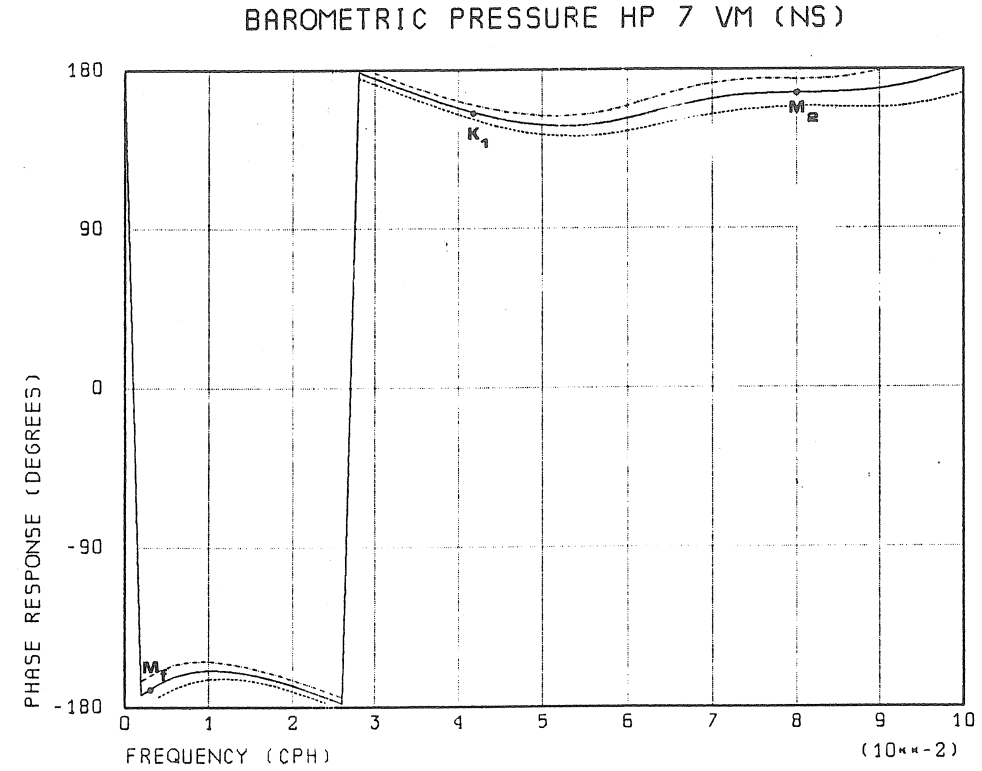

Fig. 4,e. Transferfunction of the barometric pressure corresponding to $H_5(f)$.

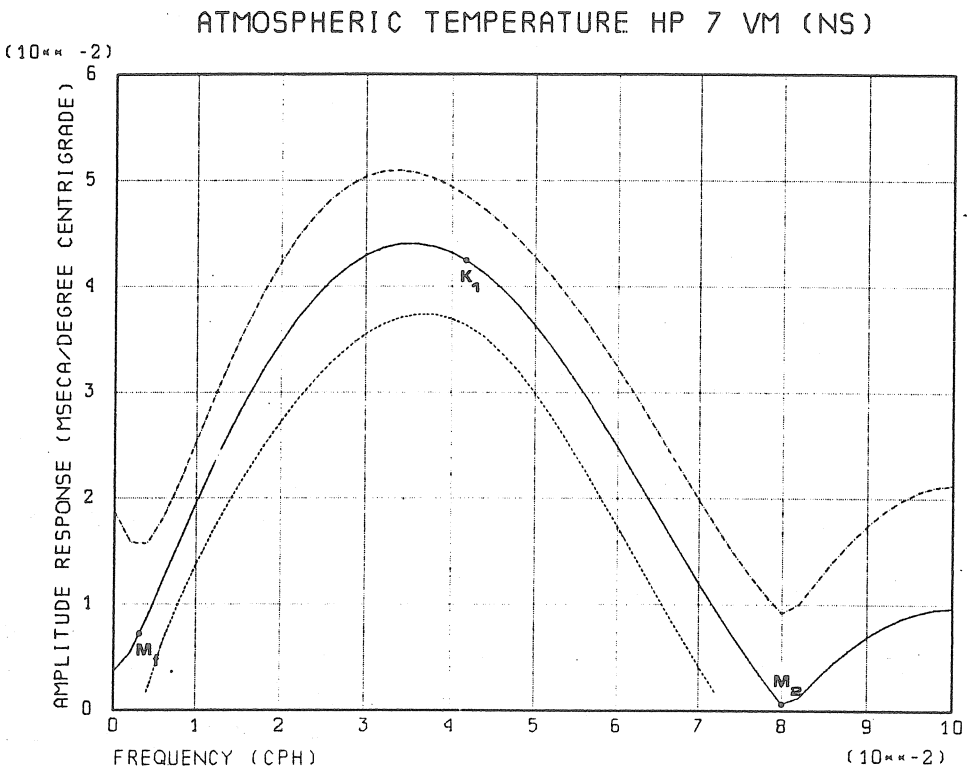

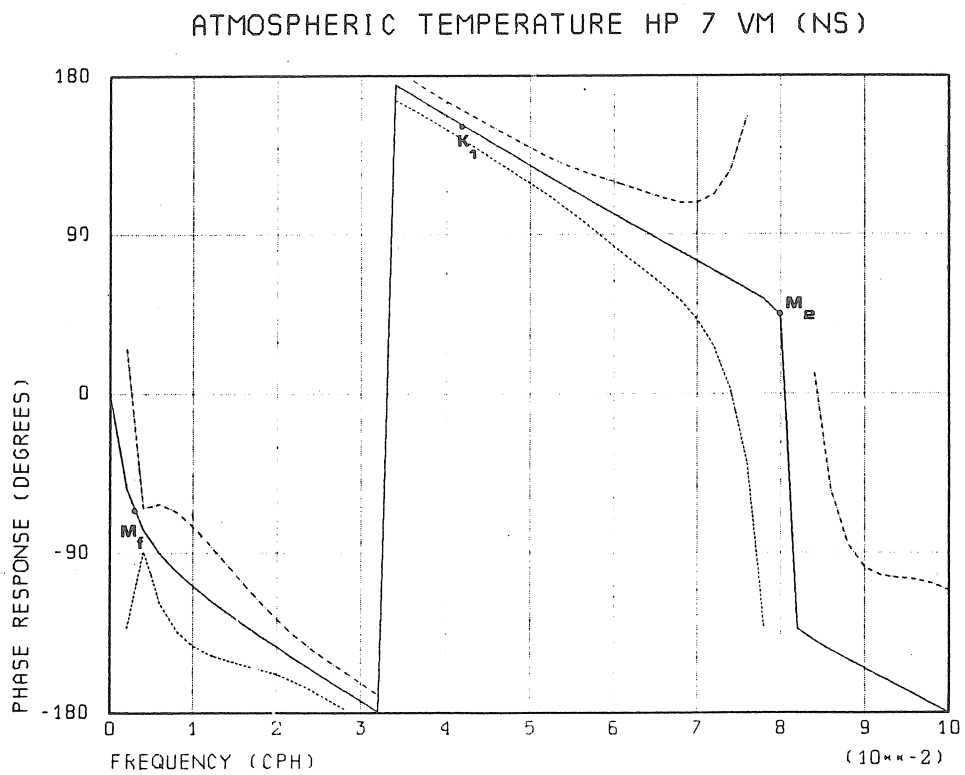

Fig. 4. f. Transferfunction of the atmospheric temperature corresponding to $H_n(r)$.

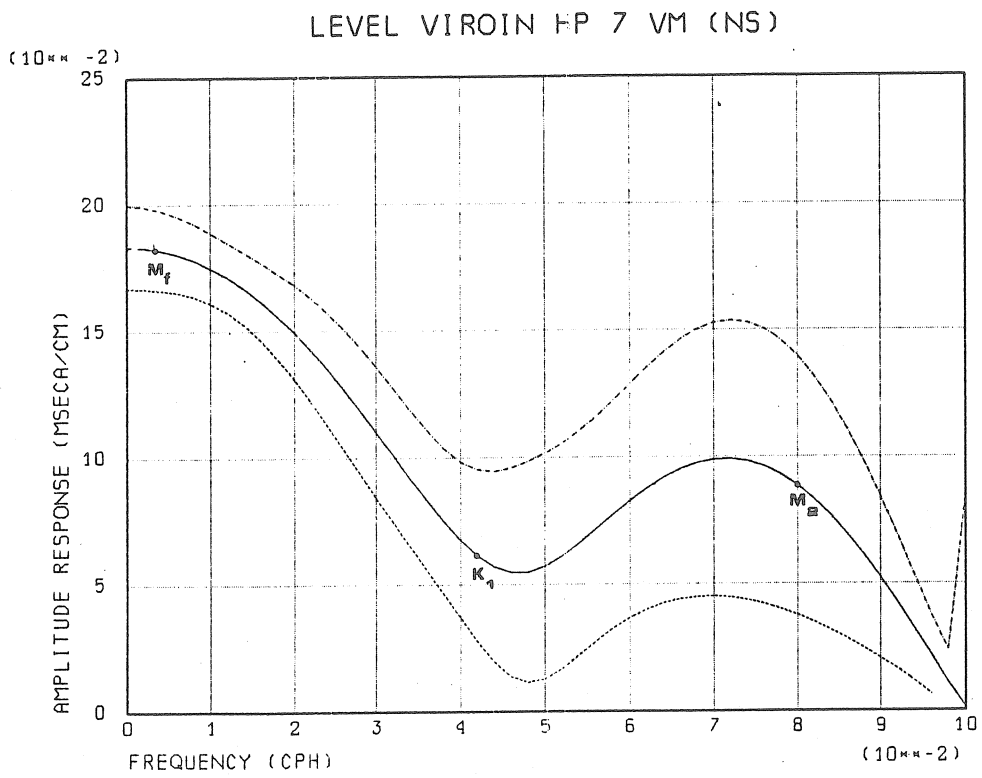

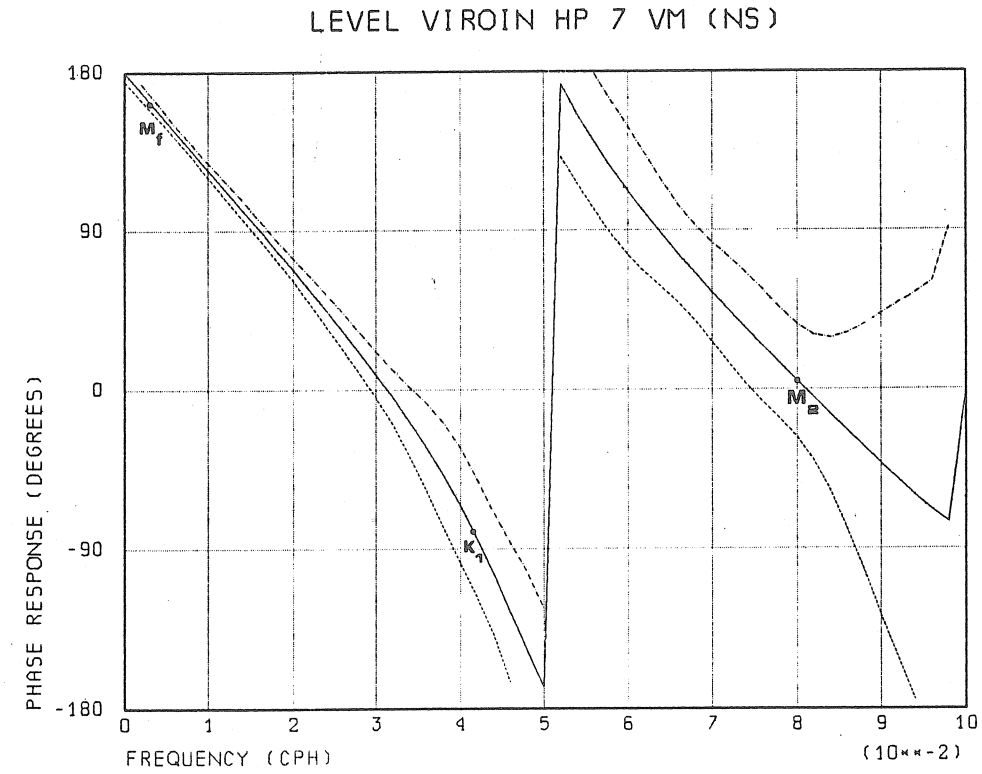

Fig. 4.g. Transferfunction of the Viroin level corresponding to $H_7(f)$.

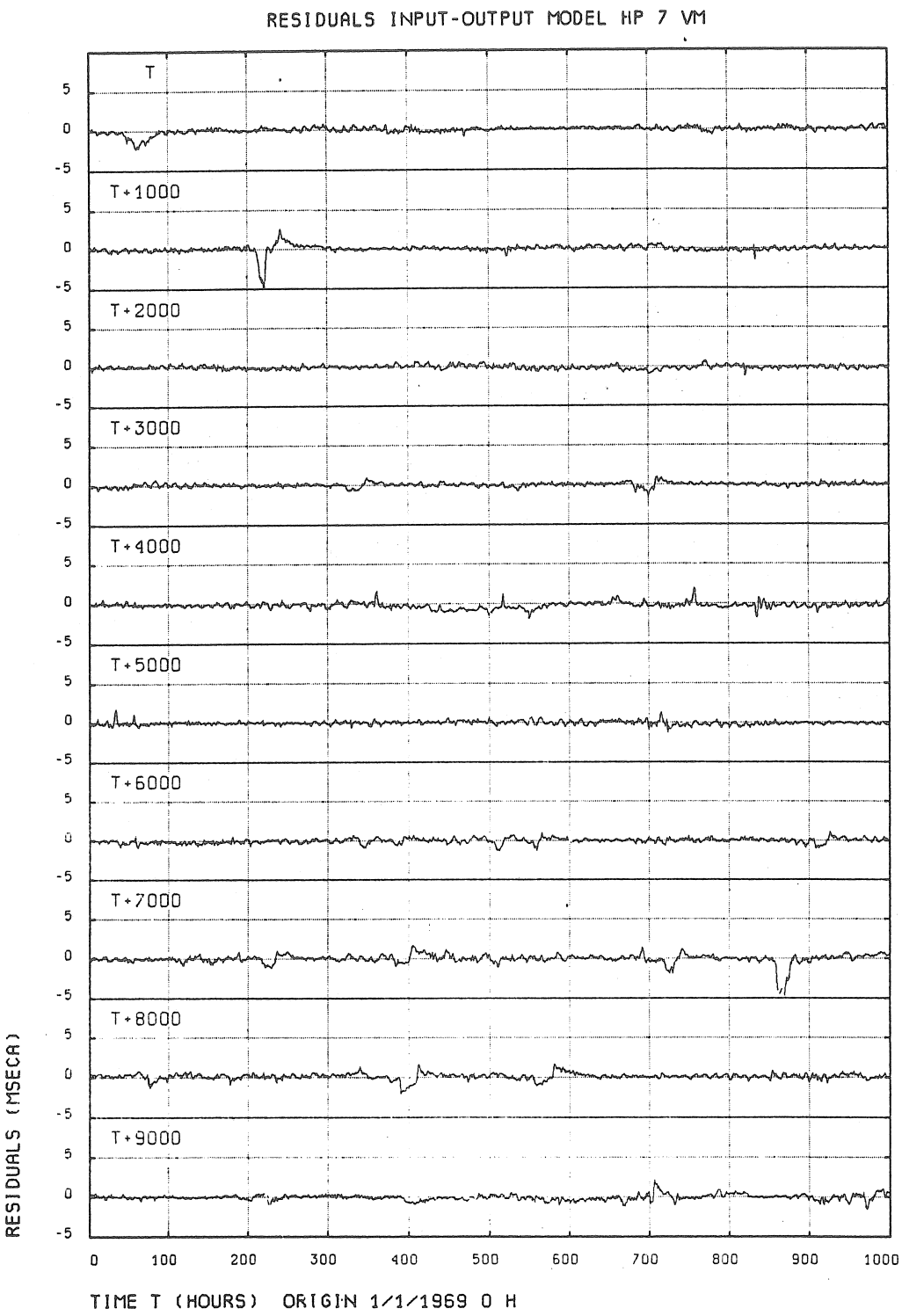

Fig. 5. Observed residuals of the MISO model.

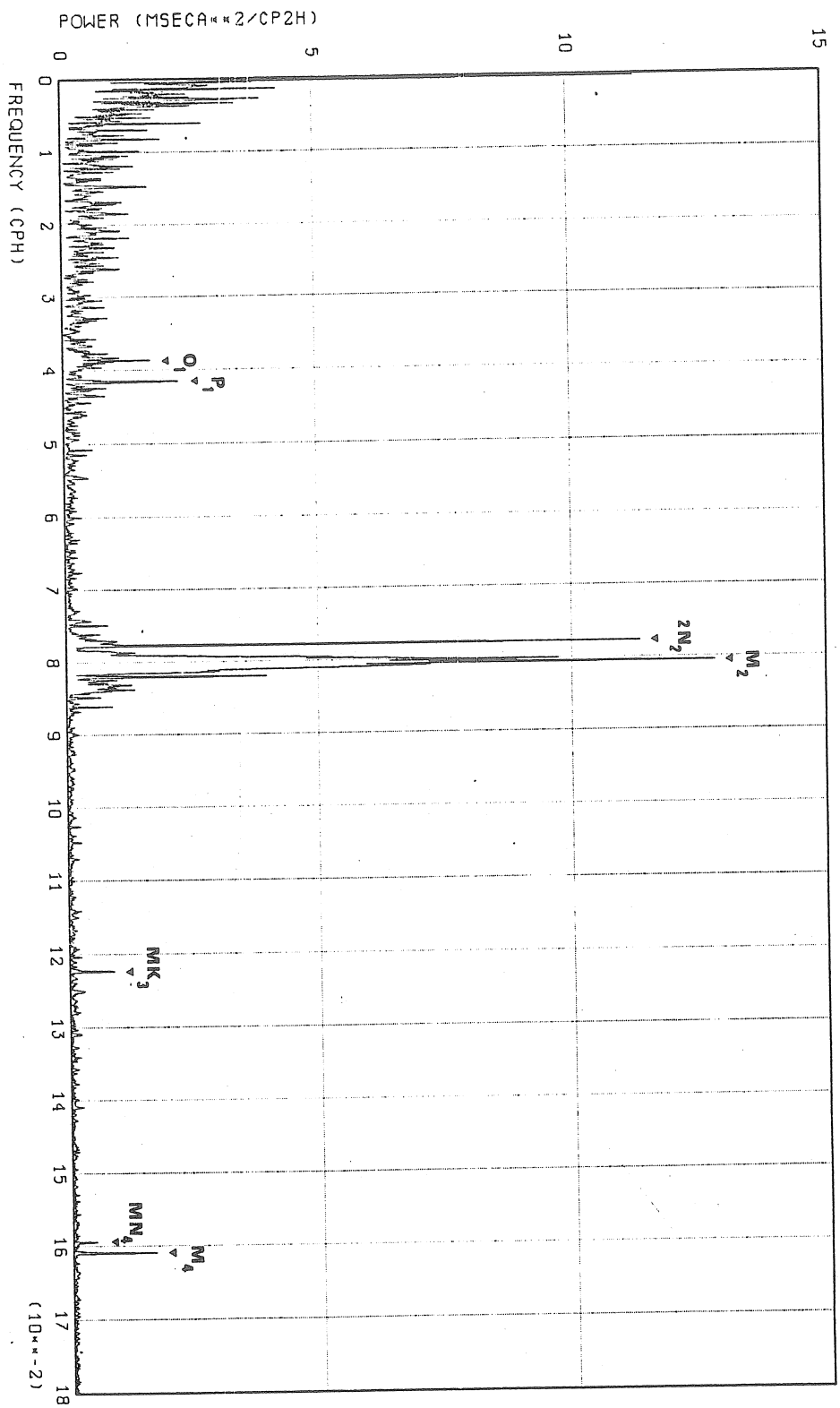

Fig. 6. a. Residual power spectrum in the frequency interval $0 \leq f \leq 0.18$ cph.

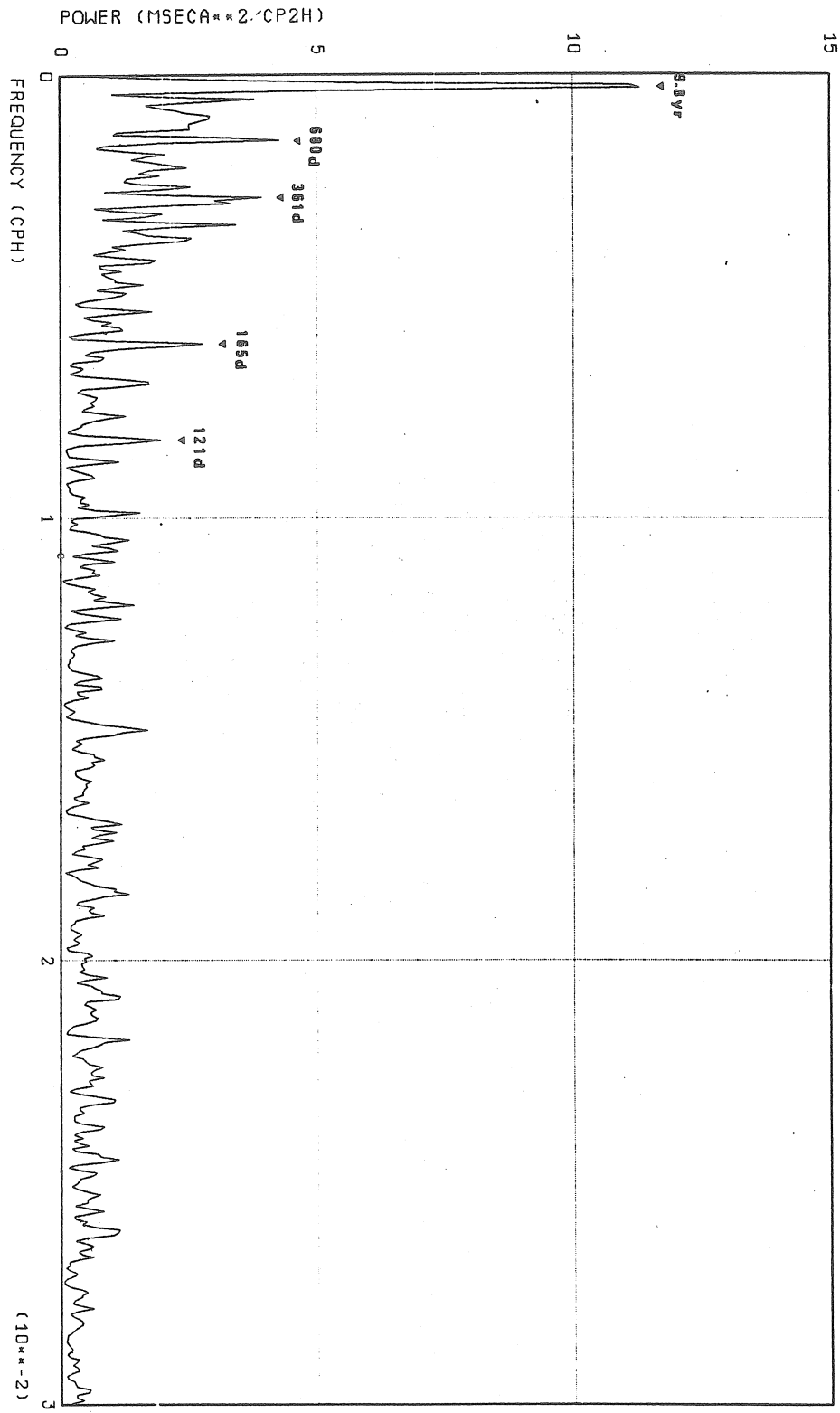

Fig. 6. b. Residual power spectrum in the frequency interval $0 \leq f \leq 0.03$ cph.

Agterberg F.P., 1974, Geomathematics, Elsevier, Amsterdam.

Bennet R.J., 1979, Spatial time series, Pion Ltd, London.

Box G.E., G.M. Jenkins, 1970, Time series analysis, Holden-day, San Francisco.

Cameron J.M., 1960, Statistics, in Fundamental Formulas of Physics, vol.1, edited by D.H. Menzel, Dover, New York.

Cartwright D.E., 1968, A unified analysis of tides and surges round north and east Britain, Phil. Trans. Roy. Soc. London, Ser. A, 263, 1-55.

Cartwright D.E., R.J. Tayler, 1971, New computations of the tide-generating potential, Geoph. J.R. astr. Soc., 23, 45-74.

Cartwright D.E., A.C. Edden, 1973, Corrected tables of tidal harmonics, Geoph. J.R. astr. Soc., 33, 253-264.

De Meyer F., 1980, A study of various harmonic analysis methods for Earth tides observations, Bull. Inf. Mar. Terr., 83, 5187-5235.

Dopp S., 1964, La station de marées terrestres de Dourbes, Commun. Observ. Roy. Belg., 236, 187-192.

Draper N.R., H. Smith, 1966, Applied regression analysis, John Wiley, New York.

Hoerl A.E., R.W. Kennard, 1970, Ridge regression. Biased estimation for nonorthogonal problems, Technometrics, 12, 55-67.

Lambert A., 1974, Earth tide analysis and prediction by the response method, Journ. Geoph. Res., 79, 4952-4960.

Melchior P., 1978, The tides of the planet Earth, Pergamon Press, Oxford.

Munk W.H., D.E. Cartwright, 1966, Tidal spectroscopy and prediction, Phil. Trans. Roy. Soc. London, Ser. A, 259, 533-581.

Penrose R., 1955, A generalized inverse for matrices, Proc. Cambridge Phil. Soc., 51, 406-413.

Robinson E.A., 1980, Physical applications of stationary time series, Charles Griffin, London.

Rossiter J.R., G.W. Lennon, 1968, An intensive analysis of shallow water tides, Geophys. J.R. astr. Soc., 16, 275-293.

Tukey J.W., 1961, Discussion emphasizing the connection between analysis of variance and spectrum analysis, Technometrics, 3, 191-211.

Yaramanci U., 1978, Tidal analysis methods and optimal linear system approximation, Bull. Inf. Mar. Terr., 78, 4621-4634.

Yaramanci U., 1978, Principles of the response method, Bull. Inf. Mar. Terr., 78, 4649-4658.

Zetler B., D. Cartwright, W. Munk, 1970, Tidal constants derived from response admittances, Commun. Observ. Roy. Belg., Sér. Géoph. 96, 175-178.

An absolute method for the calibration of earth tides gravimeters

R. Brein

Institut für Angewandte Geodäsie, Frankfurt/Main

Summary: Defined gravity differences are produced by periodic accelerations of the measuring device of the gravimeter. This absolute method can be used for instruments with rapid feed-back control like the superconducting gravimeter. Parameters are given to achieve a good accuracy.

The digital or analogous values received by the recordings of earth tides must be transformed in gravity values by a calibration factor or perhaps by a calibration function.

For the measurement of the calibration factor one or more steps are needed. One-step methods are prefered. Difficulties which can be connected with two-steps methods are treated in [5].

An example for the one-step method can be demonstrated by the La Coste-Romberg earth tides gravimeter, where the same reading screw is used for the calibration on a calibration line and the recording of earth tides [1].

Some other methods were evaluated to achieve the one-step calibration:

1. Proposed [2] and approved [3] was a direct calibration of the recordings by moving the gravimeter on a vertical calibration line in the laboratory. Here the gravity differences caused by the vertical gradient of the gravity are used.

2. The compensation of the earth tides by an electromagnetic device with feed-back control in the gravimeter [4] enables the direct calibration by the same device on a calibration line in the field [5].

3. A combination and variation of these two systems is the calibration procedure of the superconducting gravimeter [6]. Gravity differences, produced in the laboratory by displacements of a mass, are compensated with an electromagnetic or electrostatic feed-back control. The same feed-back compensation is used for the recording. The gravity differences are calculated with Newton's inverse square law of gravitation. Unfortunately, the square of the distance must be found out from vertical displacements of the mass.

The absolute method, now described, gives also a calibration of the earth tides gravimeters in one step. It is based on the equivalence principle of the ponderous and the inert mass which is used for the theory of general relativity. The gravimeter is vertically moved with a defined acceleration during the feed-back control of the earth tides recordings. Such a system was already proposed in [7] with the argument that "problems of calibration exist in the precise gravimetry of small gravity differences similar as in earth tides recordings, because the calibration factors, determined at great gravity differences, are used with uncertain assumptions in small areas". The absolute method can be important also for the superconducting gravimeter which cannot be calibrated on points with known gravity differences.

Suitable for this method are gravimeters with rapid feed-back control like [4] where the damping device of the La Coste gravimeter must be eliminated.

The vertical displacement z of the gravimeter (only the measureing device without the dewar for the superconducting gravimeter) may be given by the time function

$$z = z_o \cos \omega t. \qquad (1)$$

(z_o = amplitude, ω = angular speed = $2\pi/T$)

The second derivative of this function

$$\frac{d^2z}{dt^2} = -z_o\omega^2 \cos \omega t = -z\omega^2 \qquad (2)$$

is used for the absolute calibration of the gravimeter. Extreme values of the acceleration $\pm z_o\omega^2$ are obtained for $t = 0 \pm n \cdot \pi$. The accuracy of the calibration can be improved by higher numbers n. As in the free rise and fall method of the absolute gravity measurement some influences, like the vertical gradient of gravity or elastic deformations of the measuring device, can be eliminated or can be examined due to the cycle process.

With T = 1 minute and z_o = 40 µm (1) we get an elongation of the gravimeter recording which is adequate to a gravity change $2z_o\omega^2$ = 87,64 µgal.

This triple seems to be well suited for the realization of the method. The phase shift between (1) and the gravimeter recording of (2) can be used to examine the influence of the feedback system. An analysis of the recorded curve can give more details about the behaviour of the gravimeter and can enlarge the accuracy of the calibration. The amount of the acceleration is great enough because of the high accuracy of the gravimeter [6,8].

The amount of the displacement render possible its realization with piezo elements. The application of these elements is also useful for the exact and undisturbed examination of the minimum sensitivity to tilts during the recordings. During the absolute calibration this minimum must be maintained by controlling two of the piezo elements with a tiltmeter. The piezo elements can also be used to avoid disturbing accelerations as was shown in the technique of absolute gravity measurement [9].

References

[1] Melchior, P.: The Earth Tides, pp 232-234

[2] Brein, R.: Photographische Registrierung der Erdgezeiten mit einem Gravimeter. DGK-Veröff., Reihe B, Nr. 21, 1954, pp 8-9.

[3] Bonatz, M.: Untersuchung des Eichfaktors der gravimetrischen Gezeitenmeßanlage der Universität Bonn Askania Gravimeter GS 15 Nr. 206 Bull, Inf. Marées Terr., 63, 1972, pp 3299-3305.

[4] Brein, R.: Le ressort électromagnétique utilisé pour l'enregistrement des marées terrestres. Proc. 4th Int. Symp. on Earth Tides, Bruxelles 1961, pp 139-143.

[5] Brein, R.: The Influence of the gravimetric springs on the calibration of earth tides recordings. Bull. Inf. Marées Terr., 74, 1976, pp 4275-4279

[6] GWR Instruments: Manual of GWR Superconducting Gravimeter, San Diego 1980.

[7] Brein, R.: Die fennoskandische Meßstrecke zur Bestimmung langzeitiger Schwereänderungen. Bericht über die Tätigkeit des Inst. f. Angew. Geodäsie im Jahre 1975, pp 67-72.

[8] Richter,B., Brein, R., Reinhart, E., Wolf, P.: First results with superconducting gravimeter registrations at the earth tides station Bad Homburg. General Meeting I.A.G., Tokio, 1982.

[9] Sakuma, A.: Gravimétrie, B.J.P.M. 1875-1975, pp 109.

Traduction

OBSERVATIONS DES INCLINAISONS DE MAREE AVEC DES CLINOMETRES PHOTOELECTRIQUES A METHODE DE ZERO

par

V.P. Chliakhovi, A.E. Ostrovski et P.S. Matvéev

Rotation et Déformation de marées 13, pp 13-18, 1981

(Abrégé)

Pour réaliser des observations d'inclinaisons on utilise beaucoup de types différents de clinomètres [1]. Les clinomètres photoélectriques d'Ostrovski ont eu une large diffusion [2]: avec ces appareils la précision de détermination des paramètres des ondes principales a atteint 1%, précision qui est garantie grâce au contrôle de la sensibilité effectué deux fois par jour par des impulsions de calibrationdans la bobine d'un électro aimant. Entre ces impulsions on interpole la sensibilité. Il en résulte des inconvénients dans la réduction. D'autres types de clinomètres n'ont pas sensiblement dépassé en précision les clinomètres photoélectriques.

Pour des développements futurs il faut créer des clinomètres de plus haute précision, très stables et très sensibles vis à vis de l'ordre de grandeur des phénomènes de marée: la précision de ces clinomètres doit être d'au moins 0.1%.

L'analyse des procédés d'amélioration de la précision indique que l'utilisation des propriétés stabilisantes du feed back est la seule voie conduisant à une amélioration sensible.

L'estimation comparative des procédés de feed back en a montré les avantages pour le clinomètre photoélectrique [3] vis à vis d'autres types d'instruments.

- En premier lieu ce clinomètre a déjà tous les éléments nécessaires pour une telle transformation: introduction du feed back depuis la sortie du canal photoélectrique de l'appareil sur l'entrée du compensateur électromagnétique [3].
- En second lieu, aucune préparation supplémentaire n'est nécessaire du point de vue mécanique, mais il faut ajouter quelques éléments électroniques courants.
- En troisième lieu, ce système peut garantir une précision plus élevée de l'installation de mesure.

On a commencé les travaux pratiques en 1974 et on a essayé plus de dix variantes différentes.
Le système doit établir automatiquement l'intensité correcte et le sens du courant électrique dans le bobinage du compensateur afin de maintenir le clinomètre au zéro.

On a constaté des difficultés du côté des hautes fréquences. Sont également possibles des perturbations des conditions de stabilité du système suiveur et une série d'autres circonstances dont nous devrons tenir compte. Ceci a requis la prise de mesures spéciales pour éliminer ces imperfections. Les enregistrements d'essai dans une des premières variantes ont été obtenus en 1975 [4] puis il a fallu vérifier le fonctionnement dans des conditions typiques d'enregistrement des marées.
Il convient de noter la stabilité de l'instrument dans des conditions variables d'environnement.

Des expériences ont été faites à Soudievka en 1977-78. Malgré quelques modifications la sensibilité déterminée par impulsions de contrôle est restée constante pendant toute l'expérience qui a duré plus d'un an et demi.
La courbe de marée est lisse et correcte même à haute sensibilité (1000 à 1500 mm/sec. angle) et l'image d'un enregistrement obtenu en EW est donnée sur la figure.

Deux appareils ont été installés à Soudievka où, à une profondeur de 13m on fait des observations régulières depuis 1971 avec les clinomètres Ostrovski photoélectriques n°57 et n°66.

La comparaison repose sur la période du 09/09/79 au 12/02/80 et dans la direction EW. L'échelle d'enregistrement du clinomètre autocompensateur était pratiquement constante [3]: les données de sensibilité sont reprises dans la Table I. Le plus grand écart atteint moins de 2%. Pour le clinomètre ancien l'écart atteint 10% [8], soit près d'un ordre de grandeur de plus que pour l'autocompensateur.

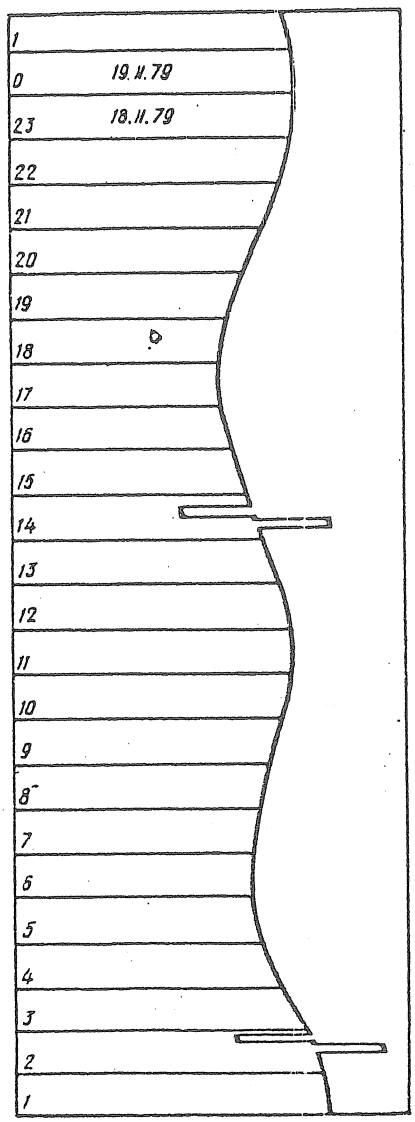

Fig. Enregistrement du clinomètre autocompensateur sur enregistreur potentiométrique KSP-4.
Echelle: 0.79 mseca/mm.

Le calcul des paramètres de marée γ, $\Delta\phi$ a été fait d'après le schéma d'analyse mensuelles établi à Poltava [9]. Les données ont été réparties en séries mensuelles avec recouvrement d'un demi mois (excepté une interruption des mesures du n°66 entre le 20/10/79 et le 2/11/79).

Les résultats sont donnés dans la Table II pour les cinq ondes principales. L'accord est satisfaisant pour les séries analysées ayant les mêmes instants initiaux.

La meilleure concordance s'observe pour les ondes lunaires O_1, M_2 et N_2.

La dérive est donnée dans la Table III mais par mois ainsi que la différence entre les deux appareils.

La différence n'est pas de plus de 0".07/mois et les dérives sont de l'ordre de celles données par d'autres auteurs [10].

TABLE I. Sensibilité (mseca/mm) du clinomètre autocompensateur n°18 et du clinomètre photoélectrique n°66.

Epoque	n° instrument		Epoque	n° instrument		Epoque	n° instrument	
	66	18		66	18		66	18
01.12.79	1.702	1.420	13.12.79	1.810	1.433	25.12.79	1.890	1.426
	1.702	1.424		1.778	1.429		1.887	1.422
02.12	1.684	1.437	14.12	1.774	1.437	16.12	1.878	1.418
	1.674	1.431		1.798	1.437		1.914	1.412
03.12	1.674	1.437	15.12	1.818	1.437	27.12	1.928	1.426
	1.649	1.433		1.814	1.433		1.923	1.420
04.12	1.709	1.441	16.12	1.818	1.451	28.12	1.909	1.443
	1.681	1.431		1.793	1.440		1.896	1.412
05.12	1.674	1.433	17.12	1.843	1.440	29.12	1.923	1.440
	1.667	1.435		1.802	1.442		1.942	1.410
06.12	1.674	1.427	18.12	1.835	1.437	30.12	1.914	1.410
	1.653	1.433		1.843	1.433		1.997	1.410
07.12	1.670	1.433	19.12	1.878	1.440	31.12	1.923	1.422
	1.681	1.433		1.848	1.445		2.041	1.426
08.12	1.709	1.439	20.12	1.878	1.422	01.01.80	1.932	1.410
	1.717	1.433		1.878	1.428		1.923	1.414
09.12	1.735	1.435	21.12	1.905	1.422	02.01	1.970	1.439
	1.695	1.422		1.914	1.433		2.000	1.407
10.12	1.702	1.425	22.12	1.874	1.420	03.01	1.990	1.408
	1.695	1.420		1.852	1.418		2.000	1.415
11.12	1.702	1.439	23.12	1.878	1.426	04.01	1.932	1.420
	1.794	1.439		1.896	1.420		1.932	1.414
12.12	1.782	1.433	24.12	1.890	1.424	05.01	1.914	1.420
	1.782	1.429		1.896	1.414		2.010	1.421

TABLE II. Résultats des analyses harmoniques pour la composante EW à Soudievka.

n° série	début série	O_1		K_1		N_2		M_2		S_2	
		γ	$\Delta\phi°$	γ	$\Delta\phi°$	γ	$\Delta\phi°$	γ	$\Delta\phi°$	γ	$\Delta\phi°$
18	09.09.79	0.646	- 0.39	1.267	- 36.95	0.779	- 5.90	0.716	-4.54	0.976	5.81
66	09.09.79	0.809	- 3.26	1.343	- 39.71	0.687	- 4.18	0.743	-3.62	1.032	3.17
18	17.09.79	0.493	-11.58	1.297	- 48.01	0.629	- 3.02	0.711	-2.11	1.017	3.63
66	17.09.79	0.542	- 9.85	1.296	- 51.95	0.667	0.151	0.739	-2.76	1.076	3.92
18	03.11.79	0.615	-12.94	0.528	- 18.24	0.787	- 2.64	0.726	-1.63	0.945	3.55
66	03.11.79	0.548	-14.82	0.576	- 18.64	0.950	-21.02	0.740	-5.10	0.988	0.21
18	18.11.79	0.531	7.51	0.590	- 4.15	0.832	- 0.23	0.722	-2.40	0.886	2.46
66	18.11.79	0.366	0.15	0.611	- 10.92	0.894	-17.04	0.705	-5.80	0.926	0.70
18	03.12.79	0.519	-38.73	0.782	- 1.98	0.912	39.55	0.785	3.85	0.632	18.40
66	03.12.79	0.563	-48.47	0.777	- 3.97	0.777	41.19	0.755	2.68	0.615	22.06
18	18.12.79	0.542	-29.92	0.596	- 27.91	0.675	70.08	0.808	-0.54	0.897	25.62
66	18.12.79	0.568	-26.40	0.576	- 27.99	0.728	154.63	0.796	-2.71	0.841	24.82
18	02.01.80	1.020	7.51	0.665	-129.95	0.628	57.13	0.715	-2.20	1.550	0.89
66	02.01.80	1.192	9.97	0.632	-137.49	0.810	52.09	0.703	-5.33	1.461	12.59

Le signe "moins" dans $\Delta\phi$ correspond à un retard de phase.

TABLE 3. Valeurs moyennes de la dérive

DEBUT DE LA SERIE MENSUELLE	DERIVE MENSUELLE MOYENNE 18	66	DIFFERENCE
09.09.79	-0.066	-0.091	+0.025
04.11.79	-0.301	-0.231	-0.070
04.12.79	-0.163	-0.156	-0.007

Le signe "plus" correspond à une inclinaison vers l'Ouest.

REFERENCES

1. MELCHIOR P.
   Marées Terrestres MIR 1968 - 482 pages

2. OSTROVSKI A.E.
   Le clinomètre photoélectrique
   Etudes de Marées Terrestres 1961 n°2 pp 41-75

3. OSTROVSKI V.E. MATVEEV P.S. et SCHLIAKOVI V.P.
   Sur la possibilité d'utilisation du clinomètre photoélectrique en méthode de zéro.
   Rot. et Déform. Marées Terre. 1975 n°7 pp 42-49.

4. OSTROVSKI A.E. SCHLIAKOVI V.P. et MATVEEV P.S.
   Sur l'efficacité du feed back pour la stabilisation de la sensibilité du clinomètre photoélectrique.
   Rot. et Déform. Marées Terre. 1977 n°9 pp 44-50.

5. SCHLIAKOVI V.P.
   Analyse des schémas de structure des clinomètres photoélectriques à feed back.
   Rot. et Déform. Marées Terre. 1978 n°10 pp 58-63.

6. SCHLIAKOVI V.P. KOUTNII A.M.
   Utilisation de photorésistances pour des déplacements faibles dans les enregistreurs de marées.
   Rot. et Déform. Marées Terre. 1977 n°9 pp 51-56.

7. SCHLIAKOVI V.P.
Choix d'un procédé de stabilisation de la source d'illumination des photoémetteurs d'une installation d'enregistrement de marée.
Rot. et Déform. Marées Terre. 1978 n°10 pp 63-68.

8. BAGMET A.L. · MICHATKIN V.N. et KOUTNII A.N.
Amélioration de la stabilité de la sensibilité des clinomètres photoélectriques.
Rot. et Déform. Marées Terre. 1973 n°5 pp 56-63.

9. MATVEEV P.S.
Analyse harmonique d'une série mensuelle
Marées Terrestres, Kiev, Naouk Doumka 1966 pp 51-79.

10. OSTROVSKI A.E.
Déformations de l'écorce terrestre d'après les observations d'inclinaisons.
M: Naouka 1978, 184 pages.

Traduction

SUR QUELQUES COMBINAISONS QUI PEUVENT AVOIR UNE APPLICATION DANS LA REDUCTION DES OBSERVATIONS DE MAREES TERRESTRES

B.S. Doubik

Rotation et Déformation de marées 13, pp. 56-57
1981

1. Combinaisons pour la détermination de deux ordonnées manquantes.

Nous introduisons la notation

$$D(t) = Z_{0,5}^2 \left(4Y_1 - 7\frac{Y_0}{2} \right),$$

où t est l'époque centrale de la partie d'enregistrement à laquelle s'applique la combinaison

A. $15D(t) + 22D(t+1)$,
60, -137, 0, 259, -270, 88;

B. $22D(t) + 15D(t+1)$,
88, -270, 259, 0, -137, 60;

C. $Z_{0,5}^2 Z_1 \left(Y_2 - \frac{Y_0}{2} \right)$ [1],
1, -2, -7, 4, 0, -4, 1, 2, -1;

D. $Z_{0,5}^2 Z_1 \left(4Y_1 - 7\frac{Y_0}{2} \right)$;
-4, 15, 18, 0, -18, 15, -4;

E. $Z_{0,5}^2 Z_1 \left(4Y_1 - 7\frac{Y_0}{2} \right)$,
-4, 23, -52, 51, 0, -51, 52, -23, 4.

2. Combinaisons pour la détermination de trois ordonnées manquantes. Dans ce cas on recommande d'utiliser séparément une combinaison pour la détermination de l'ordonnée centrale et une combinaison pour la détermination des deux autres ordonnées.

A. $65 Z_{0,5}^3 \left(Y_2 - \frac{Y_0}{2}\right) + Z_{0,5}^5 \left(4Y_1 - 7\frac{Y_0}{2}\right)$,

69, -222, 209, 0, 0, -209, 222, -69;

B. $35 Z_{0,5}^3 \left(Y_2 - \frac{Y_0}{2}\right) + 2 Z_{0,5}^7$,

37, -119, 112, 0, 0, -112, 119, -37;

C. $483 Z_{0,5}^5 \left(4Y_1 - 7\frac{Y_0}{2}\right) + 130 Z_{0,5}^3 \left(4Y_1 - 7\frac{Y_0}{2}\right)^2$,

146, -479, 453, 0, 0, -453, 479, -148;

D. $-Z_{0,5}^2 \left(Y_2 - \frac{Y_0}{2}\right)$,

1, -2, 0,2, 0 -2, 1;

E. $Z_{0,5}^4 \left(Y_2 - \frac{Y_0}{2}\right)$,

1, -4, 5, 0, -4, 0, 5, -4, 1;

F. $Z_{0,5}^2 \left(Y_2 - \frac{Y_0}{2}\right)\left(4Y_1 - 7\frac{Y_0}{2}\right)$,

-4, 15, -18, 0, 14, 0, -18, 15, -4.

3. Combinaisons éliminant la marée et la dérive représentée sous forme d'un polynome du premier degré dans un intervalle d'un jour.

A. $Y_6 \left(Y_2 - \frac{Y_0}{2}\right)^2 Z_1 Z_{0,5}$,

-1; 1, 3, -3, -5, 5, 5, -5, -3, 3, 1, -1, / -1, 1, 3,... ;

B. $Y_6 Y_3 \left(4Y_1 - 7\frac{Y_0}{2}\right) Z_1 Z_{0,5}$,

-4, 11, -7, -7, 11, -4, -4, 11, -7, -7, 11 -4, / -4, 11, -7,... .

4. Combinaisons pour la séparation de la marée diurne par intervalles journaliers.

A. $Z_6 Z_3 \left(Y_2 - \frac{Y_0}{2}\right) Y_{0,5}$,

-1, -1, 1, 1, -1, -1, 1, 1, -1, -1, 1, 1, / 1, 1, -1,... ;

B. $Z_4 \left(Y_2 - \frac{Y_0}{2}\right)\left(Y_4 + \frac{Y_0}{2}\right) Z_1 Y_{0,5}$,

-1, -1, 2, 2, -1, -1, -1, -1, 2, 2, -1, -1, / -1, -1, 2,... ;

C. $Z_6 Z_3 \left(Y_2 - 1,0598\frac{Y_0}{2}\right) Y_{0,5}$,

D. $Z_{6,5} \left(Y_4 + \frac{Y_0}{2}\right) Z_1 Y_{0,5}$.

-1, -1, 1, 1, -1, -1, 1, 1, -1, -1, 1, 1, 0, 1, 1, -1, -1, 1, 1, -1, -1, 1, 1, -1, -1.

5. Combinaisons pour la séparation de la marée semi diurne par intervalles journaliers

$$A.\ Y_6\left(Y_4 - \frac{Y_0}{2}\right) Z_1 Z_{0,5},$$

$$-1, 1, 1, -1, 1, -1, -1, 1, -1, 1, 1, -1, / -1, 1, 1, \ldots;$$

$$B\ Y_6\left(Y_4 - 1{,}1184\,\frac{Y_0}{2}\right) Z_1 Z_{0,5};$$

$$C.\ Y_{6,5}\left(Y_4 - \frac{Y_0}{2}\right) Z_1 Z_{0,5},$$

$$-1, 1, 1, -1, 1, -1, -1, 1, -1, 1, 1, -1, 0, -1, 1, 1, -1, 1, -1, 1, 1, -1, 1, 1, -1.$$

En remplaçant Y_k par 2 cos k g_i et ℓ_k par 2 sin k g_i dans n'importe laquelle des combinaisons données nous obtiendrons le facteur de sélectivité correspondant[2].

On peut également utiliser les combinaisons (1) et (2) (par applications glissantes) pour découvrir des erreurs inhérentes aux ordonnées. On peut utiliser les combinaisons (3) pour la détermination de l'erreur quadratique moyenne d'une ordonnée. On peut appliquer les combinaisons (4) et (5) pour la séparation d'une des marées; elles peuvent être également utilisées dans les schémas d'analyse harmonique.

Références

[1] DOUBIK B.S.

Certaines remarques sur la réduction initiale des observations des marées terrestres.

[2] MELCHIOR P.

Marées Terrestres
M: Mir 1968 482 pages.

A Proposal for Acceleration of Spectral Estimation of Accuracy in the Least Square Analysis by CHOJNICKI

Kurt ARLT
Zentralinstitut für Astrophysik
Akademie der Wissenschaften der DDR

In order to estimate the accuracy of the observation adjustment at different frequency bands in the programs from 15H up to 15K, CHOJNICKI (1978) applied the subroutine FORIT (a FOURIER-Transformation). His algorithm is modified with the aim to obtain a faster and more efficient program. This is done by changing Chojnicki's direct translation of the formules involved.
We determine the coefficients a and b in the harmonic representation (G. GOERTZEL, 1967).

$$f_i(x) = \frac{1}{2} a_o + \sum_{j=1}^{M} (a_j \cos \pi j x + b_j \sin \pi j x) \qquad (1)$$

with $x = 2\,i/(2N+1)$ and $i = 0,(1),\ 2N$
recursively, after setting

$$s = 0,\ c_1 = 1, \qquad (2)$$

$$u_o = u_{-1} = 0, \qquad (3)$$

by the formula :

$$u_i = f_{2N+1-i} + 2c_j \cdot u_{i-1} - u_{i-2} \quad \text{for } i = 1(1)2N. \qquad (4)$$

The coefficients now read

$$a_j = (f_o + c_j \cdot u_i - u_{i-1}) \cdot \frac{2}{2N+1}, \qquad (5)$$

$$b_j = s \cdot u_i \cdot \frac{2}{2N+1}, \qquad (6)$$

with the trigonometrical terms

$$c_{j+1} = sd \cdot c_j - sd \cdot s, \qquad (7)$$

$$s = cd \cdot s + sd \cdot c_j . \qquad (8)$$

(We use the notation cd = $\cos\left(\frac{2\pi}{2N+1}\right)$ and sd = $\sin\left(\frac{2\pi}{2N+1}\right)$

We may repeat (3) ... (8) for all frequencies j = 1, (1), M of interest.

We get an essential reduction of computer time, if we now change the order of computing in the following way.

We set :

$$s = 0,\ c_1 = 1 \qquad (2')$$

$$\left.\begin{aligned} c_{j+1} &= \ldots \\ s &= \ldots \end{aligned}\right\} \text{ for } j = 1\ (1)\ K \qquad \begin{matrix} (5') \\ (6') \end{matrix}$$

$$u_{ij} = f_{2,N+1-i} + 2c_j u_{i-1j} - u_{i-2j} \qquad j=1(1)K \qquad \left.\begin{matrix} \\ \\ \\ \\ \\ \end{matrix}\right\} i=1(1)2N \qquad (4')$$

$$\left.\begin{aligned} a_j &= \ldots \\ b_j &= \ldots \end{aligned}\right\} \text{ for } j = 1(1)K \qquad \begin{matrix} (7') \\ (8') \end{matrix}$$

The formulas (5'), (6'), (4'), (7'), (8') have to be computed for l = 1, (K), M. In the presented program K = 504 was chosen analogous to the numbers of waves in the expansion of the tide potential in the versions 15H and 15J.

A small disadvantage of the new program is the requirement of more storage : An additional field C (504) with 4K Bytes is defined. Moreover it needs a little more central processor time, namely to set the fields A and B zero, and by the use of subscripted quantities instead of formerly scalar values.

As in the old version the data set of residuals was read M times (for instance for 24 000 observations 3 000 times), the data set will be rewinded in the new FORIT only INT (2N,K)+1 times (in the example 6 times). We have to keep in mind, however, that the input from external memories does not reduce to the access time, but that it is expensive in central precessor time too.

Let us denote by s a typical number of operation per unit time for the computer in question, then the old FORIT requires

$$(2N/10^3)^2/s \text{ minutes}$$

central processor time, but the new one needs only the fifth !

(At ES 1040 is s = 1,6 after optimization level 0 and s = 3 after level 2.)

On computers with 4-Byte-words it is natural to implement the double precision to the subroutines ESTIM and FORIT - above all in the view on long series.

These reflections on accelerating the estimation of accuracy were suggested by Dr. CHOJNICKI. Our revision of FORIT should be seen as thanks for his kind aid to advance the tidal analysis in Potsdam.

L i t e r a t u r

C h o j n i c k i T., 1978, Estimation of accuracy of tidal data adjustment results based on residual spectrum, Publ. Inst. Geophys. Pol. Acad. Sc., 129, 3-8

G o e r t z e l G., 1967, Fourier-Analyse (in Ralston/ Wilf, Math. Meth. für Digitalrechner, 1967, S.462-470).

```
      SUBROUTINE FORIT(FNT,N,M,A,B,K3,KR21,K252,FNTZ,KRG,KDX)
C   F O R I T :  VARIANTE POTSDAM
      DOUBLE PRECISION A(KDX),B(KDX),FNT(KRG)
      REAL*8 FNTZ,COEF,S1,C1,C,S,U0,U1,U2,AN,NAME
      REAL*8 SALT,C2(504),CONST,AN
      AN=N
      COEF=2.D0/(2.D0*AN+1.D0)
      CONST=COEF*3.14159265358979D0
      S1=DSIN(CONST)
      C1=DCOS(CONST)
      C=1.D0
      S=0.D0
      REWIND 18
      M1=M+1
      IS=1
      DO 10 JL=1,M1,KDX
      REWIND 19
      SALT=S
      JLR=KDX
      IF(M1-JL+1.LT.KDX) JLR=M1-JL+1
       DO 30 J=1,JLR
      C2(J)=C*2.D0
      Q=C1*C-S1*S
      S=C1*S+S1*C
      C=Q
      A(J)=0.D0
   30 B(J)=0.D0
      K2=2*N+K3-1
      DO 20 K1=K3,K2
      K=MOD((K1-1),252)+1
      IF(K.EQ.1.OR.K1.EQ.K3) READ(19)(FNT(L+9),L=KR21,K252)
      I=KR21+K+8
      U1=FNT(I)
      DO 20  J=1,JLR
      U0= U1+C2(J)*A(J)-B(J)
      B(J)=A(J)
   20 A(J)=U0
      IS=1
      C=C2(1)/2.D0
      S=SALT
      DO 40 J=1,JLR
      U1=A(J)
      U2=B(J)
      A(J)=COEF*(FNTZ+C*U1-U2)
      B(J)=COEF*S*U1
      Q=C1*C-S1*S
      S=C1*S+S1*C
   40 C=Q
      IF(JL.EQ.1) A(1)=A(1)/DSQRT(2.D0)
      IF(M1.LE.KDX) GOTO 50
      WRITE(18) A
      WRITE(18) B
   10 CONTINUE
      REWIND 18
      REWIND 19
   50 CONTINUE
      RETURN
      END
```

SECULAR AND SEASONAL EFFECTS IN EARTH TIDE DATA

F. DE MEYER
Royal Meteorological Institute
Av. Circulaire, 3
1180 Brussels, Belgium

Abstract

A numerical scheme is presented to study long-period variations in the instrumental drift of four Verbaandert-Melchior horizontal pendulumns at a single tidal station (Dourbes, Belgium). As a first approximation the corrected drift curve can adequately be represented by an exponential function. The secular contributions are accounted for by a truncated series of orthonormal polynomials. Constructing two sets of residuals, mechanisms for the annual and long-period fluctuations are investigated, but no unique geophysical or meteorological origin can be denoted that accounts unambiguously for the perturbations in the drift phenomena of the instruments concerned.

1. Introduction

We know that instability in azimuth of horizontal pendulumns for the observation of Earth tides gives rise to a drift of the instrumental zero that is not negligeable and frequently fluctuating. The tidal curve is superposed on these long-period waves, which act as noise in this context. Slow variations in the instrumental condition of any origin (molecular, rheologic, thermic) are one of the main causes of the drift. External effects acting on or inside the Earth's crust also influence the tidal recordings, such as changes in the underground water-level induced by variations in the flow of adjacent watercourses and distortions of the crust from loading by snow or surface water. We also observe instantaneous deformations of the crust consequent on zones of high and low pressure as reflected in the barometric pressure. A tectonic cause of the drift is situated in the flexure of the crust resulting from long-period tectonic trends affecting large areas.

Since the drift always deflects in the same direction and slowly diminishes by comparable amounts, this phenomenon may be attributed to an expansion effect of the rocks in which the pendulumns are imbedded. There are so many causes that no unambiguous solution is to be expected from a single station with a single pair of instruments. Much work has been done in this controversial domain in relation to geophysical interpretation and the disturbing effects of the drift in the deformation of Earth tide waves. Some have asserted that there are variations of the seasonal type. Nevertheless lacking accurate physical information one is compelled to work hazardously with the observations, but it can be aimed to treat the data in an optimal way. Therefore, to avoid as much as possible the personal bias it is the intention in this paper to use only unsophisticated numerical techniques in order to search for significant secular and seasonal variations in Earth tide measurements.

2. Description of the tidal station

The observation site has been described by DOPP (1964) and MELCHIOR (1978, p. 363). A single horizontal gallery in the direction N 75°W inside a hilly region gives access to a L-shaped cavity of dimension 6m x 6m, specially excavated in the limestone massif for the purpose. The distance from the entry of the gallery is 150m, the depth from the free surface is 46m. The directions of the principal dimensions of the cavity are NS and EW. The station Dourbes (λ = 04°36'E, φ = 50°06'N) is situated at an elevation of 175m and the distance from the North Sea is about 140km.

Since 1963 two pairs of Verbaandert-Melchior pendulumns are installed at the opposite extremities of the underground L-room on massif limestone pillars of surface dimensions 2m x 0.8m and height 0.35m, thus creating a direct connection with the surrounding rocks. One pillar supports the pendulumns n°7 (NS) and 8 (EW), the other is equiped with the pendulumns 29 (NS) and 28 (EW). The thermic insulation of the instruments is realised by two telescoping boxes.

3. Data description and reductions

The source data consist of the hourly values, expressed in milliseconds of arc (mseca), of the four horizontal pendulumns ; seventeen years of observations ranging from 01.01.1965 to 31.12.1981 are used. The first two years of measurements are not included since the computed drift has an erratic aspect. For the station concerned the amplitude of the tidal fluctuation is about 13 mseca in the diurnal band and 12 mseca in the semi-diurnal band.

First the daily means of 24 consecutive hourly data are obtained. Calculating the 24-hourly averages is equivalent to low-pass filtering of the observations. The frequency response of this filter or in other words, the factor of amplitude reduction of an arithmetic summation of n data, is given by

$$S(f) = \frac{1}{n} \frac{\sin n\pi f \Delta t}{\sin \pi f \Delta t} \quad , \qquad (3.1)$$

where Δt = 1 hour is the sampling interval and f is the frequency in cycles per hour (cph). With n = 24 the moving-average operation cuts off all the frequencies that are multiples of 1 cycle per day (cpd), but lets through a fair percentage of the other frequencies : 7.5 per cent of O_1, 0.3 per cent of K_1, 5.4 per cent of N_2 and 3.5 per cent of M_2. In conclusion reducing the data set to 6209 daily means only introduces an aliasing effect of the order of 0.5 mseca.

Recordings of Earth tides are frequently displaced either because a calibration has been performed or the drift is compensated by executing a correction so as to bring the recording in the middle of the paper. Since the observed curve contains several drift corrections these discontinuities have to be counteracted by a numerical procedure. To achieve the connection of two parts of a digital time series, which are separated by a jump, LECOLAZET (1961) proposes the combination $Z^7_{1/2}$ (in the Labrouste notation). This antisymmetrical filter with coefficients (-1, 7, -21, 35 : -35, 21, -7, 1) is applied "on horseback" of every discontinuity in the data set of the daily averages with the weights symmetric with respect to the gap and furnishes 20 = 35 - 21 + 7 - 1 times the value of the jump.

This combination eliminates a polynomial of the sixth degree and its amplitude response is equal to $(2 \sin \pi f \Delta t)^7$, where $\Delta t = 1$ day and the frequency f is expressed in cpd.

The resulting corrected daily means y(t) are represented by the fluctuating curves in Fig. 1. Next the best exponential function is fitted to the time series

$$y(t) = \alpha + \beta e^{-t/\tau} + \epsilon_1(t) \qquad (3.2)$$

with the NEWTON-GAUSS method of nonlinear optimization (BARD, 1974). The retardation times in years and the damping ratios $1/\tau$ in cycles per year (cpy) are summarized in Table 1. The origin t = 0 corresponds to January 1, 1965 and the exponential fits are illustrated by the dotted curves in Fig. 1. The differences $\epsilon_1(t)$ between the daily means and the ordinates of the exponential function are shown in Fig. 2. It is concluded that the nonstationary contribution in the instrumental drifts is not completely eliminated, but an annual variation becomes apparent. Figure 3 represents the vectorial diagrams of the combinations HP7 + HP8 and HP29 + HP28, which corresponds to pairs of NS and EW pendulumns placed on the same pillar. The drift rate slowly diminishes. This indicates that the drift is mainly due to relaxation of rock stresses after excavation of the underground cavity in the sense that it corresponds to stabilisation of the rock.

4. The variance spectrum

The basic principle of this technique is very simple (VANICEK, 1970). For an arbitrary angular frequency $\omega = 2\pi f$ the trigonometric term

$$y(t) = a_o + a \cos \omega t + b \sin \omega t + v(t) \qquad (4.1)$$

is fitted to the given discrete data set y_k, $0 \leq k \leq n-1$, where $v(t)$ denotes the model noise. Estimates of the coefficients a_o, a and b are obtained by the least squares algorithm. The summation of the squares of the differences between the model values and the observations

$$S(\omega) = \sum_{k=0}^{n-1} (a_o + a \cos k\omega + b \sin k\omega - y_k)^2 \qquad (4.2)$$

is used as a measure of fit and can be regarded as a function of the frequency ω.

At the minimum the quantity $S(\omega)$ is interpreted as the residual sum of squares RSS of the residuals v_k, which remain unexplained by the trigonometric model in Eq. (4.1). Defining the total sum of squares of the data

$$TSS = \sum_{k=0}^{n-1} y_k^2 \tag{4.3}$$

it then follows that SSR = TSS - RSS is the portion of the sum of squares explained by the trigonometric regression (4.1). For the purpose of spectral analysis the variance spectrum is defined by

$$\begin{aligned} V(\omega) &= 100\ SSR/TSS \\ &= 100\ (1 - RSS/TSS) \end{aligned} \tag{4.4}$$

which may be conceived as the percentage of the total variance $\sigma_y^2 = TSS/(n-1)$ explained by the harmonic wave with frequency ω.

The curve $V(\omega)$ as a function of ω provides a spectral image of the data y_k. It gives the exact location of frequency in the shape of a sharp peak when the given function happens to be the sum of an harmonic wave and purely white noise. It can be assumed that this numerical technique, as opposed to the classical methods of power spectrum analysis, permits an increased resolution in the lower frequency band and particularly so if the lower frequency constituents have larger amplitudes. Of course side-lobe effects may show up.

Figure 4 represents the variance spectra of the residual series $\epsilon_1(t)$ of the four horizontal pendulumns. An annual variation is clearly demonstrated ; several long-period contributions appear, which have no direct geophysical interpretation.

Suppose that in a time series a number of periods $T_1, T_2 \ldots, T_m$ are identified by the peaks of the variance spectrum. Mathematically these variations can be described by a trigonometric model.

$$\begin{aligned} y(t) &= a_o + \sum_{j=1}^{m} (a_j \cos 2\pi t/T_j + b_j \sin 2\pi t/T_j) + v(t) \\ &= a_o + \sum_{j=1}^{m} c_j \cos (2\pi t/T_j + \omega_j) + v(t) \end{aligned} \tag{4.5}$$

The least squares technique then determines estimates of the coefficients a_j and b_j ; the amplitudes c_j and phases φ_j are defined by $c_j = (a^2_j + b^2_j)^{1/2}$ and $\varphi_j = - \tan^{-1} b_j/a_j$, respectively. From a statistical point of view the harmonic constituent with period T_j is considered significant at the 95% confidence level whenever $t_j = C_j / \Delta C_j$ is larger than 2, where Δc_j is the estimated standard error of the amplitude c_j. Furthermore the standard error $\Delta \varphi_j$ of the phase φ_j must be reasonably small if the variation should be adequately represented by an harmonic function.

A measure of the goodness of fit of the regression model (4.5) is the multiple correlation coefficient $R^2 = SSR/TSS = 1 - RSS/TSS$, which can be interpreted as an estimation of the percentage variance in the observations y_k by the harmonic constituents. A value $R^2 = 0$ means that the harmonic model (4.5) is a completely inefficient description of the data, where a value $R^2 = 1$ indicates a perfect correspondance.

Once the periods of the apparent lines in the spectra of Fig. 4 are relatively well defined, the amplitudes and phases of the associated periodic oscillations can be computed by fitting a trigonometric model of the form (4.5) to the observations. The results are summarized in Table 2 ; the periods T_j are expressed in years. The origin $t = 0$ corresponds to January 1, 1965. From the phases we find that the maxima of the annual variation occur at March 6, April 17, May 5 and July 21 for the pendulumns 7, 8, 29 and 28, respectively, with a standard error of about 20 days.

The t_j-values in Table 2 apparently demonstrate that the amplitudes of the long-period contributions are very significant. However, because the peaks in the variance spectra are not located at the same frequencies in the four instruments concerned we have to adopt an equivocal view as to an unambiguous interpretation of these variations.

5. Orthonormal polynomial expansion

We now intend to express the long-term contributions in the residual series $\epsilon_1(t)$ by a polynomial representation. In general it is supposed that n ordinates $y_1, \ldots, y_n$ of a continuous function $y(t)$ are given at the time points $t_1, \ldots, t_n$.

From the sequence of nonorthogonal powers 1, t, t^2, ... we can construct by linear combination a sequence of polynomials $p_k(t)$, of exact degree k, which are orthonormal in the observing interval, that is, satisfy the inner product relationships

$$<p_k \mid p_j> = \sum_{i=1}^{n} p_k(t_i)p_j(t_i) = \delta_{kj} \quad , \tag{5.1}$$

with δ_{kj} the Kronecker delta. The Gram-Schmidt procedure involves building the $p_k(t)$ in a stepwize fashion and develops a recursive relation, expressing each $p_k(t)$ in terms of t^k and $p_j(t)$, $j < k$. We take $p_o(t) = 1$ and assume that p_o, p_1, ..., p_{k-1} have been constructed and satisfy Eq. (5.1). Then take

$$q_k(t) = t^k - \sum_{j=0}^{k-1} <t^k \mid p_j> p_j(t) \quad . \tag{5.2}$$

Since 1, t, ...,t^k are linearly independent, q_k cannot be zero. To obtain an orthonormal set of polynomials, we need only replace each q_k by $q_k/(q_k, q_k)^{1/2}$.

In terms of these orthonormal polymials the function y(t) is written

$$y(t) = \sum_{k=0}^{N} c_k \, p_k(t) + \nu(t), \tag{5.3}$$

where the maximum degree N has to be chosen a priori. Using Eq. (5.1) the coefficients c_k are explicitely given by the observations y_1, ..., y_n in the data interval concerned.

$$C_k = \sum_{i=1}^{n} y_i \, p_k \, (t_i). \tag{5.4}$$

Then we apply this orthonormal representation to the residual series $\epsilon_1(t)$

$$\epsilon_1(t) = \sum_{k=0}^{N} C_k \, p_k(t) + \epsilon_2(t) \tag{5.5}$$

For increasing values of the approximation degree N the standard deviation σ_ϵ of the residual sequence $\epsilon_2(t)$ is plotted in Fig. 5 for the four instruments involved as a function of N. For increasing values of N the polynomial fit evidently becomes more accurate, but we try to avoid overfitting.

The polynomial $p_k(t)$ of order k has k zeros in the observing interval. Since we have 17 years of observations at our disposal in this connection and because we are interested in periodicities in the neighbourhood of the annual variation, the series expansion in Eq. (5.5) is limited to the maximum degree N=17. For higher values of N the polynomial series will adapt to the annual variation.

The polynomial fit N=17 to the residual series $\epsilon_1(t)$ is shown in Fig.6. The residual series $\epsilon_2(t)$ obtained in this way are displayed in Fig.7. The vectorial diagrams are shown in Fig.8 and the variance spectra are illustrated in Fig.9. The results of the harmonic analysis of the residuals $\epsilon_2(t)$ are summarized in Table 3. An annual variation is clearly demonstrated in the four pendulumns, with an amplitude of the order of 100 mseca. The phases indicate that the maxima occur at September 4, October 9, October 26 and January 17 for the instruments 7, 8, 29 and 28, respectively, with a standard error of about 10 days. It is also interesting to note that all pendulums show a contribution of an amplitude of the order of 40 mseca at a period of 1.10 years.

However, a concordant geophysical interpretation as to the cause of these fluctuations is not evident.

Finally, in an attempt to find a significant correlation with meteorological information we analyzed the time series of the barometric pressure and atmospheric temperature, measured at the synoptic station Florennes, situated about 18km to the north of the station of Dourbes and subjected the daily means records for the time interval 1965-1981 to the very same numerical procedure. Furthermore the daily means of the small river Viroin, situated 2km to the south of the station, are incorporated. Therefore the amplitudes of the associated variations are expressed in mbar, degrees centigrade and cm, respectively. Figure 10 shows the computed variance spectra of the data sets concerned and Table 4 summarizes the results of the matching harmonic analysis. The dates of the maximum of the annual variation in these time series occur at September 14, July 24 and February 19, respectively, with standard deviations 8,1 and 7 days. However, no clear and unique meteorological cause can be attached to the main disturbances in the drift of the horizontal pendulumns studied. Both the atmospheric pressure and the level of the river Viroin show an important perturbing effect at a period of 1.10 years.

It is remarked that the resulting phase and the dates of the maximum of the annual variation largely depend on the pretraitment of the data, in the sense that a representation of the long-period contributions by a trigonometric or a polynomial model leads to quite different results. Nevertheless it seems that the annual variation in the second residual series situates its maximum in the autumn for the four pendulumn concerned.

For the station in question the sensitivity determination still rests upon measurements of the free period of the instrument. The sensitivity S of the apparatus is linked to its period T by the basis formula $K = S\ T^2$, where K is the fundamental constant of the inclinometer. For the V M pendulumns a period of the order of 80 seconds is recommended. Figure 11 shows the evolution in time of the period of the four instruments.

6. Conclusions

Seventeen years of hourly values of four horizontal Verbaandert-Melchior pendulumns, placed in pairs on two stone pillars in the underground tidal station of Dourbes, have been used to make a detailed search for significant nontidal periodic behaviour. First the daily means are obtained and the drift corrections are intercepted by a simple numerical filter. As a whole the resulting daily averages can be reasonably well approximated by an exponential curve. The differences between the observations and the exponential drift are analyzed and apart from an annual variation several long-period fluctuations are found. To avoid an harmonic description of these secular trends a truncated series of orthonormal polynomials is fitted to the residuals and a second set of residuals is derived. Nevertheless no unique geophysical or meteorological cause can be indicated to account unambiguously for the perturbations in the drift curves of the instruments.

Acknowledgment

The author acknowledges his indebtedness to Prof. P. MELCHIOR for offering helpful suggestions and for reading the manuscript.

Table 1.- Retardation times and damping ratios

HP	α (mseca)	β (mseca)	τ (years)	$1/\tau$ (cpy)
7 (NS)	-13467.4	14766.3	50.58	0.0198
8 (EW)	-25507.5	26895.0	10.75	0.0931
29 (NS)	-11103.1	14354.8	2.86	0.3498
28 (EW)	- 8313.3	11878.5	6.31	0.1585

Table 2.- Harmonic analysis residuals $\epsilon_1(t)$

HP 7 VM (NS)					HP 8 VM (EW)					HP 29 VM (NS)					HP 28 VM (EW)				
T_j	$C_j^{\otimes}$	t_j	$\varphi_j^{\otimes}$	$\Delta\varphi_j$	T_j	C_j	t_j	φ_j	$\Delta\varphi_j$	T_j	C_j	t_j	φ_j	$\Delta\varphi_j$	T_j	C_j	t_j	φ_j	$\Delta\varphi_j$
11.90	97	60	-146	9	8.30	433	115	-115	10	11.90	1088	168	52	11	9.13	193	80	-96	11
5.59	158	100	141	7	4.49	179	47	145	16	5.17	331	52	-126	20	5.07	221	89	-178	10
5.28	36	23	3	15	2.68	92	24	48	23	3.22	317	49	123	21	3.80	116	47	97	13
2.14	43	27	35	14	2.19	67	17	65	27	2.61	180	28	94	27	2.59	59	25	- 12	18
1.63	41	26	1	14	1.86	94	24	-18	23	2.25	126	20	58	32	2.06	37	15	172	24
1.10	29	18	-7	17	1.58	113	30	-58	20	1.97	125	20	- 1	33	1.78	33	14	121	24
1	65	41	-64	11	1.16	57	15	-10	29	1	244	39	-120	23	1.59	38	15	11	23
0.87	26	17	110	17	1.08	65	17	-96	27						1.27	47	20	-118	20
					1	118	31	-106	20						1	73	30	161	17
					0.91	73	19	167	25						0.93	45	18	139	21
															0.89	48	20	96	20
R^2	0.88					0.89					0.93					0.90			

⊗ amplitudes in mseca, phases in degrees.

5703

Table 3.- Harmonic analysis' residuals $\epsilon_2(t)$

HP 7 VM (NS)					HP 8 VM (EW)					HP 29 VM (NS)					HP 28 VM (EW)				
T_j	$C_j^{\otimes}$	t_j	$\varphi_j^{\otimes}$	$\Delta\varphi_j$	T_j	C_j	t_j	φ_j	$\Delta\varphi_j$	T_j	C_j	t_j	φ_j	$\Delta\varphi_j$	T_j	C_j	t_j	φ_j	$\Delta\varphi_j$
2.40	39	34	67	10	2.38	78	38	23	13	1.96	50	25	129	16	2.09	26	17	-27	17
1.98	23	20	84	14	1.88	67	32	159	15	1.23	60	30	-174	15	1.73	40	27	-112	13
1.65	35	32	-142	11	1.63	78	37	148	14	1.11	30	15	80	21	1.57	43	29	174	13
1.10	31	28	-168	12	1.38	61	30	-59	15	1	200	99	65	8	1.29	44	29	24	13
1	61	54	116	8	1.20	71	33	-150	14	0.86	61	31	-67	15	1.13	39	26	140	14
0.86	20	18	54	14	1.10	50	24	100	17	0.75	51	26	-147	16	1	66	44	-17	11
0.73	21	19	6	14	1	105	49	82	12						0.90	41	28	-100	13
0.49	22	20	93	14	0.92	72	35	-37	14										
0.47	20	18	61	14	0.64	60	30	-141	15										
R^2	0.59					0.67					0.70					0.53			

⊗ amplitudes in mseca, phases in degrees

Table 4.- Harmonic analysis meteorologic phenomena

Pressure					Temperature					Level Viroin				
T_j	C_j	t_j	φ_j	$\Delta\varphi_j$	T_j	C_j	t_j	φ_j	$\Delta\varphi_j$	T_j	C_j	t_j	φ_j	$\Delta\varphi_j$
12.09	1.1	7	95	9	1.11	0.2	3	-78	9	11.41	17	40	-87	6
4.15	1.1	7	100	9	1	7.4	112	158	1	3.92	7	16	-120	9
2.78	1.1	7	16	9	0.94	0.2	3	19	8	2.28	4	10	-127	12
1.61	0.6	4	-27	12	0.89	0.2	3	-148	9	1.14	6	14	115	10
1.35	0.9	6	-114	9	0.84	0.2	3	121	8	1	13	31	-49	7
1.14	1.6	10	-30	7	0.80	0.2	3	145	8	0.90	5	11	-33	11
1	1.3	8	106	8	0.74	0.5	8	85	5	0.79	4	9	137	12
0.77	1.0	6	15	9										
0.72	0.9	6	173	10										
0.67	0.7	4	-80	11										
0.58	0.7	4	-161	11										
0.48	0.8	5	-114	10										
R^2	0.08				0.70					0.43				

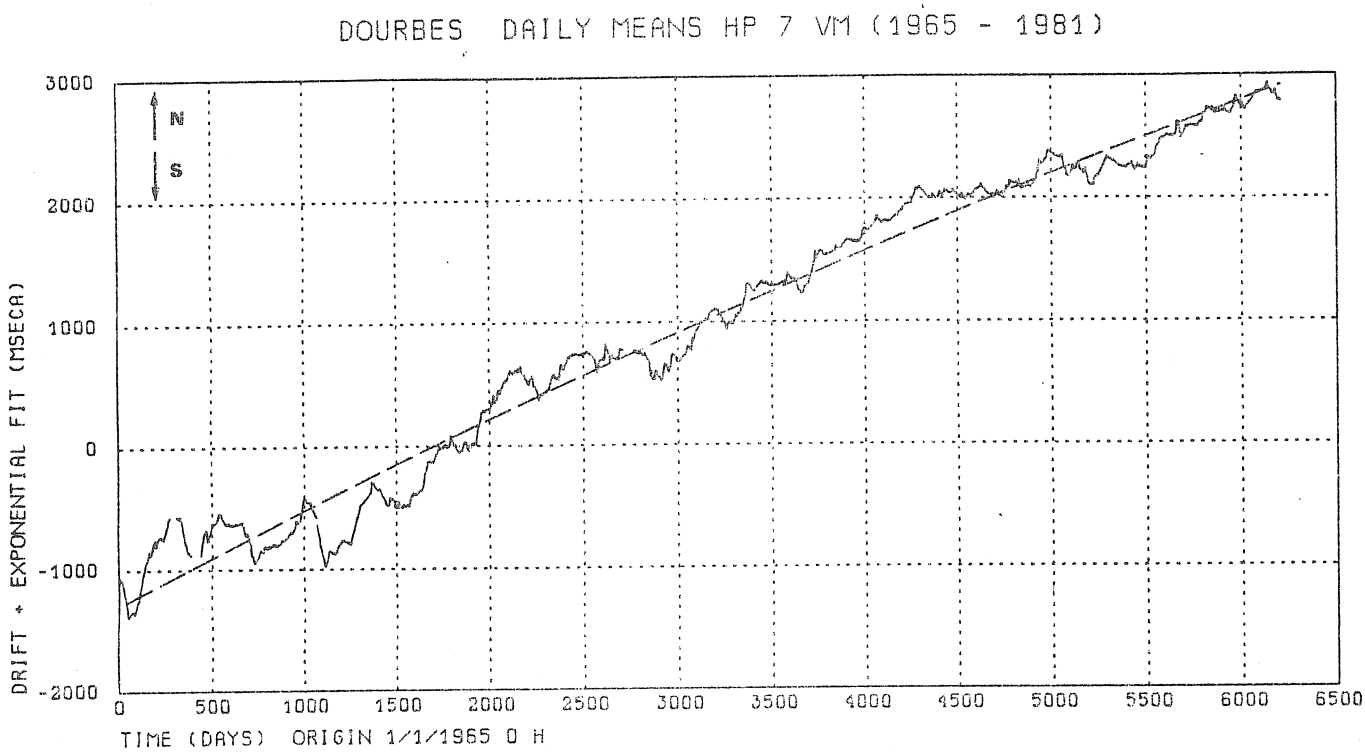

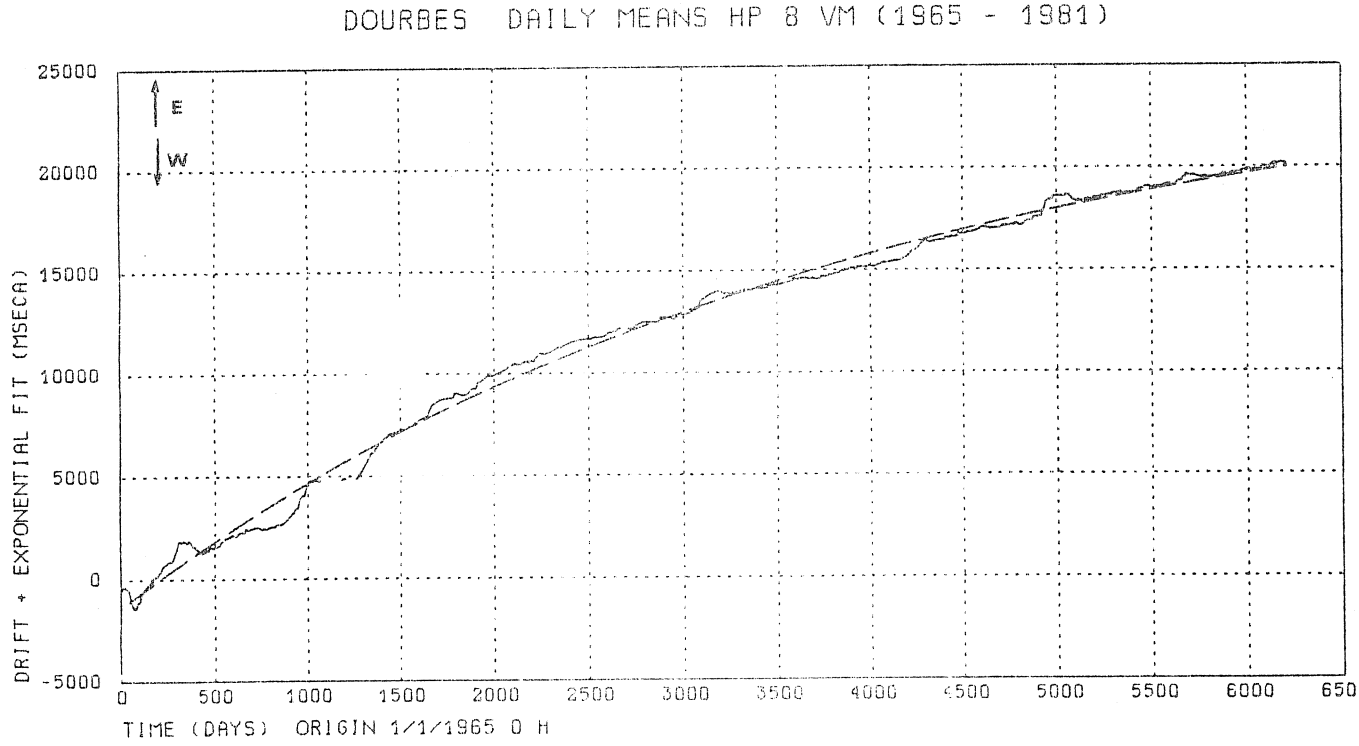

Fig. 1.a.- Daily means of horizontal pendulum observations.

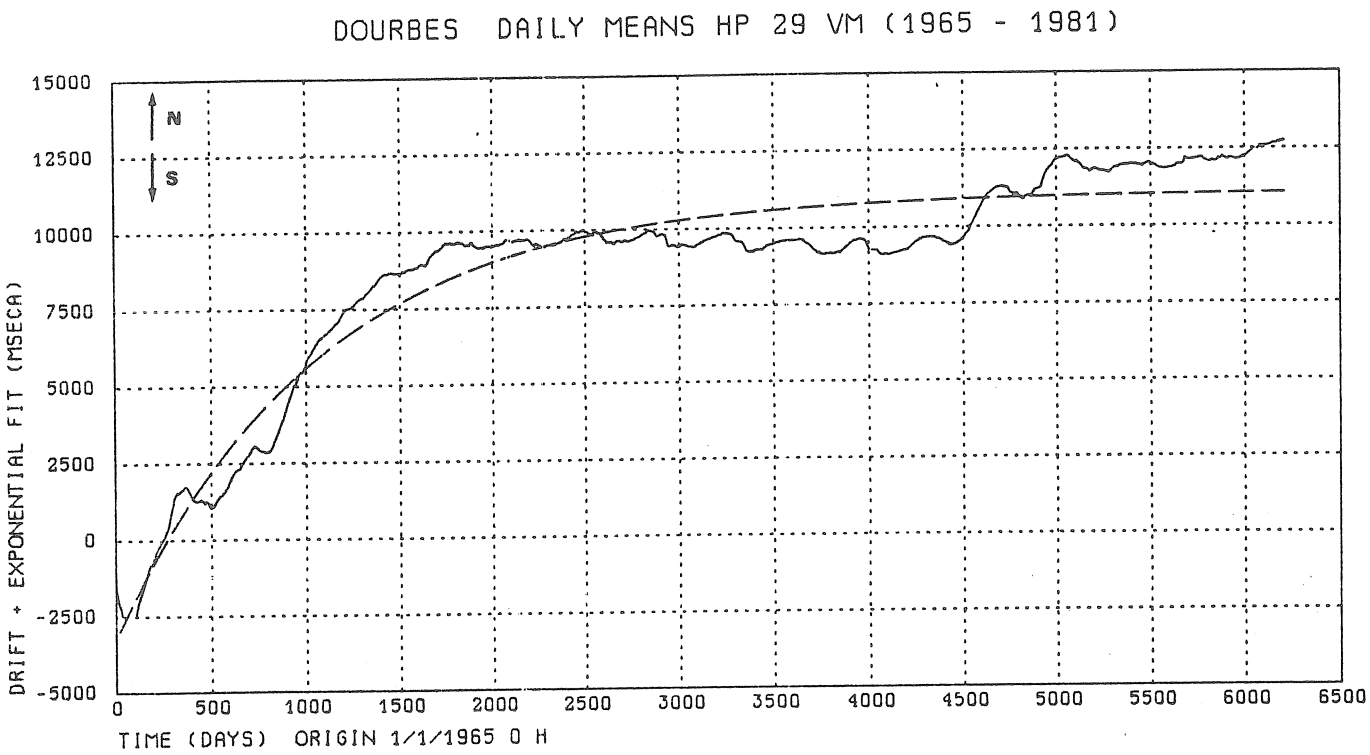

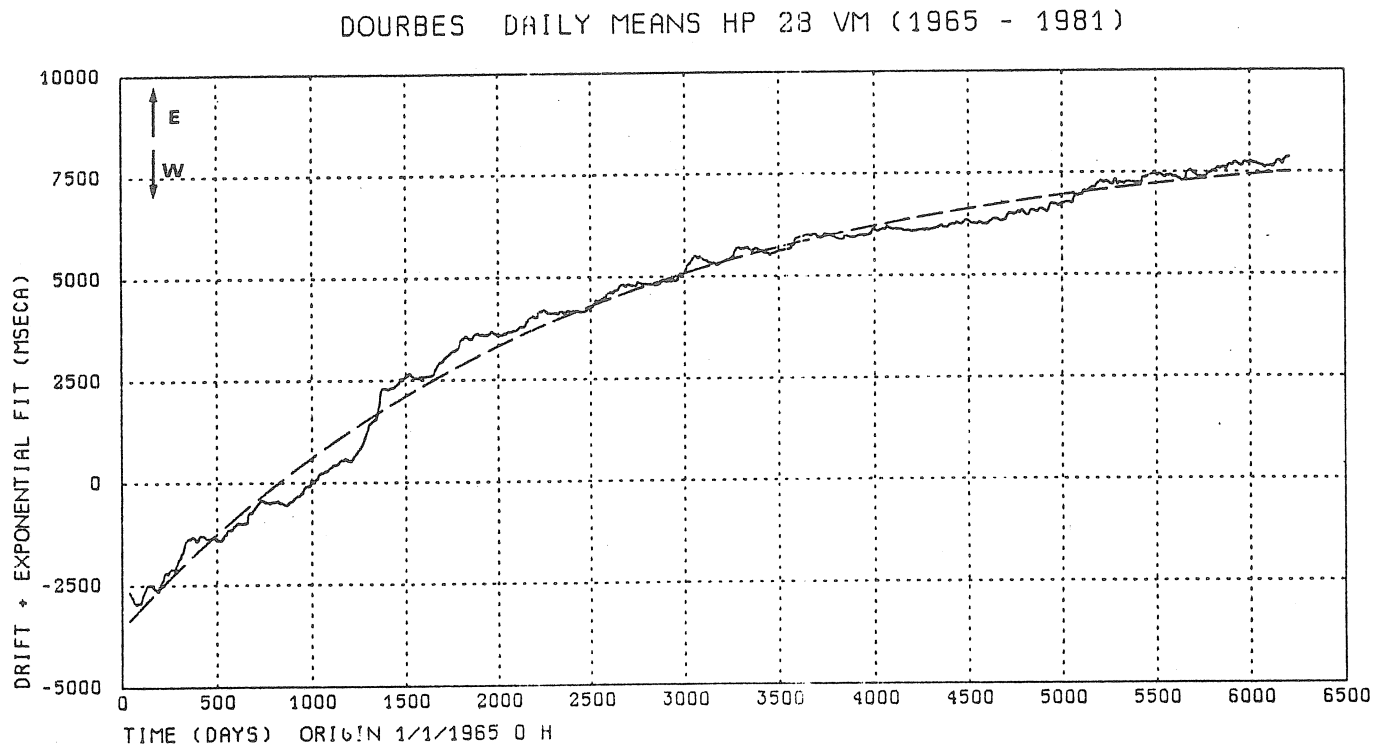

Fig. 1.b.- Daily means of horizontal pendulumn observations.

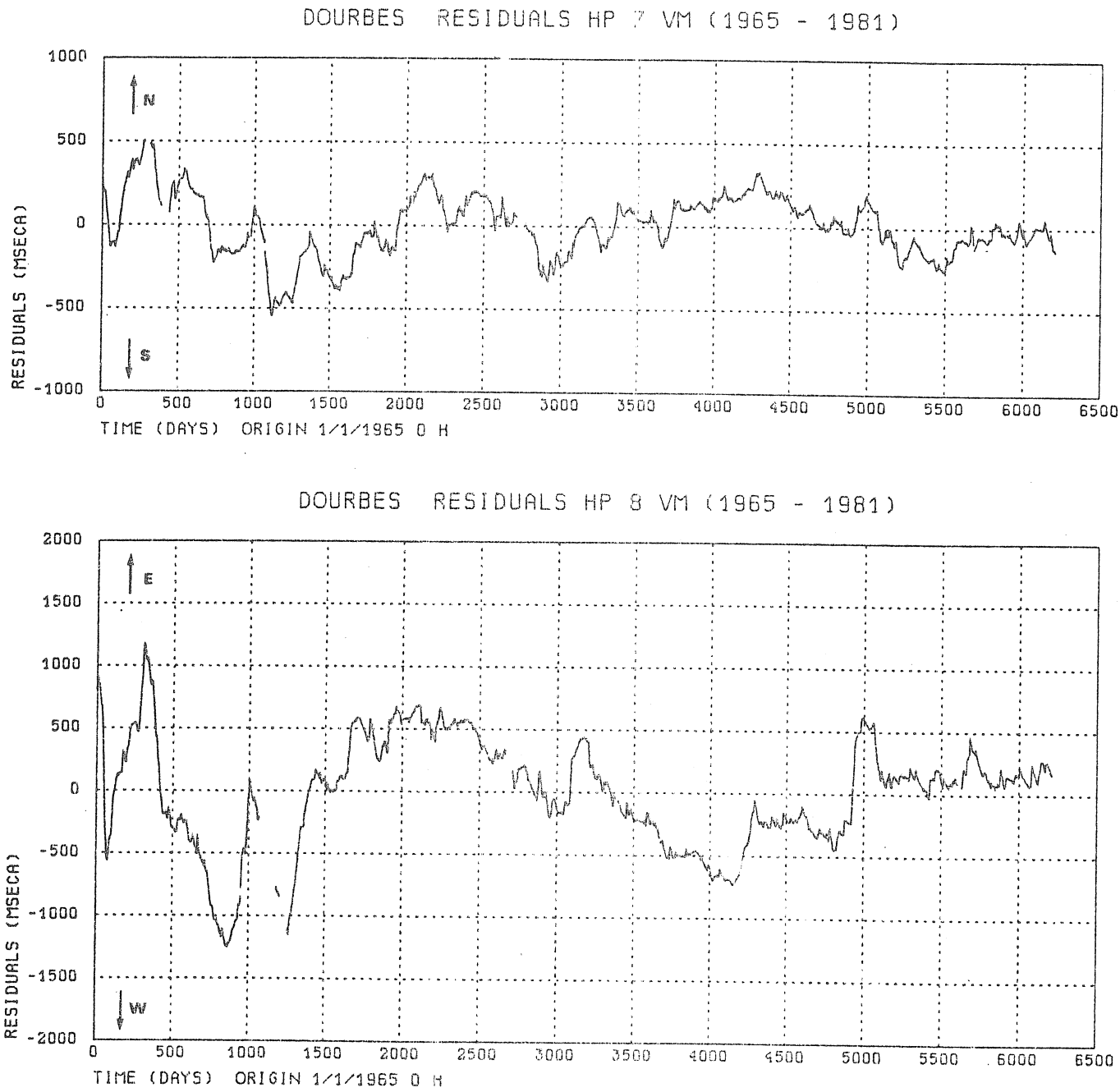

Fig. 2.a.- Residuals $\epsilon_i(t)$ = daily means - exponential fit.

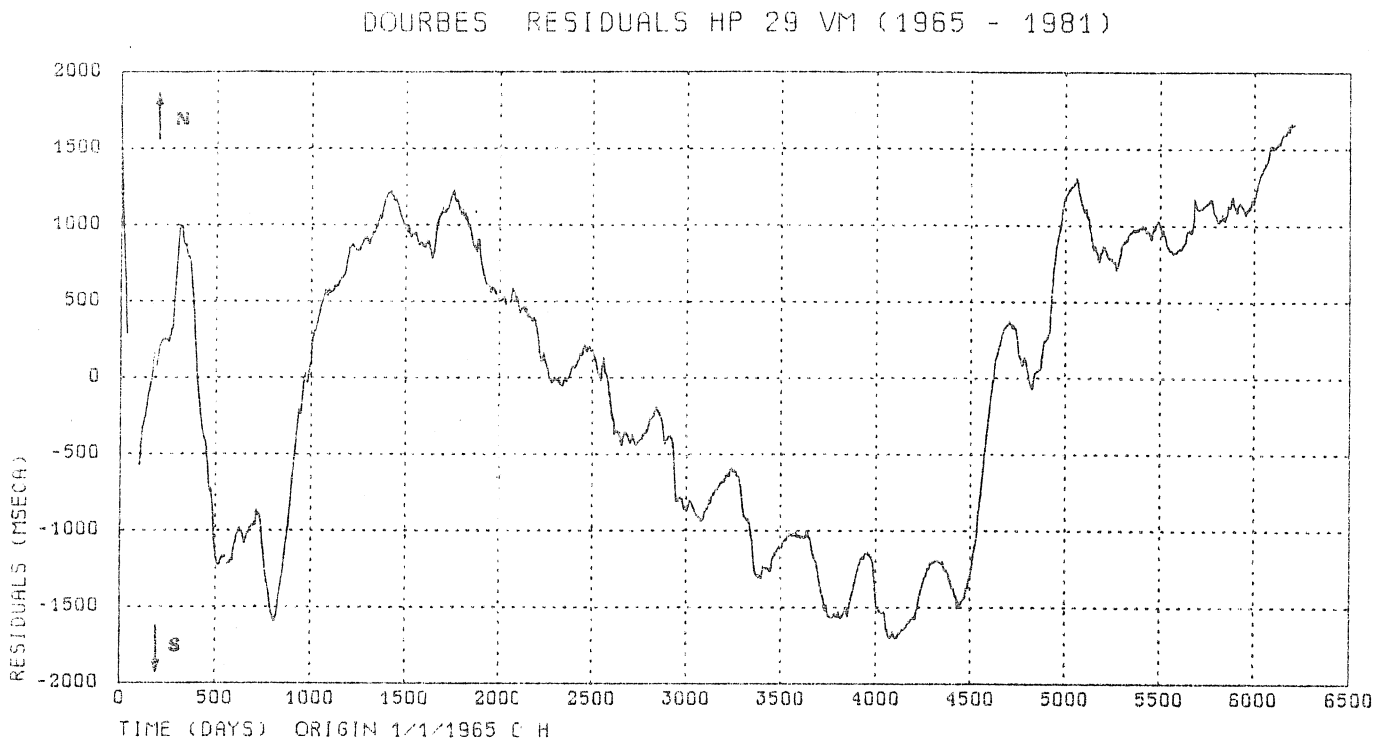

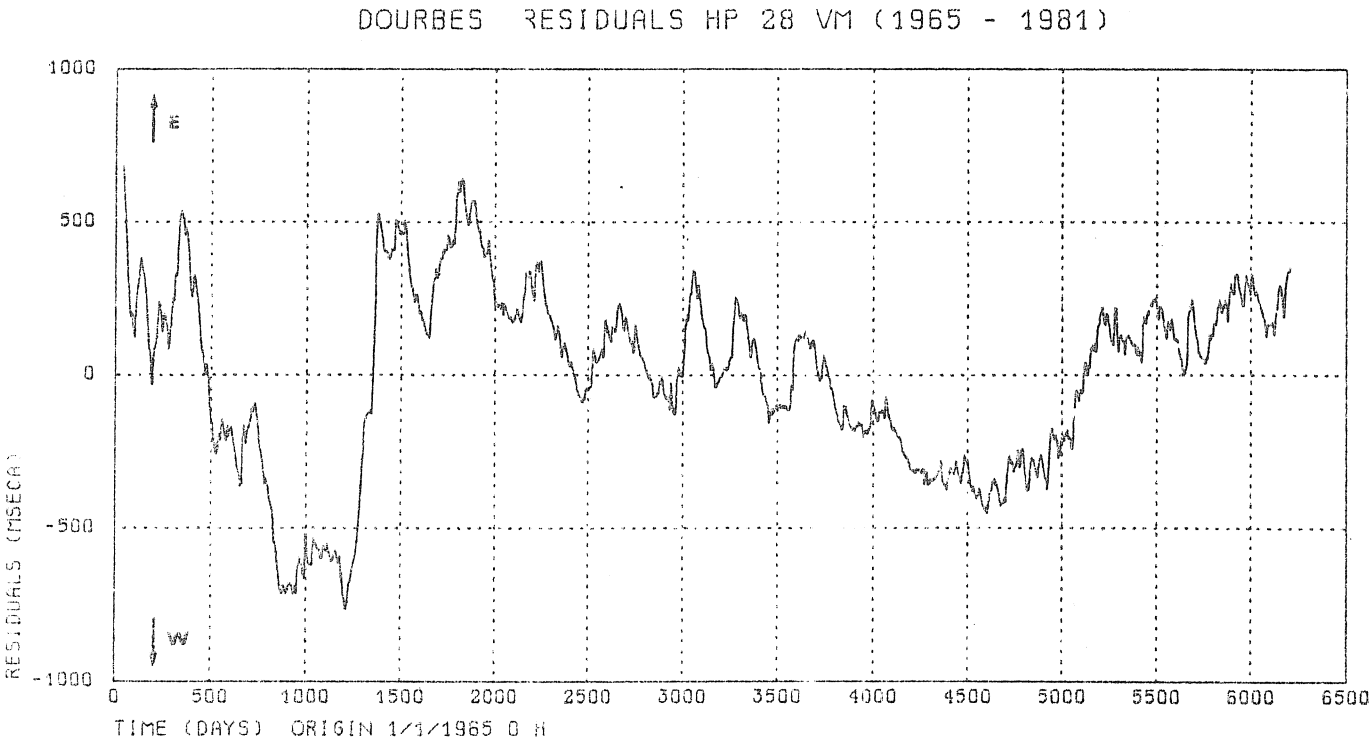

Fig. 2.b.- Residuals $\varepsilon_1(t)$ = daily means - exponential fi

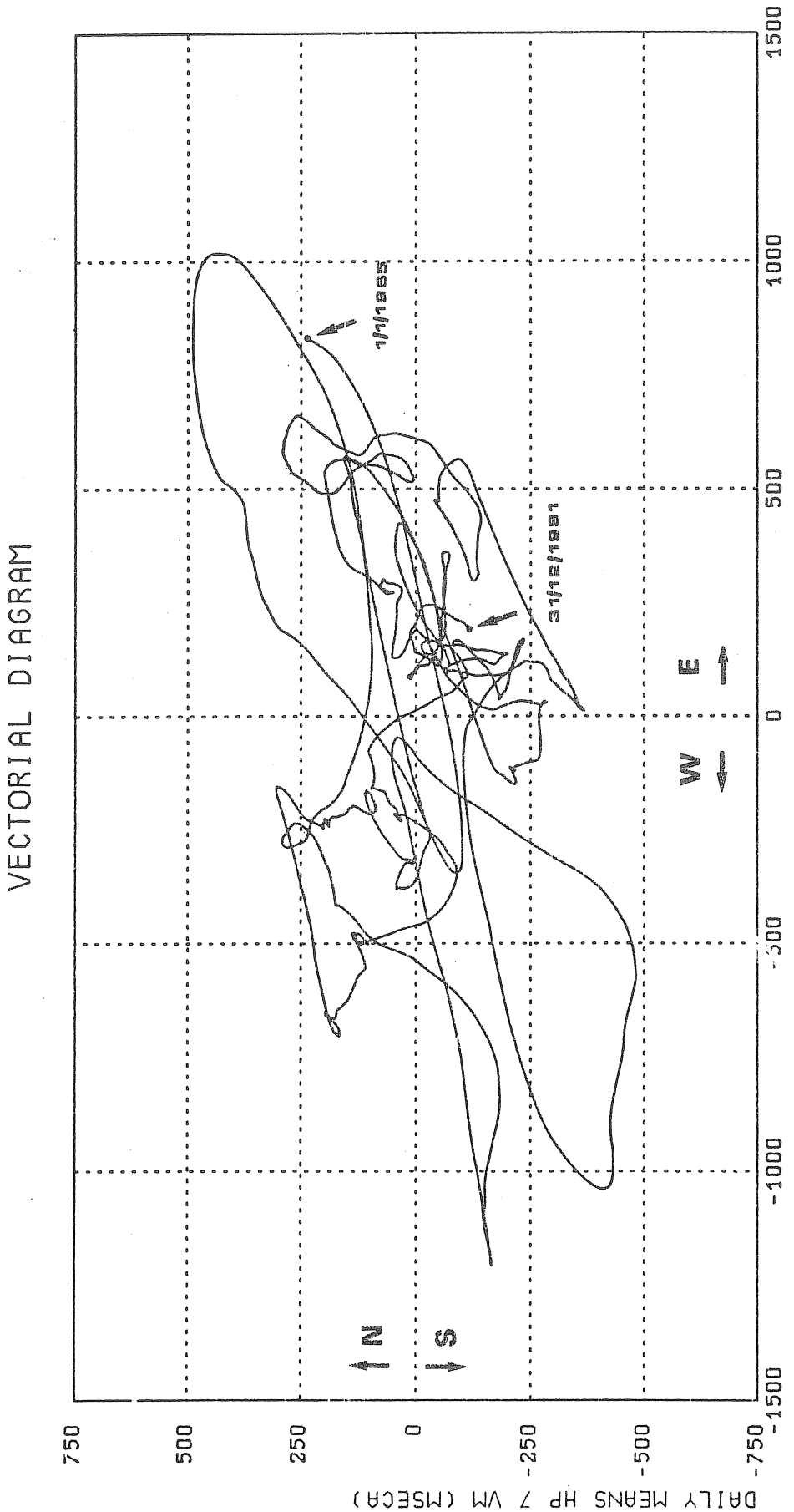

Fig. 3.a.- Vectorial diagram residuals $\epsilon_1(t)$.

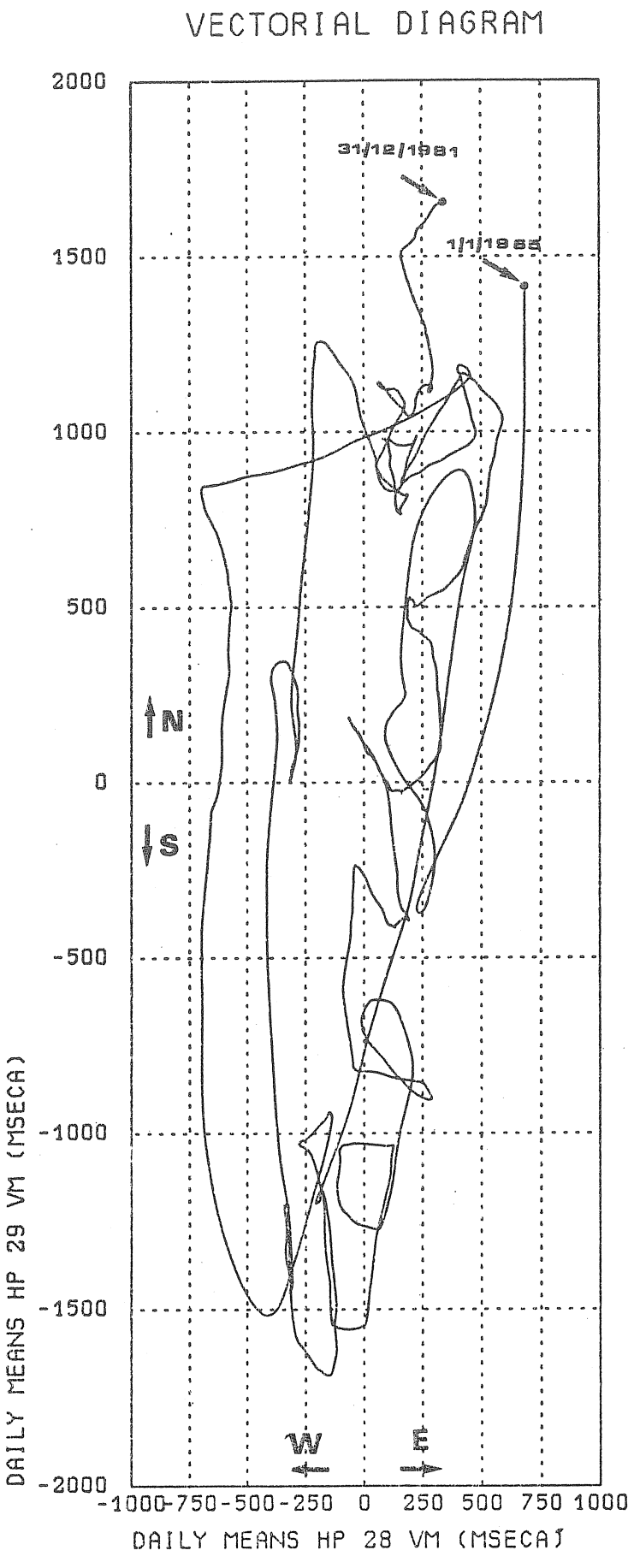

Fig. 3.b.- Vectorial diagram residuals $\epsilon_1(t)$.

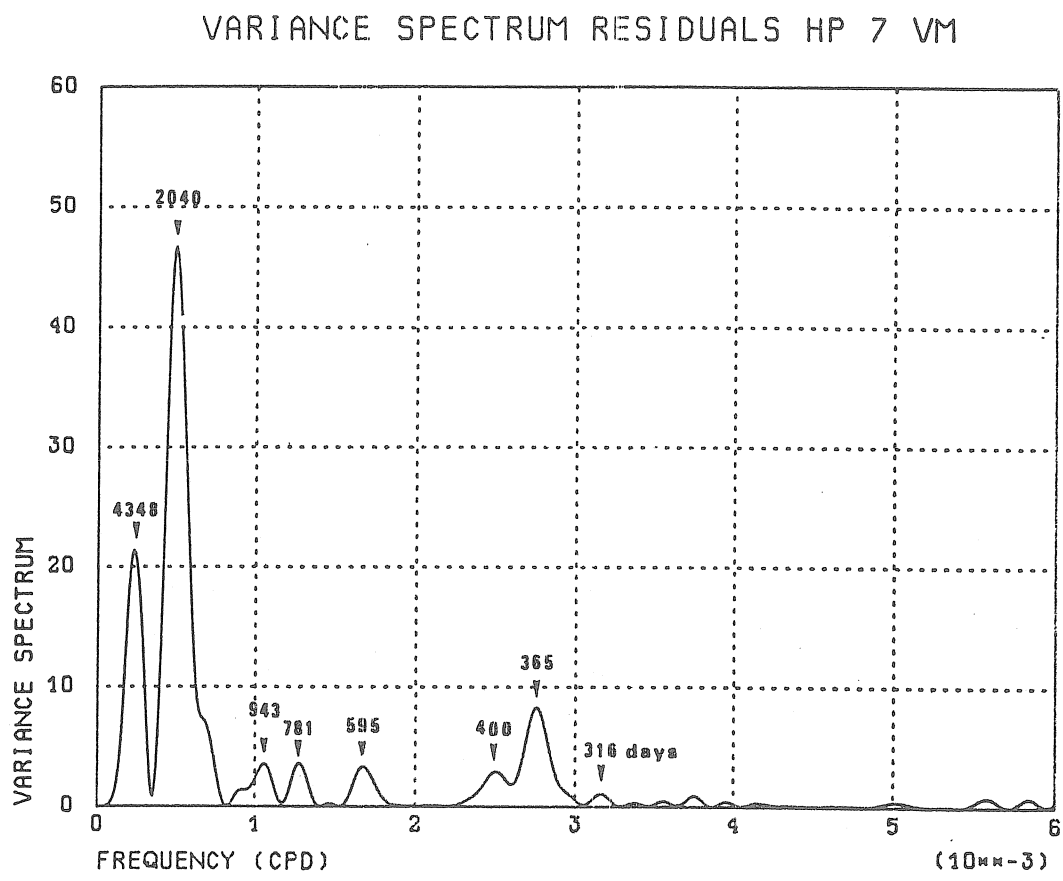

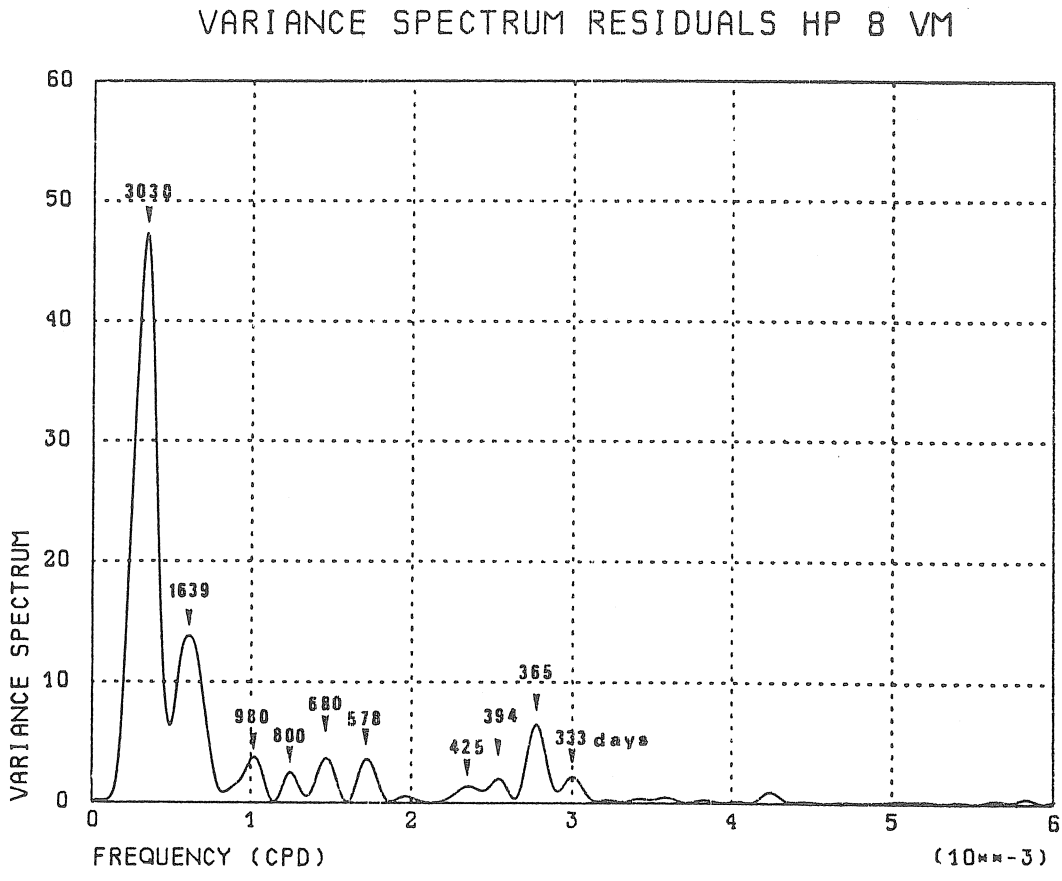

Fig. 4.a.- Variance spectrum of the residuals $\epsilon_1(t)$.

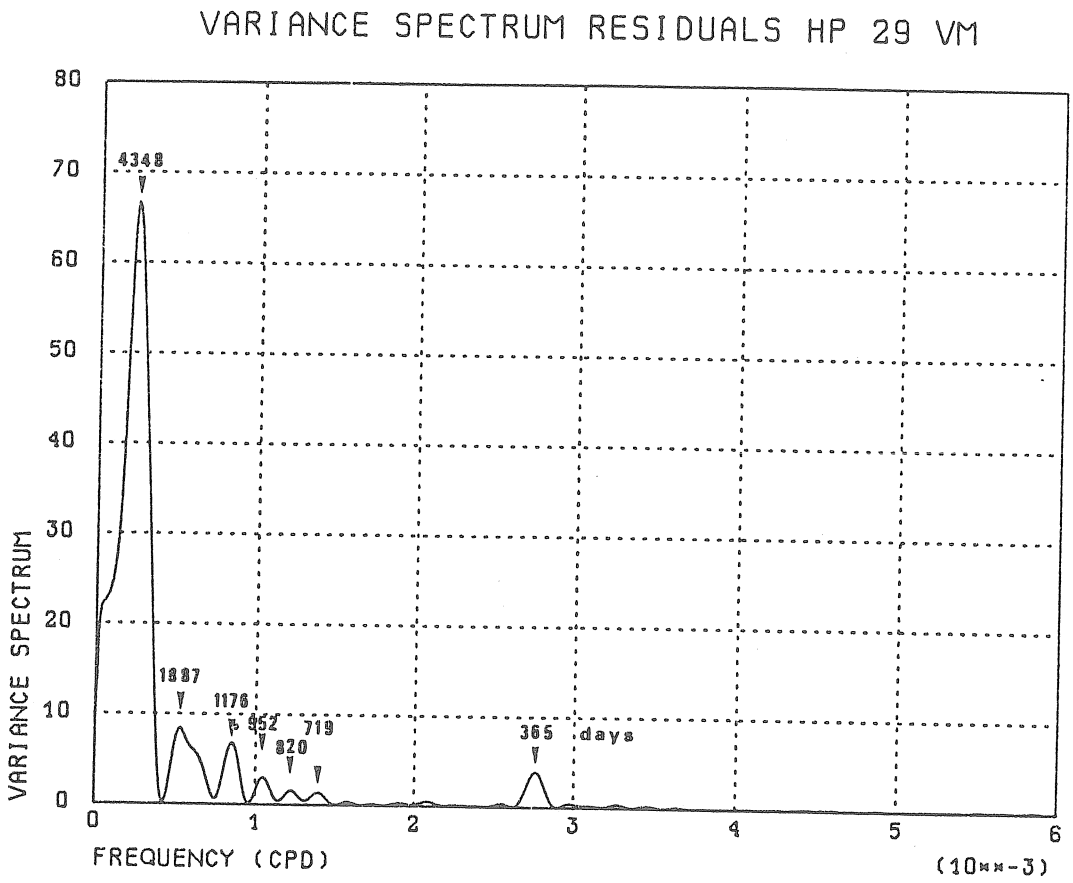

Fig. 4.b.- Variance spectrum of the residuals $\epsilon_1(t)$.

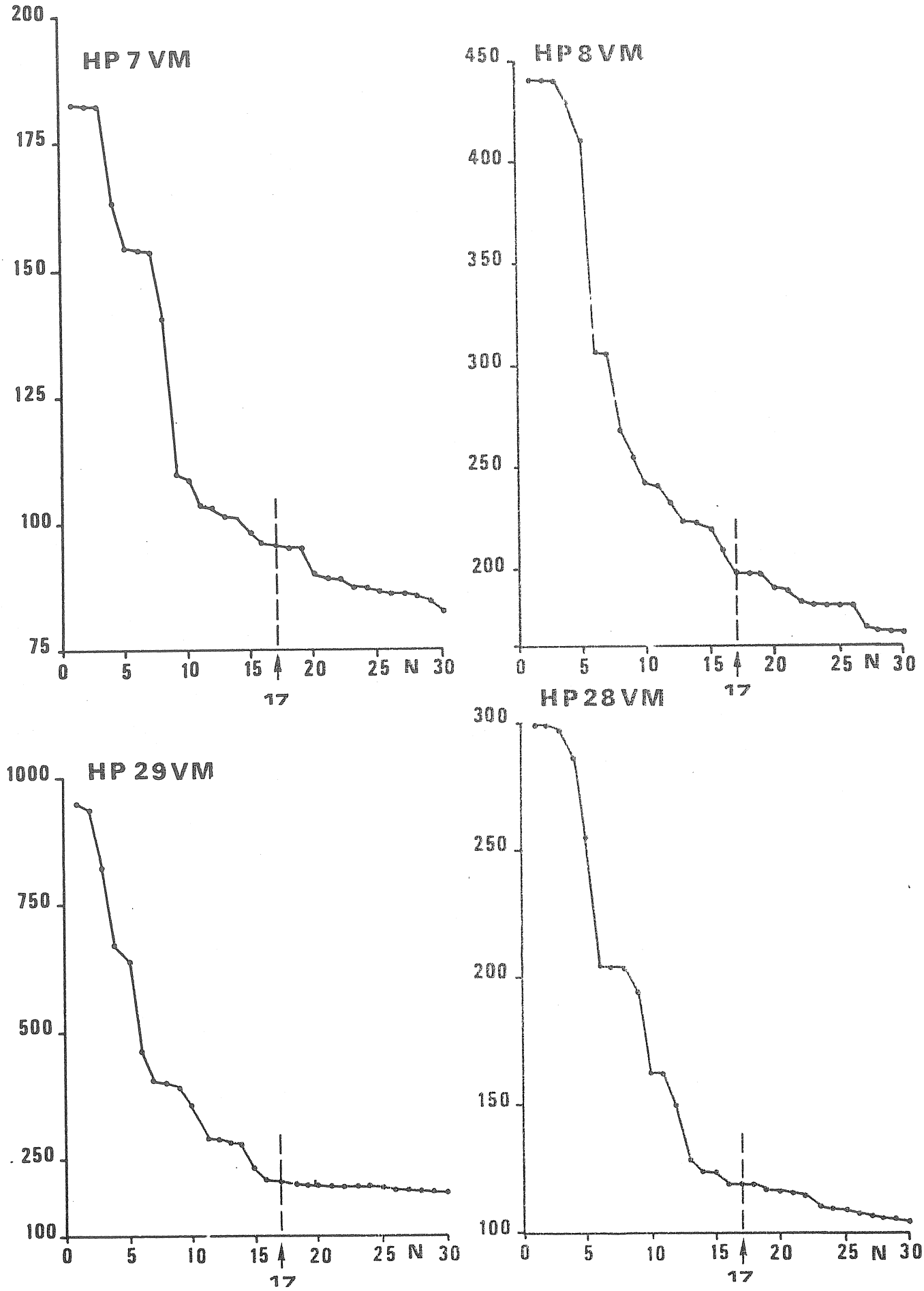

Fig. 5.- Standard deviation of $\epsilon_2(t)$ as a function of N.

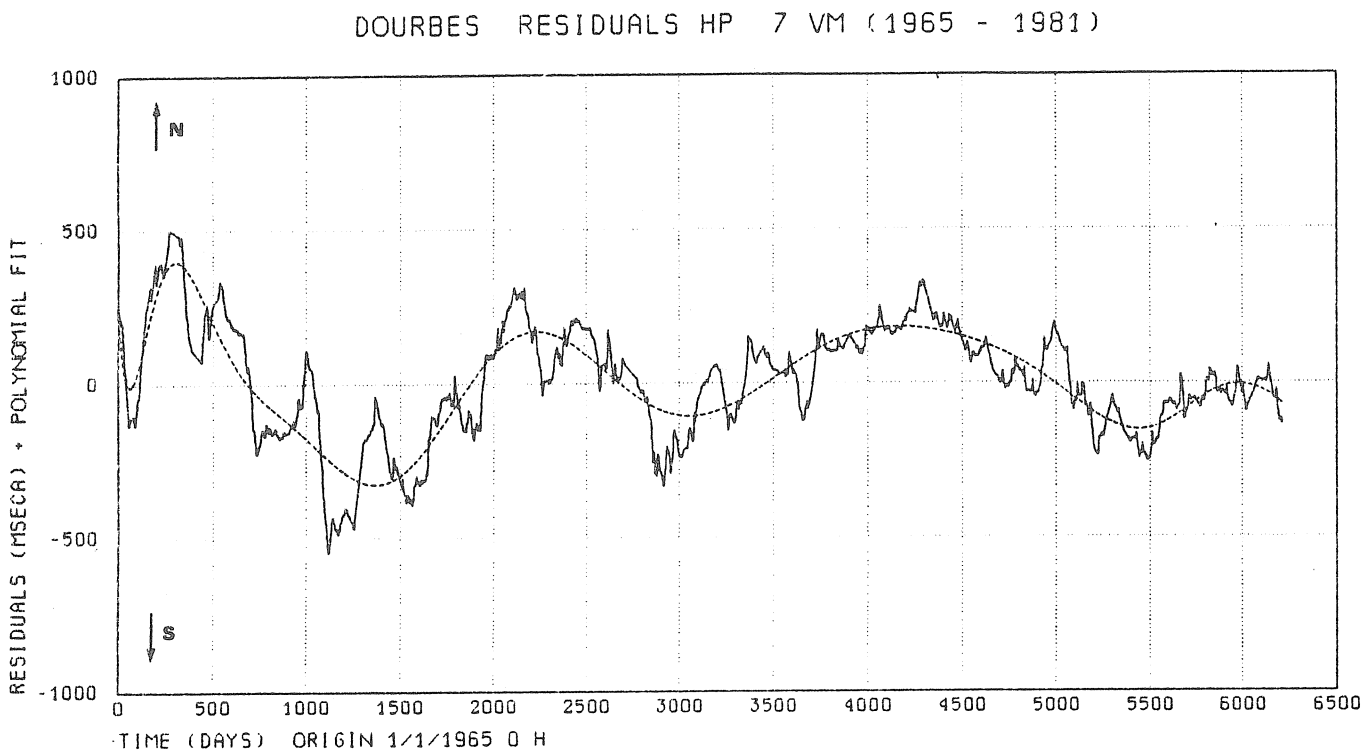

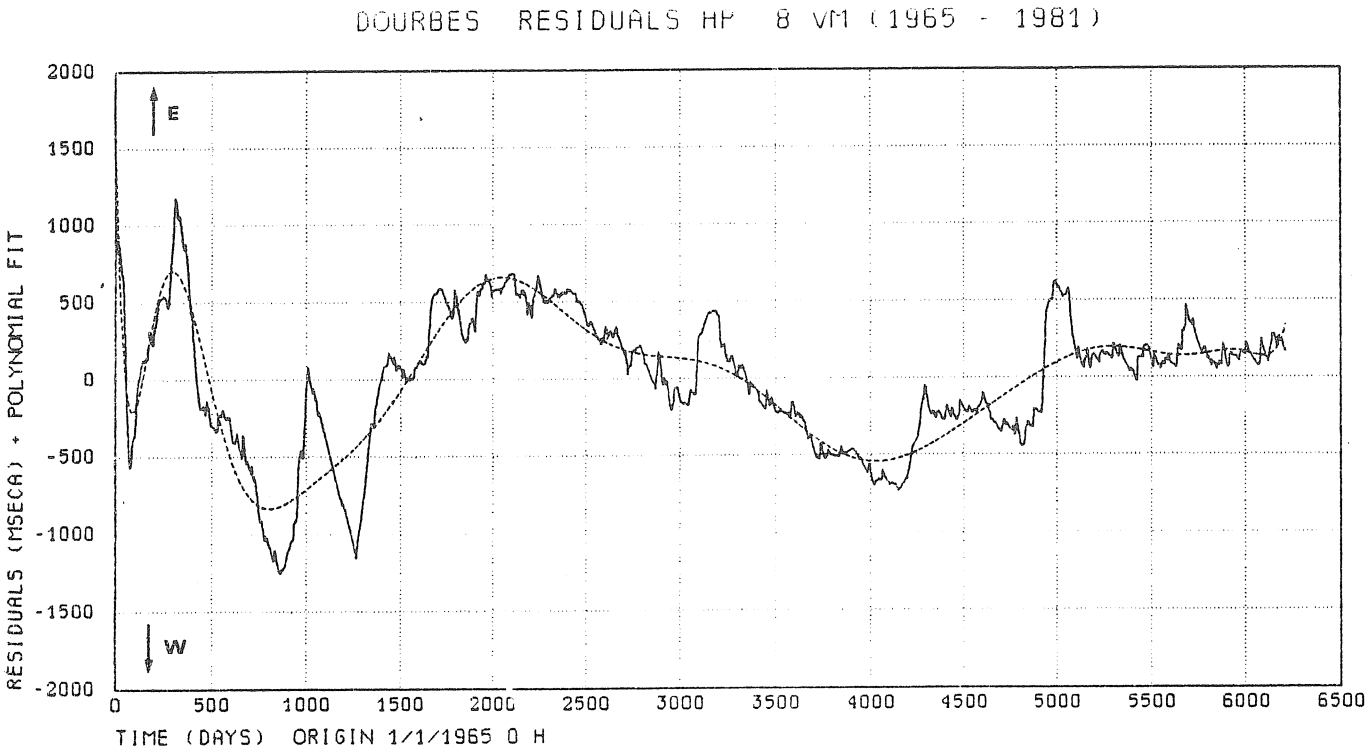

Fig. 6.a.- Polynomial fit to the residual series $\epsilon_1(t)$; linear interpolation of $\epsilon_1(t)$.

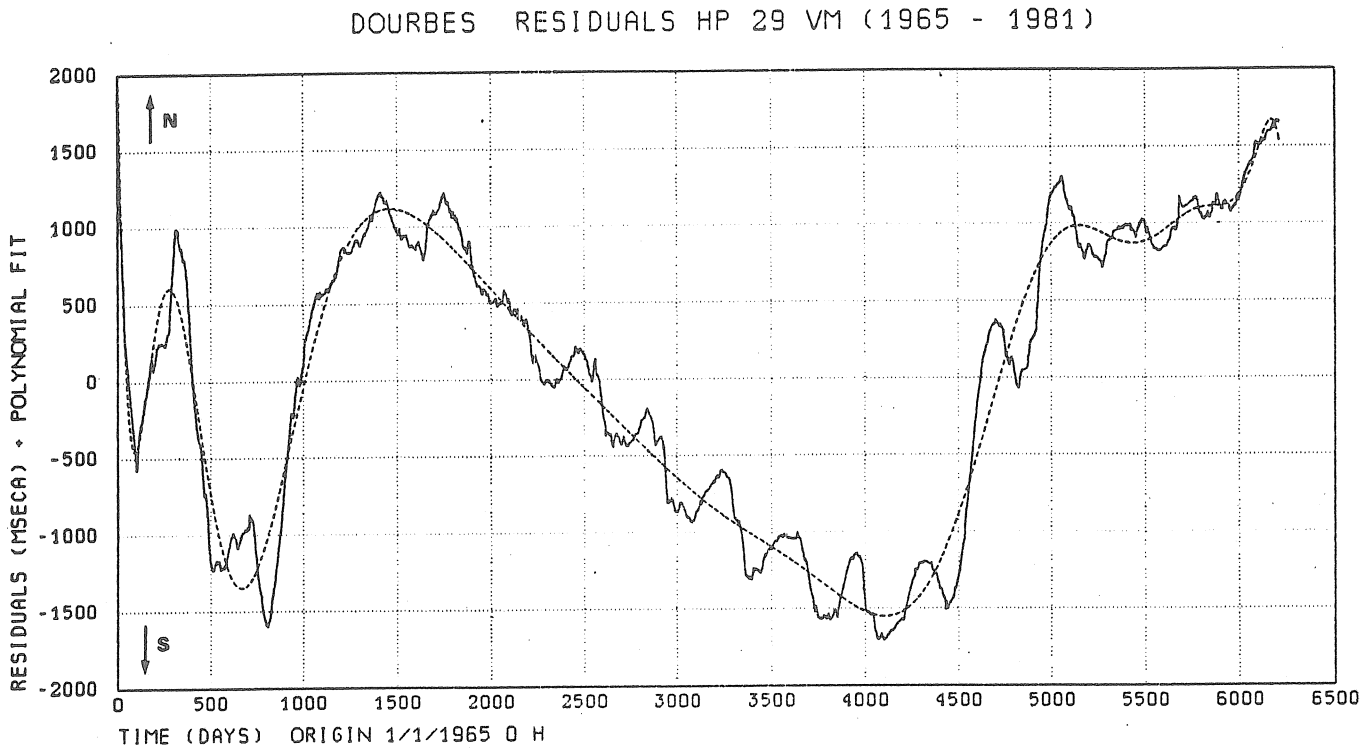

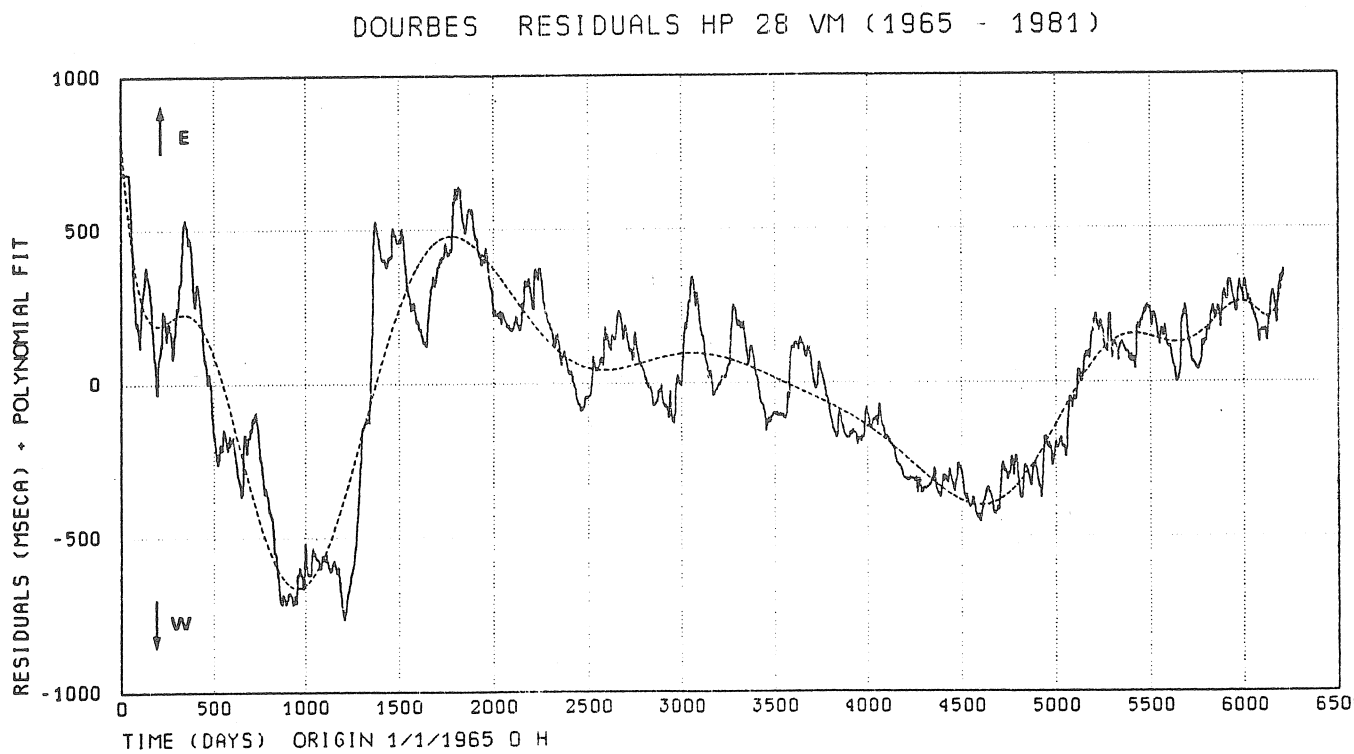

Fig. 6.b.- Polynomial fit to the residual series $\epsilon_1(t)$; linear interpolation of $\epsilon_1(t)$.

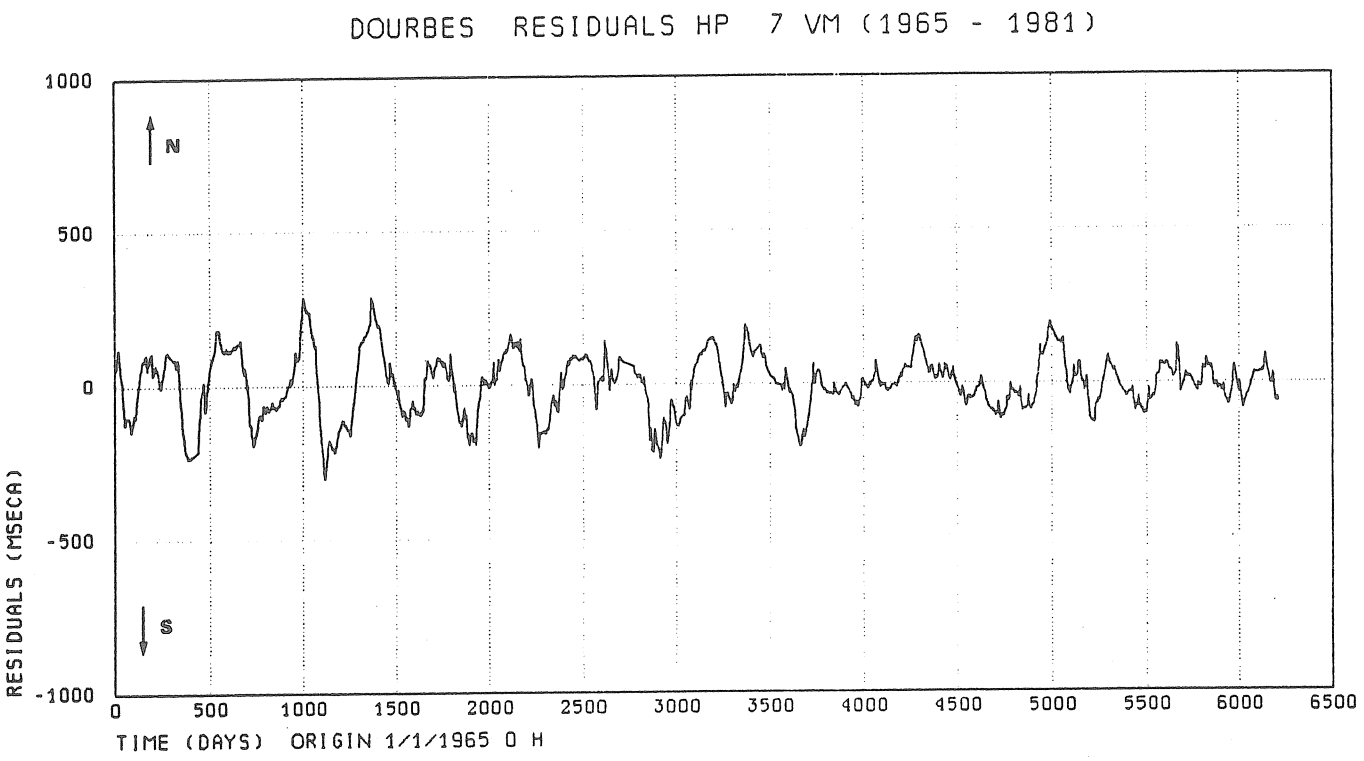

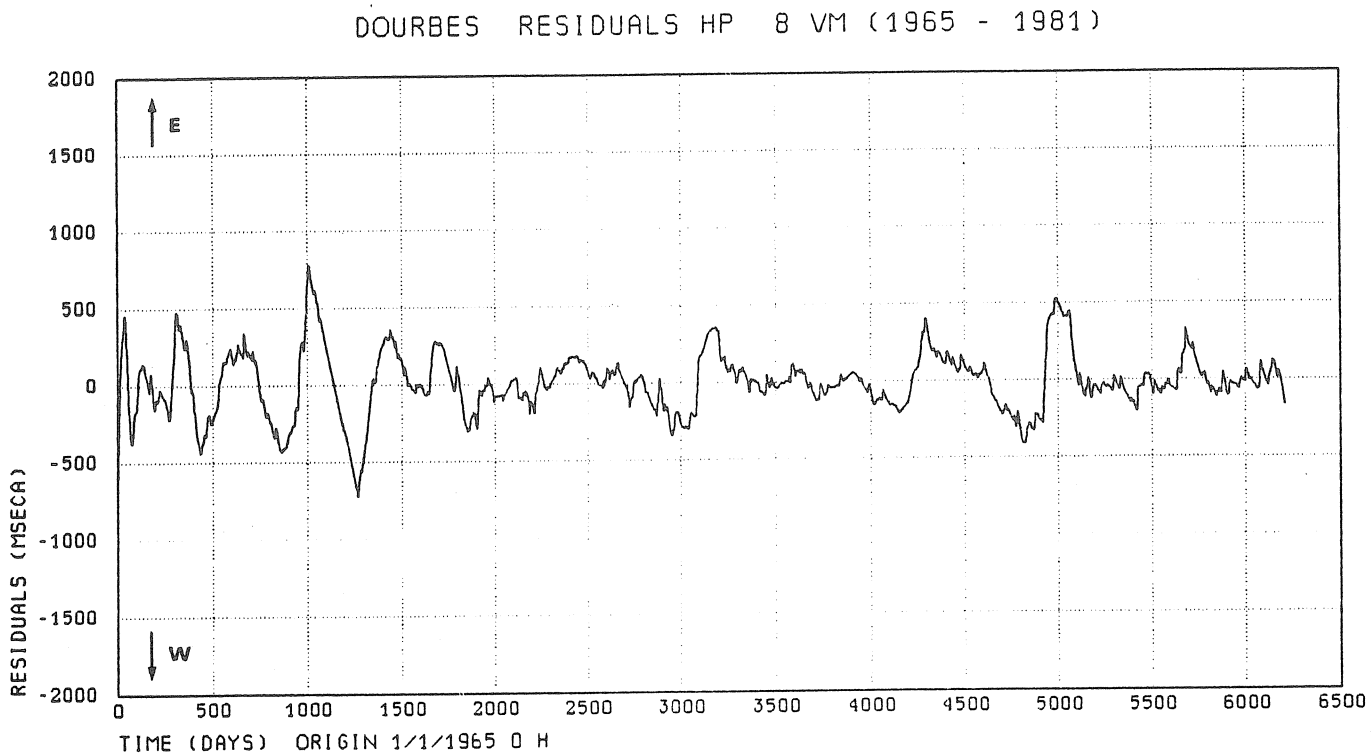

Fig. 7.a.- Residuals $\epsilon_2(t)$ = daily means - exponential fit - polynomial fit.

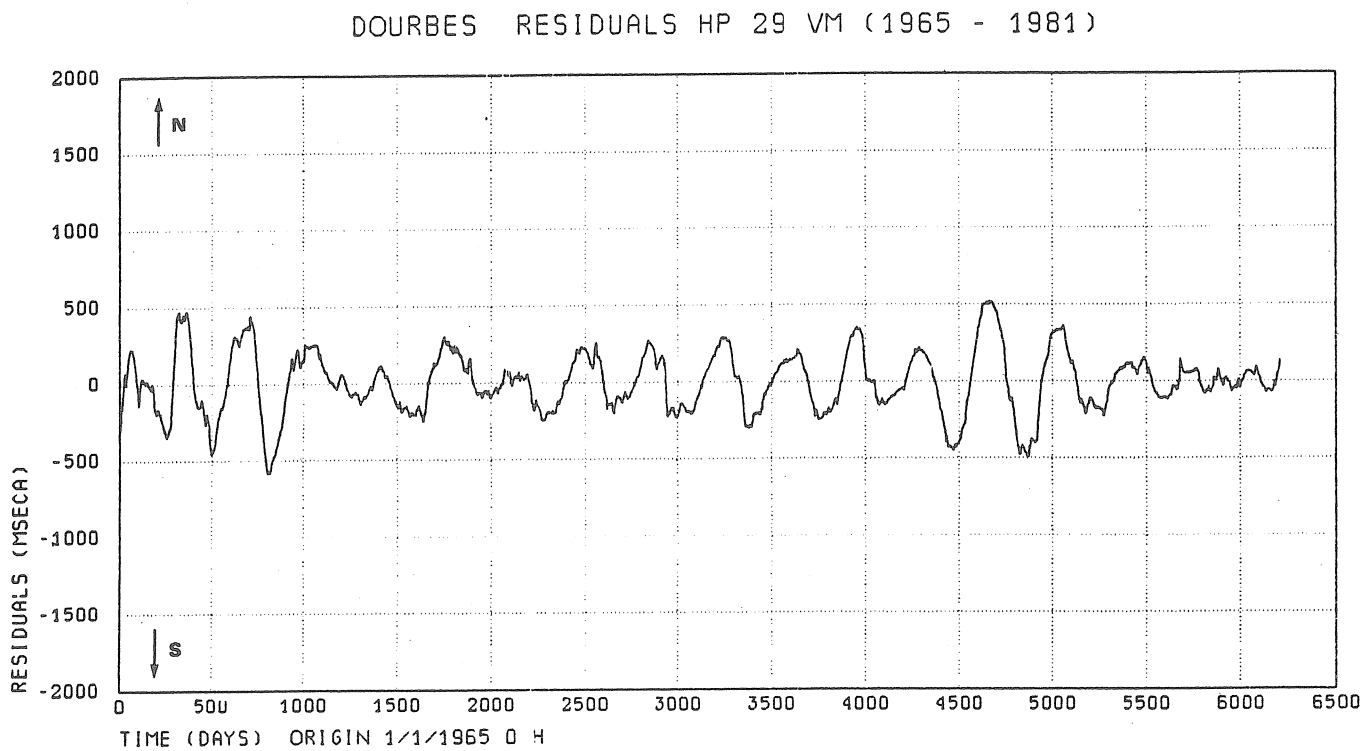

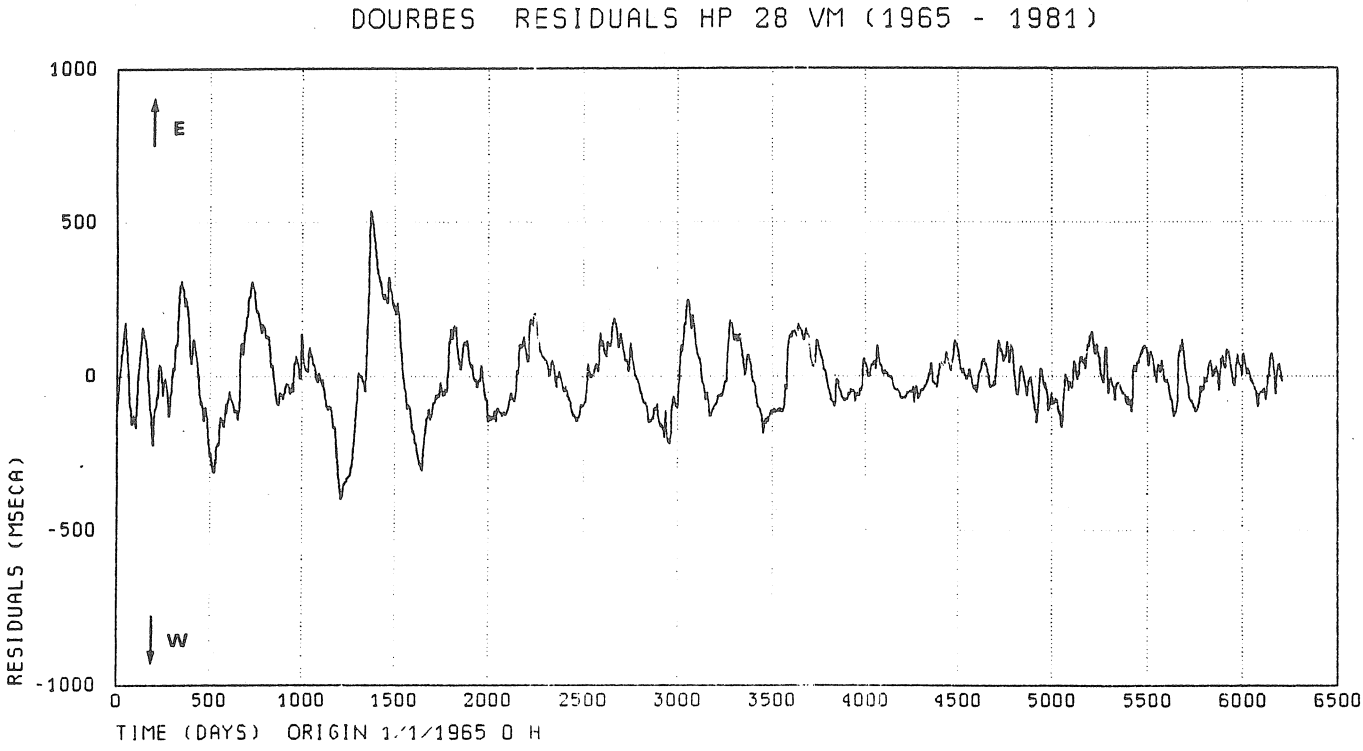

Fig. 7.b.- Residuals $\epsilon_2(t)$ = daily means - exponential fit - polynomial fit

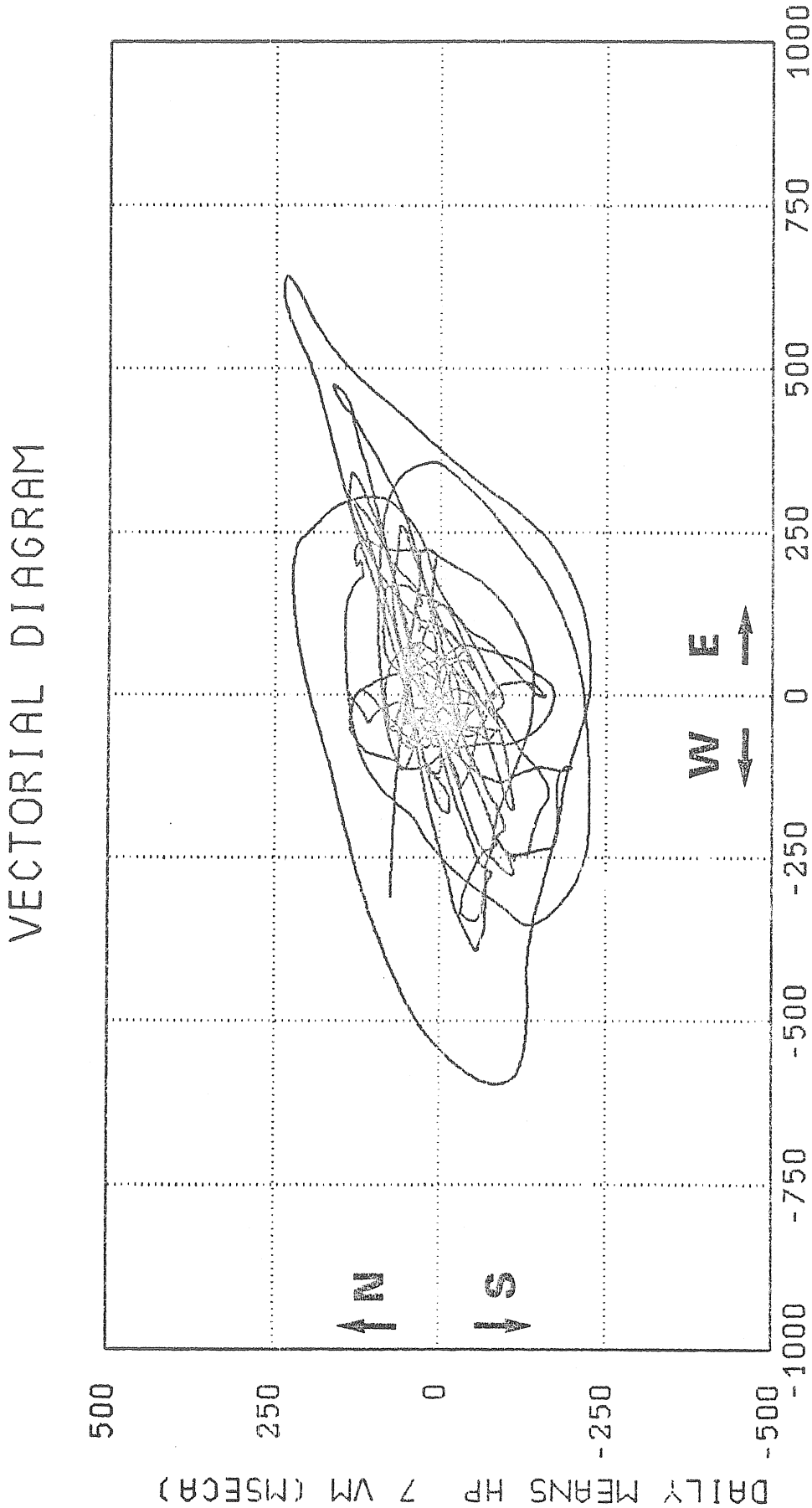

Fig. 8.a.- Vectorial diagram residuals $\epsilon_2(t)$.

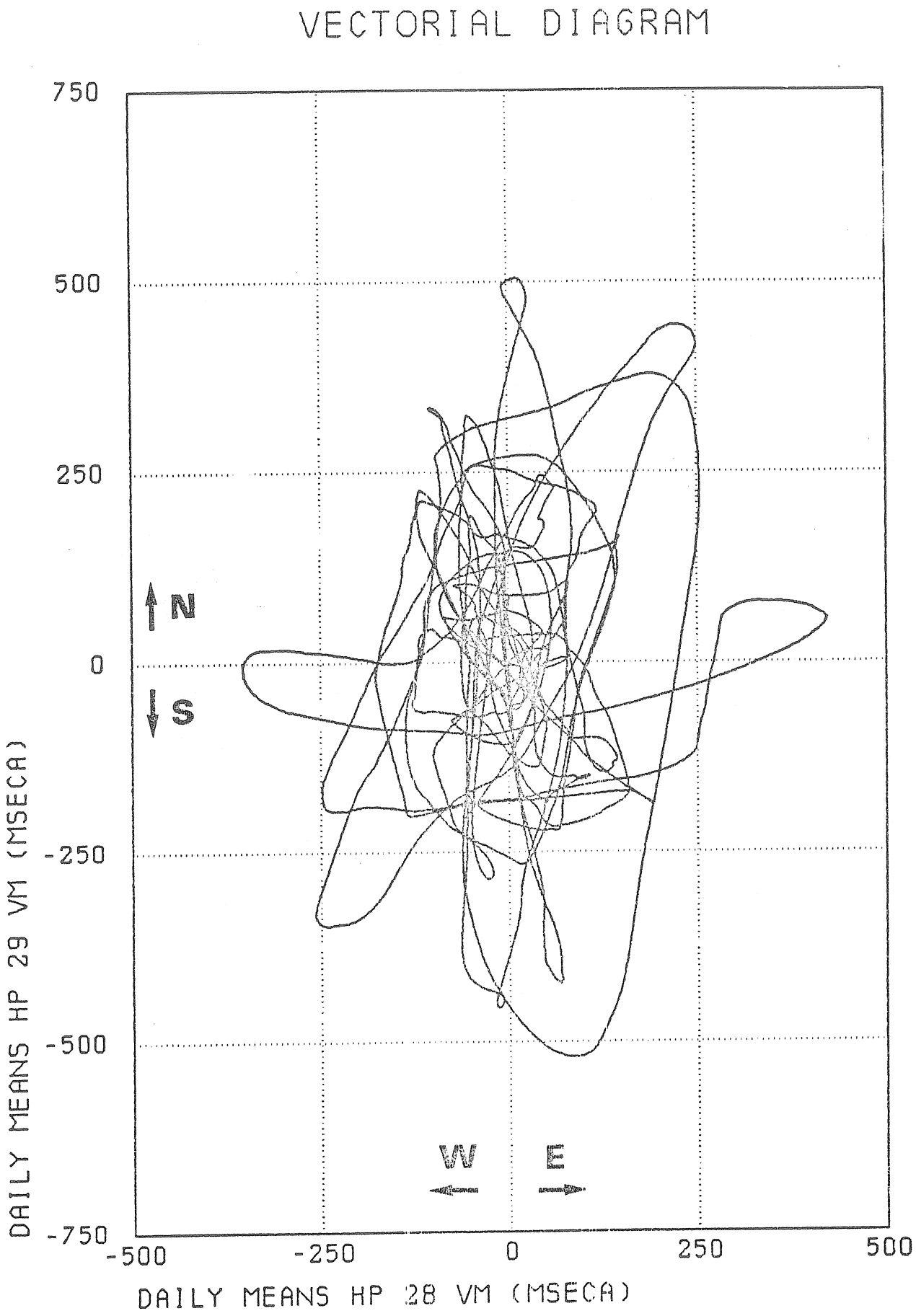

Fig. 8.b.- Vectorial diagram residuals $\epsilon_2(t)$.

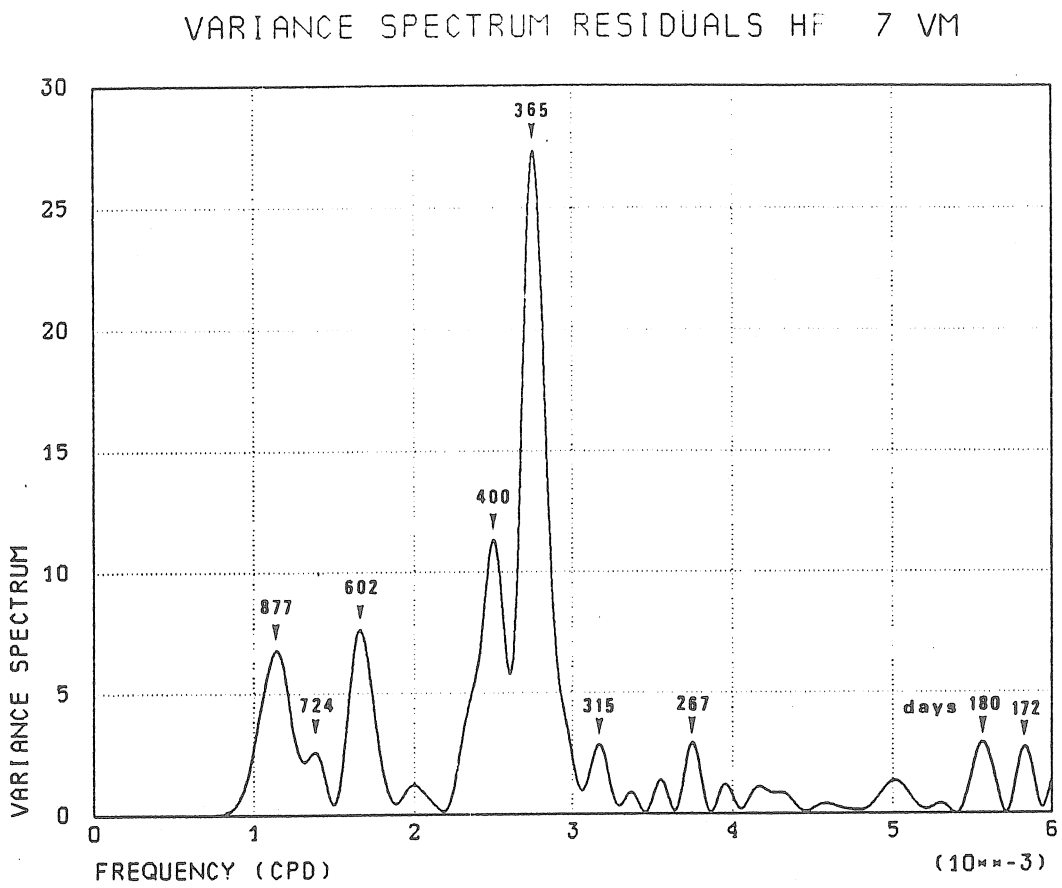

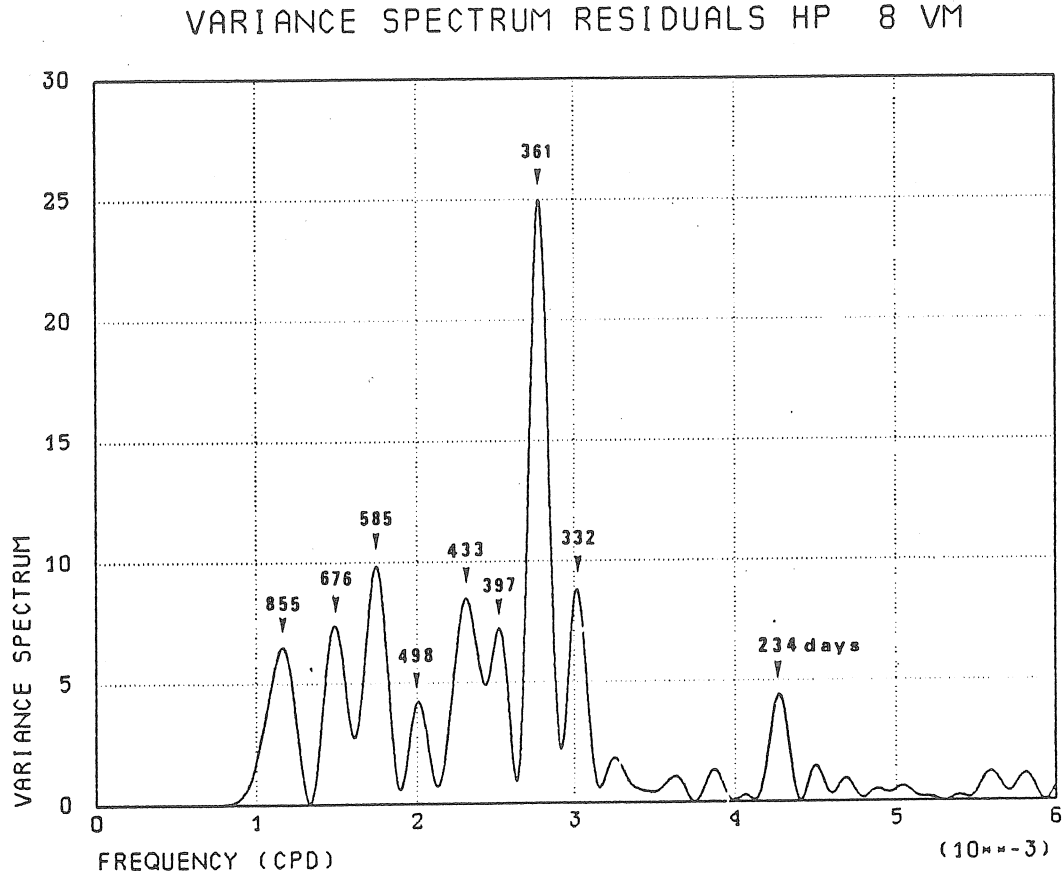

Fig. 9.a.- Variance spectrum of the resuduals $\epsilon_2(t)$.

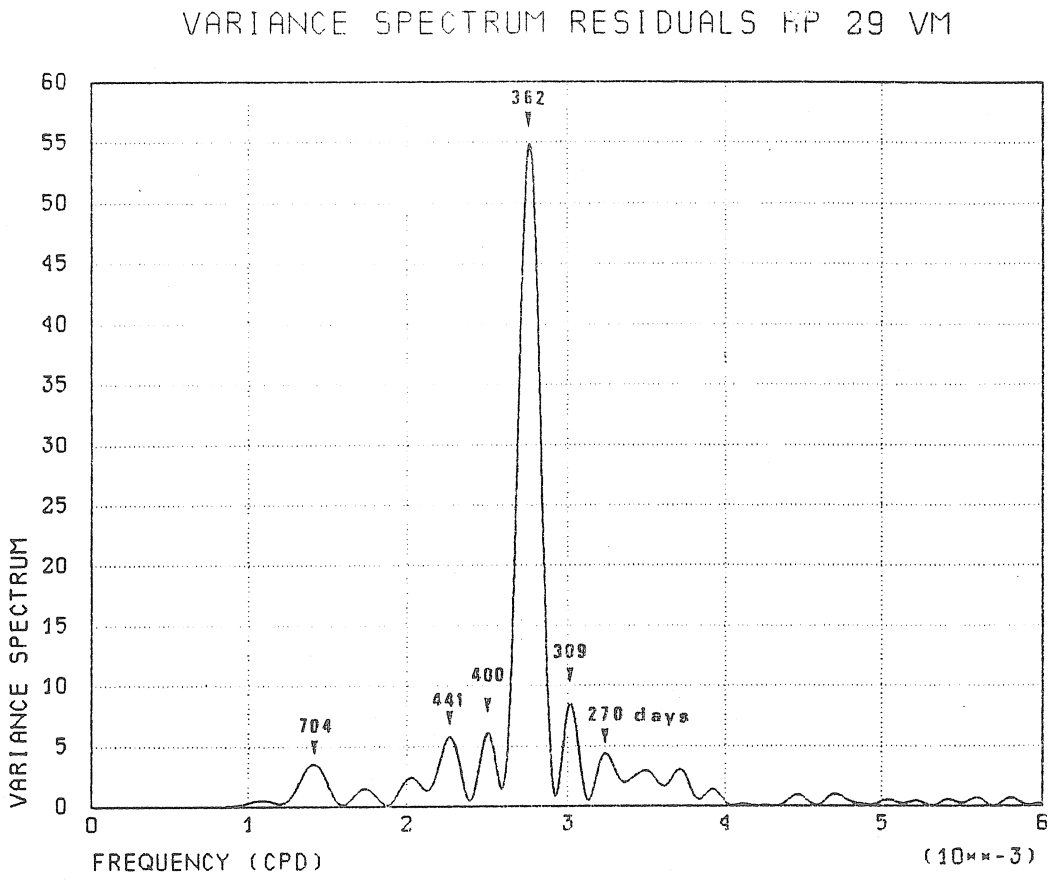

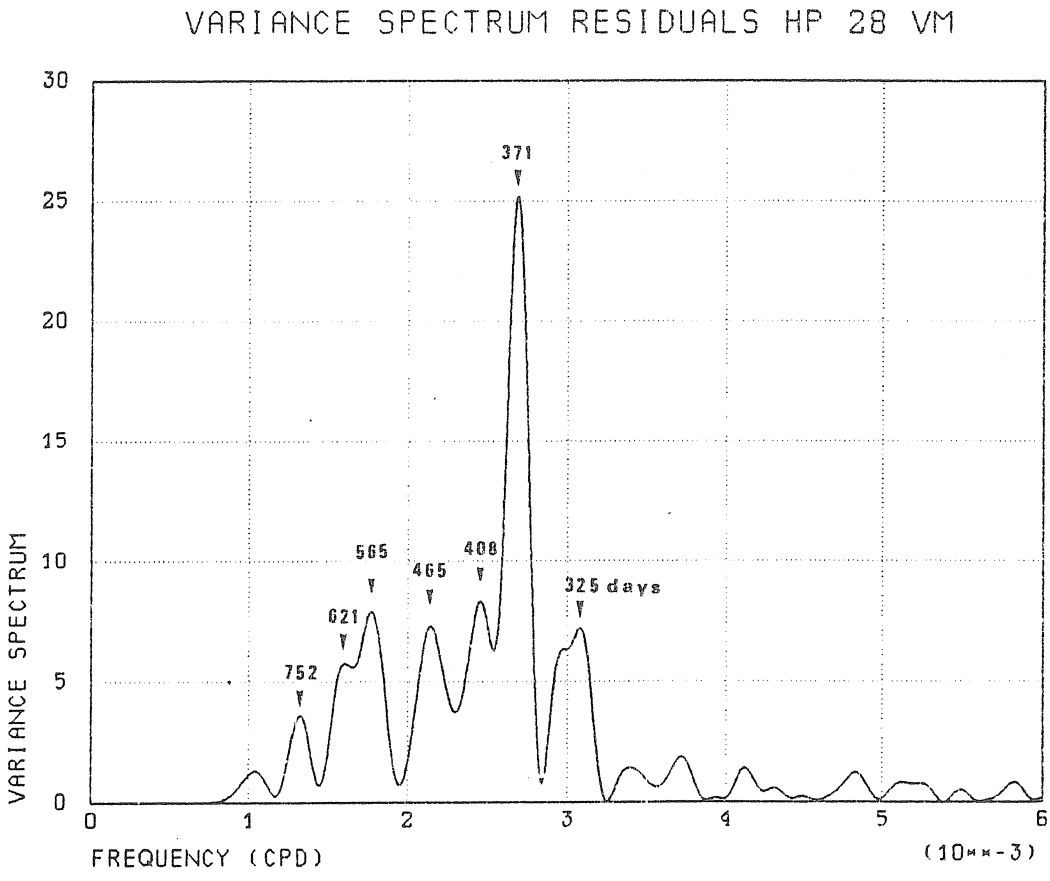

Fig. 9.b.- Variance spectrum of the residuals $\epsilon_2(t)$.

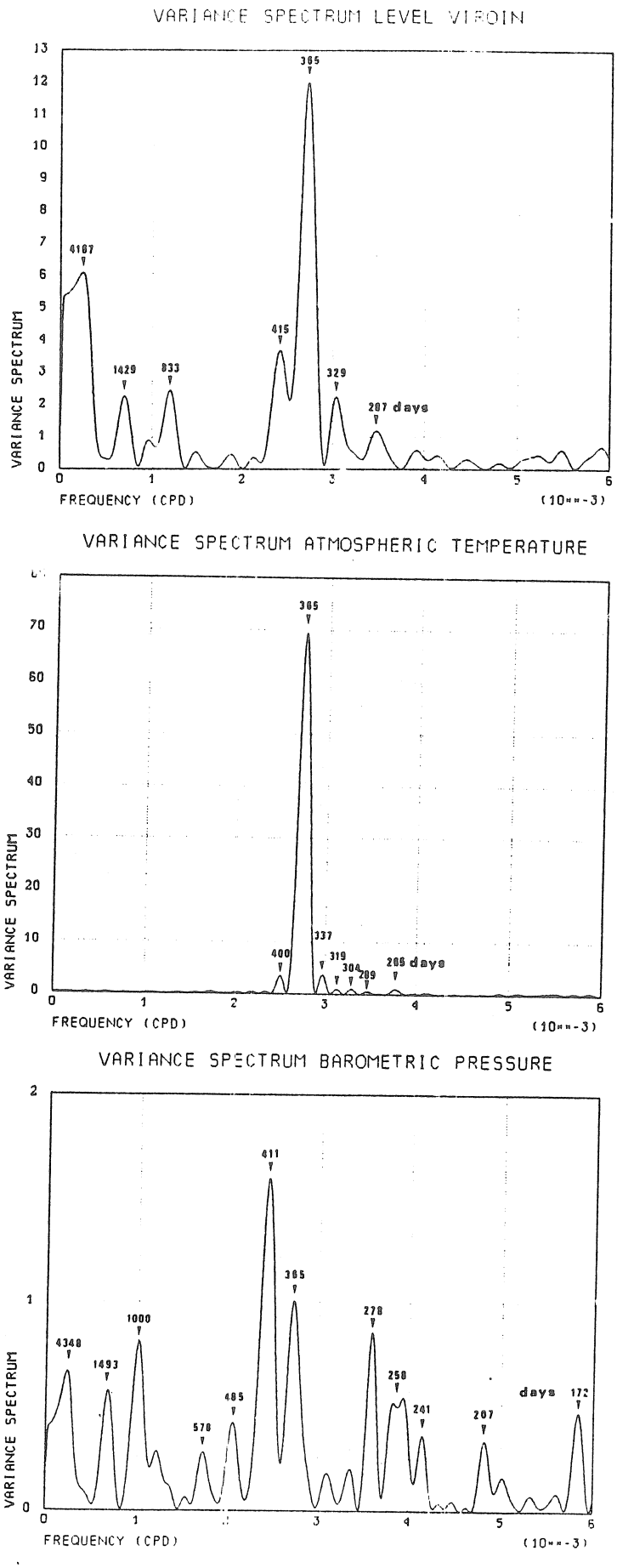

10.- Variance spectrum of the daily means of the atmospheric temperature, barometric pressure and level of the river Viroin.

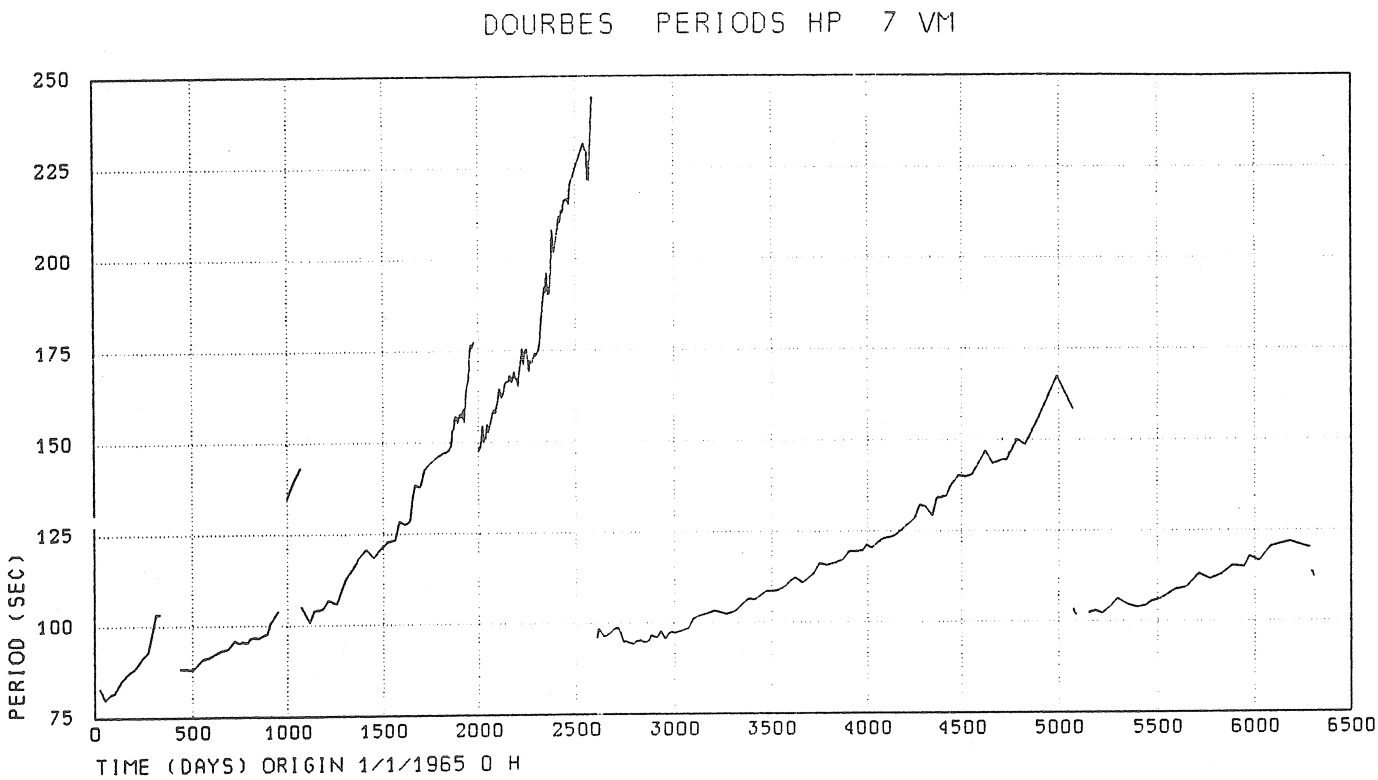

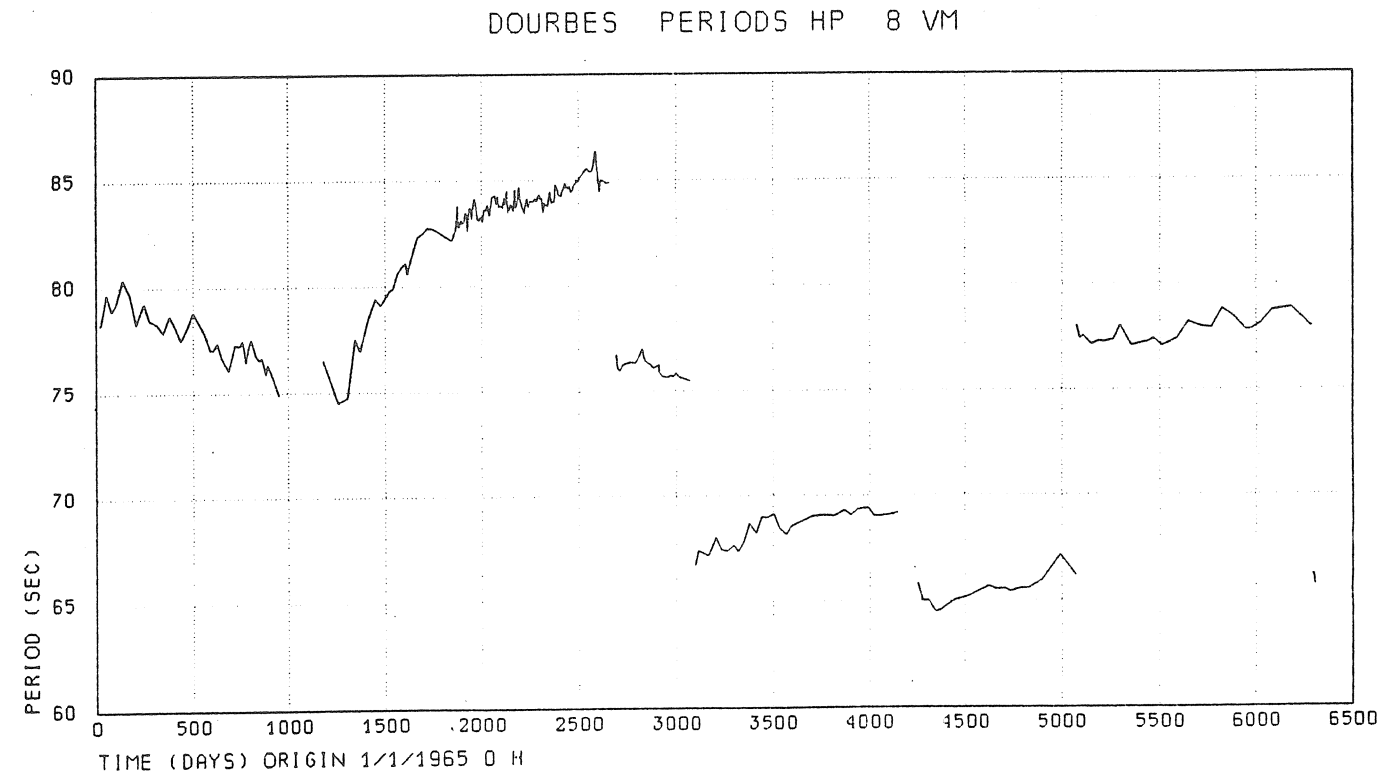

Fig. 11.a.- Period of the VM inclinometers.

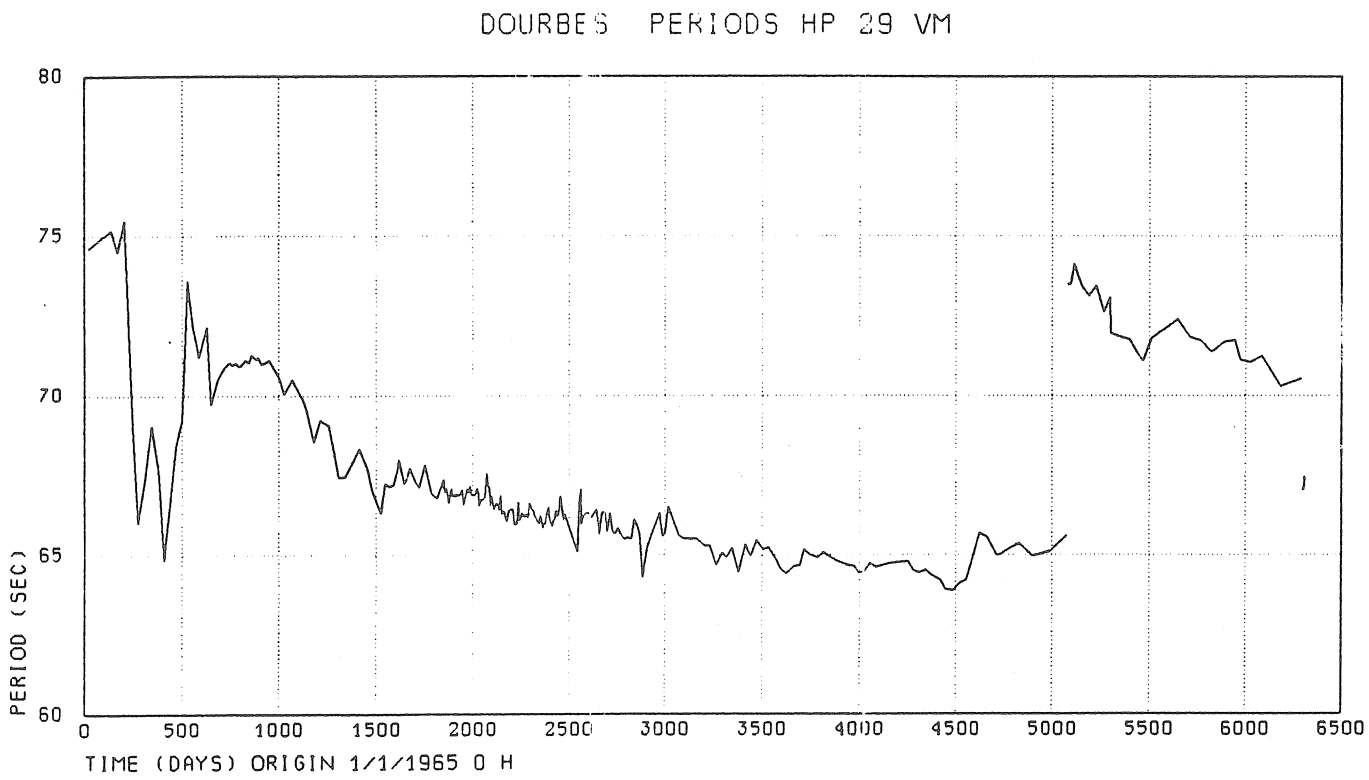

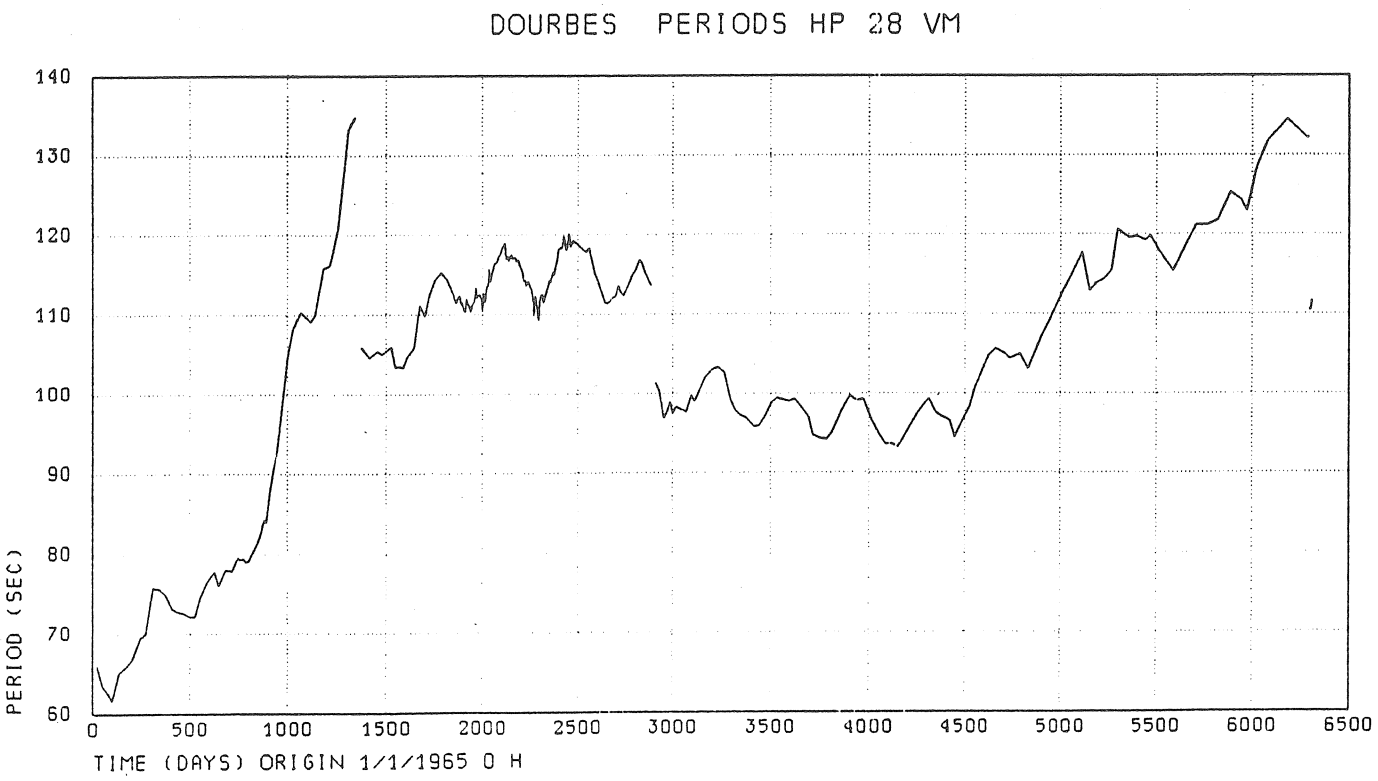

Fig. 11.b.- Period of the VM inclinometers.

REFERENCES

BARD Y., 1974, Nonlinear parameter estimation, Academic Press, New-York.

DOPP, S., 1964; La station de marées terrestres de Dourbes, Cinquième Symposium International sur les Marées Terrestres, Obs. Roy. Bel., Comm. 236, série Géoph. 69, 187-193.

LECOLAZET, R., 1961, Sur l'interpolation de données manquantes, Quatrième Symposium International sur les Marées Terrestres, Obs.Roy.Bel., Comm. 188, série Géoph. 58, 267-272.

MELCHIOR, P., 1978, The tides of the Planet Earth, Pergamon Press, Oxford.

VANICEK, P., 1970, An analytical technique to minimize noise in a search for lines in the low frequency spectrum, Obs. Roy. Belg., Comm. série A, 9, série Géoph. 96, 170-173.

RESULTATS DE LA REDUCTION PAR SERIES MENSUELLES D'UNE SERIE ANNUELLE D'OBSERVATIONS D'INCLINAISONS DE MAREES PAR TROIS METHODES DIFFERENTES

B.S. Doubik et P.S. Matvéev

Rotation et Déformations de Marées de la Terre n°13 pp38-45, 1981

(Abrégé)

Au cours des vingt dernières années des méthodes de réduction par séries mensuelles ont été développées en URSS et l'on peut en distinguer quatre qui sont décrites dans les travaux [1, 11, 2, 12]. Une particularité des deux premières est qu'elles sont connues en détails et basées sur la théorie des combinaisons d'ordonnées élaborée par Labrouste [3 p48].

Dans les schémas de calcul des deux méthodes suivantes (Venedikov, Matvéev) les valeurs les plus probables des paramètres des ondes de marée sont déterminées en utilisant sous la même forme la méthode des moindres carrés. Ceci garantit une bonne stabilité des résultats.

L'un des auteurs a proposé récemment une nouvelle méthode [4] dans laquelle aussi bien qu'en [12,2] il utilise la méthode des moindres carrés. Cette méthode a été vérifiée par comparaison avec la méthode Venedikov [12] et sa précision ne le cède en rien à celle-ci.

Nous donnons dans les Tables 1 et 2 les résultats de la nouvelle méthode appliquée mois par mois sur une série clinométrique ininterrompue de Soudievka, composante EW, du 20 février au 31 décembre 1971 obtenue avec le clinomètre Ostrovski n°9 [5].

TABLE 1: Valeurs de γ, $\Delta\phi$ en composante EW à la station Soudievka
Ondes Diurnes

Début de la série	Méthode	O_1		Q_1		K_1		M_2	
		γ	$\Delta\varphi$	γ	$\Delta\varphi$	γ	$\Delta\varphi$	γ	$\Delta\varphi$
71 022 000	М	0,628	40,62°	0,592	-21,48°	0,984	30,37°	2,065	-159,75°
	Д	0,724	59,01	0,572	-23,72	0,983	29,76	2,092	-149,23
	В	0,719	31,40	0,625	-22,75	0,978	32,56	2,381	-177,43
71 031 700	М	0,181	-44,33	0,688	- 9,37	0,548	4,28	1,227	2,66
	Д	0,175	-47,76	0,668	-10,01	0,523	3,69	1,044	11,46
	В	0,383	-34,53	0,730	-12,17	0,572	0,57	0,876	- 8,40
71 041 100	М	1,115	-12,87	0,689	-11,88	0,683	4,33	0,697	52,99
	Д	1,066	- 5,91	0,688	-10,75	0,662	3,86	0,520	57,88
	В	1,245	10,03	0,768	-15,65	0,634	5,04	1,589	54,52
71 050 600	М	0,560	-23,72	0,718	- 4,48	0,621	-12,69	1,278	-31,15
	Д	0,621	-25,63	0,717	- 4,19	0,621	-13,83	1,253	- 22,15
	В	0,612	-24,91	0,675	- 5,12	0,579	-12,01	0,863	- 6,56
71 053 100	М	0,625	-44,38	0,692	3,83	0,781	- 2,11	0,620	14,67
	Д	0,516	-52,29	0,713	4,27	0,797	- 4,25	0,799	38,23
	В	0,518	-37,99	0,626	3,44	0,842	- 4,42	1,398	- 4,62
71 062 500	М	1,434	1,44	0,781	- 4,26	0,815	4,94	0,946	-117,80
	Д	1,178	- 1,59	0,784	- 3,28	0,835	5,32	1,035	-119,80
	В	1,338	12,71	0,716	- 6,50	0,850	5,60	0,945	-140,35
71 072 000	М	0,722	14,69	0,763	-10,72	0,760	2,30	0,433	- 52,22
	Д	0,889	17,43	0,772	-11,80	0,761	1,98	0,603	- 37,59
	В	0,735	9,17	0,801	- 9,83	0,758	3,49	0,227	- 45,24
71 081 400	М	1,117	-22,35	0,604	-17,59	0,877	- 1,75	1,162	20,44
	Д	1,091	-20,06	0,615	-17,06	0,858	- 1,84	1,052	22,29
	В	0,847	-34,63	0,545	-20,46	0,818	- 2,04	1,453	- 1,90
71 090 800	М	1,099	-32,25	0,765	4,25	0,920	-14,78	1,475	26,01
	Д	0,773	-53,08	0,713	1,82	0,918	-12,20	1,616	33,76
	В	0,697	-20,16	0,647	- 2,24	1,028	- 4,67	1,340	35,91
71 100 300	М	0,950	- 7,09	0,572	5,94	0,711	- 3,33	0,710	22,85
	Д	0,960	0,90	0,560	7,33	0,701	- 3,62	0,721	16,53
	В	0,950	-40,02	0,805	6,27	0,809	- 3,72	1,276	-52,49
71 102 700	М	1,118	10,85	0,747	9,47	0,725	2,23	2,269	18,32
	Д	1,238	9,08	0,756	11,99	0,751	1,84	2,385	19,54
	В	1,102	3,38	0,689	16,48	0,658	5,33	3,431	23,03
71 112 100	М	1,071	35,04	0,647	- 3,28	0,782	- 2,55	1,293	55,25
	Д	1,046	32,27	0,647	- 3,70	0,775	- 3,52	1,226	68,63
	В	1,152	10,03	0,662	- 7,67	0,719	2,39	0,951	18,11
71 120 200	М	0,526	11,13	0,689	-12,07	0,751	-0,36	2,283	73,80
	Д	0,560	11,20	0,678	-10,10	0,750	0,75	2,235	91,40
	В	1,059	-19,92	0,867	-10,16	0,734	0,52	5,412	115,38
Moyenne Vectorielle ($n = 13$)	М	0,7740	-3,29	0,6652	-5,23	0,7344	1,24	0,6520	24,11
		±950	±7,02	± 205	±2,48	± 272	±3,52	± 2621	±20,48
	Д	0,7185	-1,06	0,6588	-5,02	0,7333	1,07	0,6000	30,15
		± 969	±7,91	± 211	±2,62	± 290	±3,42	± 2586	±23,60
	В	0,7914	-6,65	0,6775	-6,48	0,7371	2,77	0,6666	45,64
		± 858	±6,27	± 256	±2,87	±347	±3,35	±4058	±34,90

TABLE 2: Valeurs de γ, $\Delta\phi$ en composante EW à la station Soudievka

Ondes semi diurnes

M Matvéev D Doubik V Venedikov

Début de la série	Méthode	N_2		M_2		S_2		K_2 ($2N_2$)	
		γ	$\Delta\varphi$	γ	$\Delta\varphi$	γ	$\Delta\varphi$	γ	$\Delta\varphi$
71 022 000	M	0,641	-9,43°	0,745	-4,28°	0,788	-1,24°	0,913	0,41°
	Д	0,649	-5,27	0,738	-4,65	0,791	-0,65	1,022	4,76
	В	0,675	-5,34	0,752	-4,59	0,780	-2,51	0,783	-0,08
71 031 700	M	0,651	-8,80	0,730	-5,67	0,873	3,83	0,333	83,96
	Д	0,643	-5,88	0,733	-5,49	0,885	4,11	0,324	9,48
	В	0,630	-6,62	0,732	-5,74	0,864	3,75	0,411	72,88
71 041 100	M	0,749	-4,49	0,745	-3,50	0,858	6,73	1,280	-4,44
	Д	0,766	-4,80	0,747	-3,98	0,857	5,09	1,125	12,61
	В	0,769	-2,33	0,738	-3,54	0,838	6,64	0,964	12,39
71 050 600	M	0,833	-3,70	0,740	-2,34	0,902	1,97	1,228	18,50
	Д	0,840	-2,13	0,740	-2,56	0,892	0,65	0,764	42,70
	В	0,826	-0,90	0,747	-2,81	0,908	2,18	0,761	44,85
71 053 100	M	0,755	-0,92	0,737	-3,10	0,910	8,56	1,171	-9,77
	Д	0,762	1,07	0,738	-3,10	0,954	9,65	1,202	15,26
	В	0,776	3,14	0,742	-3,20	0,926	8,31	1,501	14,68
71 062 500	M	0,866	-3,17	0,726	-4,67	0,771	16,97	0,732	-17,05
	Д	0,896	-0,69	0,730	-4,70	0,780	19,78	1,141	-20,84
	В	0,901	-2,10	0,725	-4,17	0,756	18,34	1,511	-71,77
71 072 000	M	0,811	-0,50	0,721	-3,71	0,761	5,54	0,456	-53,03
	Д	0,837	-1,86	0,715	-4,05	0,768	4,48	0,394	70,52
	В	0,834	0,51	0,727	-4,17	0,761	5,57	0,393	17,86
71 081 400	M	0,880	0,79	0,737	-2,12	0,781	2,90	0,297	-53,51
	Д	0,890	-1,23	0,737	-2,43	0,786	2,40	0,323	17,13
	В	0,891	1,32	0,743	-2,06	0,775	2,63	0,377	31,63
71 090 800	M	0,743	-5,77	0,762	-2,34	0,767	4,09	0,979	-32,15
	Д	0,769	-3,13	0,767	-2,24	0,744	5,50	1,056	-15,22
	В	0,769	-0,41	0,751	-2,23	0,750	5,77	0,823	-21,27
71 100 300	M	0,730	-13,46	0,736	-1,61	0,774	7,66	0,385	-62,60
	Д	0,742	-13,72	0,737	-2,19	0,773	8,41	0,441	-36,50
	В	0,747	-8,27	0,759	-1,32	0,783	6,12	0,302	21,69
71 102 700	M	0,722	- 0,78	0,735	-3,34	0,782	6,41	0,581	-26,69
	Д	0,728	- 1,32	0,735	-3,22	0,771	6,12	0,692	-14,30
	В	0,714	- 2,30	0,734	-3,37	0,772	6,22	0,765	- 8,65
71 112 100	M	0,736	2,94	0,722	-3,62	0,756	10,26	0,596	-45,03
	Д	0,746	2,32	0,721	-3,57	0,759	9,61	0,814	-27,06
	В	0,705	2,24	0,727	-3,63	0,752	8,85	0,865	-27,75
71 120 200	M	0,688	8,12	0,720	-2,81	0,737	7,04	1,174	1,35
	Д	0,685	8,12	0,720	-2,78	0,720	6,54	0,979	28,98
	В	0,712	10,11	0,711	-3,27	0,741	8,77	1,063	33,86
Moyenne Vectorielle (n = 13)	M	0,7340	-2,89	0,7182	-3,31	0,7841	6,15	0,6756	-12,23
		± 211	±1,46	± 30	±0,31	± 166	±1,18	± 1183	±6,53
	Д	0,7457	-2,15	0,7183	-3,45	0,7849	6,23	0,7001	4,14
		± 228	±1,31	± 36	±0,29	± 191	±1,38	± 955	±7,17
	В	0,7457	-0,76	0,7206	-3,38	0,7797	6,12	0,6365	1,94
		± 224	±1,22	± 37	±0,32	± 177	±1,26	± 954	±12,92

Les décalages des 13 analyses mensuelles sont de 25 jours ce que nous faisons usuellement dans notre méthode [6].

La comparaison des valeurs obtenues par les trois méthodes pour γ et $\Delta\phi$, leurs moyennes vectorielles et leurs erreurs quadratiques moyennes, montre le bon accord des résultats.

Il convient de noter ici que les valeurs du paramètre γ sont corrigées par un facteur $k_{09} = 0,97721$ qui tient compte d'une correction à l'étalonnage de l'appareil [6].

Aucun des paramètres calculés par les différentes méthodes ne sort des limites des intervalles déterminés par les erreurs quadratiques moyennes correspondantes.
Pour M_2 par exemple, la valeur relative de l'erreur est de moins de 0,5% pour chacune des méthodes.

La diminution peu importante des erreurs pour l'une des méthodes (M) ne suffit pas à attribuer à celle-ci une qualité supérieure et on peut en fait considérer les trois méthodes comme équivalentes.

Quand on a la possibilité de déterminer des poids p_n avec certitude on appliquera des moyennes vectorielles pondérées ce qui garantit des résultats plus sûrs mais la base du système de poids présente toujours un problème compliqué. On a fait en [10] une estimation de l'efficacité de plusieurs variantes de poids en prenant des valeurs inversément proportionnelles au carré de l'erreur quadratique moyenne σ_n d'une ordonnée (calculée par la combinaison de Doubik [8].

L'ensemble des valeurs des erreurs quadratiques moyennes $(m_x)_n$ de la détermination de chacun des paramètres de marée X_i peut constituer une bonne base du système des poids p_n. La méthode de Venedikov permettant d'estimer la précision de détermination de chacun des paramètres pour chaque série analysée, nous avons utilisé cette possibilité pour clarifier la question de savoir si le fait d'utiliser le système de poids

$$p_n = \frac{1}{(m_x)^2_n}$$

améliore les résultats par rapport à la moyenne vectorielle simple.

Les résultats sont donnés dans les Tables 3 et 4 comme suit:

en première ligne	calcul avec poids égaux à 1
dans les lignes suivantes	moyennes pondérées suivant diverses variantes.

TABLE 3: Valeurs moyennes de γ et $\Delta\phi$ pour différentes variantes de pondérations (méthode Venedikov).

Ondes diurnes

Poids	Q_1		O_1		K_1		M_2	
$(\rho_X)_n$	γ	$\Delta\varphi$	γ	$\Delta\varphi$	γ	$\Delta\varphi$	γ	$\Delta\varphi$
$(\rho_X)_n=1$	0,7914 ± 858	−6,65° ±6,27	0,6775 ± 256	− 6,48° ± 2,87	0,7371 ± 347	2,77° ±3,35	0,6666 ± 4058	45,64° ±34,90
$(\rho_{Q1})_n$	0,8088 ± 892	−8,09 ±6,01	0,6561 ± 271	− 9,80 ± 2,75	0,7035 ± 333	0,85 ±2,30	0,9875 ± 2772	21,33 ±15,02
$(\rho_{O1})_n$	0,8198 ± 935	−5,07 ±5,67	0,6701 ± 239	− 8,47 ± 2,62	0,6975 ± 329	0,64 ±2,26	0,8799 ± 2886	24,67 ±18,38
$(\rho_{K1})_n$	0,8544 ± 922	−4,07 ±5,52	0,6664 ± 246	− 7,82 ± 2,68	0,7105 ± 299	0,68 ±1,88	0,8843 ± 3132	27,79 ±20,45
$(\rho_{M1})_n$	0,7941 ± 902	−8,61 ±6,14	0,6560 ± 272	−10,44 ± 2,60	0,7037 ± 339	0,84 ±2,40	0,9431 ± 2630	19,15 ±14,42

TABLE 4: Valeurs moyennes de γ et $\Delta\phi$ pour différentes variantes de pondérations (méthode Venedikov)

Ondes semi-diurnes

Poids	N_2		M_2		S_2		$2N_2$	
$(\rho_X)_n$	γ	$\Delta\varphi$	γ	$\Delta\varphi$	γ	$\Delta\varphi$	γ	$\Delta\varphi$
$(\rho_X)_n=1$	0,7457 ± 224	−0,76° ±1,22	0,7206 ± 37	−3,38° ±0,32	0,7797 ± 177	+6,12° ±1,26	0,6365 ± 954	1,94° ±12,92
$(\rho_{N2})_n$	0,7479 ± 210	−0,38 ±1,10	0,7209 ± 34	−3,18 ±0,29	0,7796 ± 171	6,18 ±1,00	0,6553 ± 929	1,89 ±10,56
$(\rho_{M2})_n$	0,7537 ± 209	0,11 ±1,07	0,7198 ± 33	−3,25 ±0,26	0,7852 ± 190	6,69 ±1,09	0,6963 ± 1002	0,79 ±11,45
$(\rho_{S2})_n$	0,7562 ± 226	−0,87 ±1,04	0,7225 ± 33	−3,14 ±0,32	0,7779 ± 155	5,61 ±1,03	0,6028 ± 909	3,68 ±10,84
$(\rho_{2N2})_n$	0,7402 ± 210	−1,21 ±1,10	0,7228 ± 34	−3,11 ±0,33	0,7738 ± 139	5,43 ±0,82	0,5992 ± 803	3,84 ± 8,58

On constate que la pondération améliore la précision de tous les résultats, à l'exception de $\gamma(Q_1)$.

On peut se demander si une pondération basée sur l'une des ondes principales K_1 ou M_2 n'apparaitrait pas comme utile pour la recherche d'une solution optimale mais aucune des deux ondes n'offre une telle propriété car elles ne minimisent les erreurs que sur leurs propres paramètres. Ceci peut s'étendre à d'autres ondes de moindre amplitude. Les résultats de la variante optimale sont soulignés dans les tables 3 et 4.

Un résultat intéressant concerne la comparaison, faite dans la Table 5, des valeurs de γ pour les ondes O_1 et K_1 en relation avec les effets dynamiques du noyau liquide.

TABLE 5: Comparaison des valeurs conclues de la Table 3 pour $\gamma(O_1)$, $\gamma(K_1)$ avec la théorie de Molodensky sur les effets dynamiques du noyau liquide [3, p400].

Variante	$\gamma(O_1)$	$\gamma(K_1)$	$\gamma(O_1)-\gamma(K_1)$
Observations de Soudievka Composante EW, 1971 Clinomètre Ostrovski 09 méthode Venedikov			
1) moyenne vectorielle non pondérée	0,6775	0,7371	-0,0596
2) moyenne vectorielle pondérée	0,6701	0,7105	-0,0404
Théorie de Molodensky			
1) Modèle I	0,688	0,730	-0,042
2) Modèle II	0,686	0,727	-0,041

Conclusions:

1 - Les méthodes Venedikov [12], Matvéev [2] et Doubik [4] sont de même valeur dans une application mois par mois.

2 - Les résultats mensuels doivent être combinés par moyennes vectorielles pondérées suivant les erreurs quadratiques moyennes de l'onde considérée.

BIBLIOGRAPHIE

1. PERTSEV B.P.
Analyse harmonique des marées élastiques.
Isvestia Akad Naouk SSS R, Serie Geoph 1958 n°8 pp 946 - 958.

2. MATVEEV P.S.
Analyse harmonique d'une série mensuelle d'observations de marées terrestres.
Marées Terrestres, Kiev, Naoukova Doumka 1966, pp 51 - 79.

3. MELCHIOR P.
Marées Terrestres.
Mir 1968, 482 pages.

4. DOUBIK B.S.
Analyse d'une série mensuelle d'observations de marées.
Rot. et Déf. de Marées, 1978, n°10 pp 34 - 39.

5. MATVEEV P.S., OSTROVSKI A.E., GOLOUBITSKI V.G. et alii
Observations clinométriques à Soudievka.
Rot. et Déf. de Marées, 1973, n°5, pp 11 - 16.

6. MATVEEV P.S., OSTROVSKI A.E., GOLOUBITSKI V.G. et alii
Résultats de l'analyse harmonique des observations clinométriques à la station de Soudievka de 1971 à 1973.
Rot. et Déf. de Marées, 1975, n°7, pp 3 - 8.

7. MATVEEV P.S.
Remarques au sujet de la moyennisation de résultats d'analyses harmoniques de marée terrestre.
Travaux Obs. Grav. Poltava, 1963,vol.12, pp 115 - 124.

8. DOUBIK B.S.
Estimation de l'erreur quadratique moyenne d'une ordonnée de courbe de marée et moyennisation des résultats d'analyses harmoniques.
Rot. et Déf. de Marées, 1975, n°7, pp 62 - 66.

9. MATVEEV P.S., GOLOUBITSKI V.G., BOGDAN I. Yu. et alii
Précision des paramètres de marée terrestre pour les points du profil clinométrique Soumi - Kherson.
Rot. et Déf. de Marées, 1977, n°9, pp 16 - 32.

10. DOUBIK B.S., GOLOUBITSKI V.G.
Sur l'attribution de poids à des séries mensuelles séparées dans la réduction des observations de marées terrestres.
Rot. et Déf. de Marées, 1978, n°10, pp 51 - 58.

11. LECOLAZET R.
La méthode utilisée à Strasbourg pour l'analyse harmonique de la marée gravimétrique.
Marées Terrestres Bull. Inform. Assoc. Int. Géod. Commis. perman. marées Terrestres, 1958, n°10, p. 153 - 178.

12. VENEDIKOV A.P.
Une méthode pour l'analyse des marées terrestres à partir d'enregistrements de longueur arbitraire.
Com. Obs. Roy. Belg., Ser. Geophys., 1966, n°250, N°71, p. 463 - 485.